Universitat Autònoma de Barcelona

Multifunctional Materials based on TTF-PTM dyads: towards new Molecular Switches, Conductors and Rectifiers

Manuel Souto Salom

Universitat Autònoma de Barcelona

Multifunctional Materials based on TTF-PTM dyads: towards new Molecular Switches, Conductors and Rectifiers

Manuel Souto Salom

Tesi doctoral

Programa de Doctorat en Ciència de Materials

Directors

Prof. Jaume Veciana i Dr. Imma Ratera

Departament de Química

Facultat de Ciències

2016

Memòria presentada per aspirar al Grau de Doctor per:

Manuel Souto Salom

Dr. Imma Ratera

Prof. Jaume Veciana

Bellaterra, 13 de juny de 2016

El Prof. **Jaume Veciana**, investigador principal, i la Dr. **Imma Ratera**, científic titular del CSIC a l'Institut de Ciència de Materials de Barcelona (ICMAB-CSIC)

CERTIFIQUEN

Que Manuel Souto Salom, llicenciat en Química i Enginyeria Química, ha realitzat el treball d'investigació que porta per títol "Multifunctional Materials based on TTF-PTM dyads: towards new Molecular Switches, Conductors and Rectifiers" i que aquest treball s'ha desenvolupat en el marc del programa de doctorat en Ciència de Materials del Departament de Química de la Universitat Autònoma de Barcelona.

I perquè així consti, signen el present certificat

Prof. Jaume Veciana

Dr. Imma Ratera

Bellaterra, 13 de juny de 2016

“If you're going to try, go all the way.
Otherwise, don't even start.”

Charles Bukowski

A mis abuelos,

Acknowledgements

La realización de esta Tesis no hubiera sido posible sin la ayuda y el apoyo de numerosos colaboradores, amigos y familiares. Es por ello por lo que me gustaría dar las gracias a todos ellos.

En primer lloc, voldria agrair molt especialment al Prof. Jaume Veciana per haver-me donat l'oportunitat de formar part del seu grup i per haver-me fet confiança per la realització d'aquesta Tesi. Agraeixo molt tots els seus consells durant aquesta Tesi a nivell científic així com a l'hora de redactar un article. Vull agrair també a la Dra. Imma Ratera per tot el seu ajut i suport, tant a nivell professional com personal, i per la seva amabilitat al llarg d'aquests anys. També voldria donar les gràcies a la Prof. Concepció Rovira, que ha estat com una tercera directora i amb la que he après molt sobre conductors moleculars. Moltes gràcies a tots tres per tot el que m'heu ensenyat durant aquests anys i per l'entusiasme que m'heu transmès per la recerca.

Quisiera agradecer a todos los miembros del grupo Nanomol con los que he tenido el gusto y la suerte de compartir todo este tiempo tanto dentro como fuera del ICMAB. Muchas gracias a la pequeña gran familia por tantos momentos vividos durante estos años: Carlos, Amable, Núria, María, Lidia, Francesc, Antonio, Davide, Toni, Inés, Víctor, Serena, Sergi, Gonca, Ajay, Stefano, Francesca, Carles, Luiz, Dolores, Elena M., Adriana, Diego, Elisabet, Nathaly, Natascia, Quioaming, Jose, Judit, Marta, Santi, Nora, Vega, Pepe, Carme, Elena L., Volodia… Tampoco me olvido de los que no están: César, Elisa, Witold, Eva, Rapha, Elena R., Javi, Eve, Ingrid, José, Isaac, Dayana, Freddy, Lourdes… ¡Muchas gracias a todos!

Como se verá a lo largo de esta Tesis, buena parte de los estudios se han realizado en colaboración con diversos grupos de investigación por lo que me gustaría dar las gracias a todos ellos. Ha sido un verdadero placer colaborar con todos vosotros:

Muchas gracias a Paula Mayorga, Juan Casado y Teo López por la ayuda con las medidas Raman y por la amabilidad con la que me recibieron durante mi pequeña estancia en la Universidad de Málaga.

Moltes gràcies a Sergi Vela i Maria Fumanal (Université de Strasbourg) per tots els càlculs teòrics i per les discussions tan interessants que hem mantingut en aquest temps.

I would like to thank very much Dr. Francesca Delchiaro, Prof. Alberto Girlando and Prof. Anna Painelli from the University of Parma for all the theoretical calculations as well as for the Raman measurements of the crystals. Grazie mille!

I also want to thank Valentina Pia, Stein, Dr. Jochen Campo and Prof. Wim Wenseelers for all the help and support during my stay at the University of Antwerp where I could perform the HRS measurements.

También quisiera agradecer a Enrique Ortí (Universidad de Valencia) por todos los cálculos teóricos y por su predisposición a la hora de realizarlos.

I would like to thank Dr. Marta Vico, Morten Jensen, Dan Bendixen and Prof. Jan O. Jeppesen (University of Southern Denmark) for the synthesis of the TTF derivative that was the precursor for obtaining very interesting materials.

Thank you very much to Dr. HengBo Cui (RIKEN) for the resistivity measurements of the single crystals at high pressure.

I would like to thank Harald O. Jeschke, Milan Tomic and Roser Valentí (University of Frankfurt) for the crystal and band structures calculations at high pressures.

Quisiera dar igualmente las gracias a Miriam Peña y Valentín Baonza por las medidas de Raman y fotoluminiscencia a alta presión.

I would also like to thank Dr. Li Yuan and Prof. Christian Nijhuis for their help and support during my stay at the National University of Singapore where I could perform the charge transports measurements through the SAMs.

Asimismo, me gustaría agradecer el financiamiento de esta Tesis al MECD, al CSIC y al CIBER-BBN.

Por último, me gustaría dedicarle esta Tesis a toda mi familia y en especial a mis abuelos. A mi abuelo Julio, por inculcarme desde pequeño la pasión por la investigación. A mi abuelo Pepe, por enseñarme a ser perseverante y a esforzarme frente a las adversidades. A mis abuelas Sefa y Amparo, por todo el cariño y alegría que siempre me han transmitido. A mis padres, por todas las oportunidades que me han dado en la vida y porque todo lo que soy es gracias a ellos. A mis hermanos Julio e Iria, porque siempre me han estado animando a pesar de la distancia. A Ariadna, por estar a mi lado cuidándome y apoyándome en el día a día durante todos estos años.

List of abbreviations

6OP di-*tert*-butyl-6-oxophenalenoxyl

A Acceptor

A-D-A Acceptor-Donor-Acceptor

AFM Antiferromagnetic

BE Binding Energy

BLA Bond Length Alternation

C-SFM Conductive Scanning Force Microscopy

CT Charge Transfer

CV Cyclic Voltammetry

D Donor

D-A Donor-Acceptor

DCC N,N'-Dycyclohexulcarbodiimide

DMAP 4-(Dimethylamino)pyridine

DMF N,N-Dimethylformamide

DMSO Dimethyl Sulfoxide

DT Dithiazolyl

EGaIn Eutectic Gallium-Indium

EFISHG Electric-Field-Induced Second Harmonic Generation

ESR Electron Spin Resonance

Fc Ferrocene

Fc-PTM Ferrocene-Polychlorotriphenylmethyl

FM Ferromagnetic

GGA Generalized Gradient Approximation

HOMO Highest Occupied Molecular Orbital

HS High-Spin

HRS Hyper-Rayleigh Scattering

ICT Intramolecular charge transfer

IR Ion-Radical

IET Intramolecular Electron Transfer

ITO Indium tin oxide

LB Langmuir-Blodgett

LS Low-Spin

LUMO Lowest Unoccupied Molecular Orbital

MPTTF Monopyrrolo-Tetrathiafulvalene

MV Mixed-Valence

N Neutral

NEXAFS Near-Edge X-ray Absorption Fine Structure spectroscopy

NIR Near-Infrared

NLO Non Linear Optics

NMR Nuclear Magnetic Resonance

PES Photoemission Spectroscopy

PTM Polychlorotriphenylmethyl

RR Rectification Ratio

SBP Spirobis(phenalenyl)

SAM Self-Assembled Monolayer

SERS Surface-enhancement Raman spectroscopy

SOMO Semi Occupied Molecular Orbital

SC Spin-Crossover

STM Scanning Tunneling Microscopy

SUMO Singly Unoccupied Molecular Orbital

TBAOH Tetrabutylammonium hydroxide

THF Tetrahydrofuran

ToF-SIMS Time-of-flight secondary ion mass spectrometry

TCNQ Tetracyanoquinodimethane

TTF Tetrathiafulvalene

TTF-PTM Tetrathiafulvalene-Polychlorotriphenylmethyl

UV-vis-NIR Ultraviolet-visible-near-infrared spectroscopy

U Coulomb energy

UPS Ultraviolet Photoemission Spectroscopy

VASP Vienna *ab* initio simulation package

VT Valence Tautomeric

W Electronic bandwidth

XPS X-ray Photoemission Spectroscopy

Z Zwitterionic

Summary

This Thesis is focused on the design, synthesis and characterization of new multifunctional molecular materials based on donor-acceptor (D-A) dyads formed by the electron-donor tetrathiafulvalene (TTF) unit linked to the electron-acceptor polychlorotriphenylmethyl (PTM) radical moiety through different π-conjugated bridges. These compounds can exhibit interesting physical properties such bistability and nonlinear optical properties in solution, conductivity in the solid state or electrical rectification when anchored on surfaces. Thus, these systems could find potential applications in the field of molecular electronics as switches, conductors or rectifiers.

In the first part of the Thesis, we have studied the bistability phenomenon in solution of a D-A dyad based on a PTM radical linked to a TTF moiety through a vinyelene bridge. This system exhibited a temperature-induced switching between diamagnetic dimers at room temperature and paramagnetic monomers at high temperature. The two different states showed different optical and magnetic properties when using the temperature as external input. On the other hand, we have also reported the A-D-A diradical triad based on two PTM radical subunits connected through a TTF-vinylene bridge that can reversibly modify the optical, electronic and magnetic properties by one-electron reduction and oxidation in CH_2Cl_2 solution. The modification of electron delocalization and magnetic coupling was observed when the charged species were generated and the changes were rationalized by theoretical calculations.

In the second part of the Thesis, we have reported the synthesis and characterization of different TTF-π-PTM dyad derivatives increasing the number of vinylene units between the D and A moieties. We have studied the intramolecular charge transfer and non-linear optical (NLO) properties in solution and their dependence on the open-shell structure as well as on the bridge length for this family of compounds.

In the third part of the Thesis, we have studied self-assembled architectures in the solid state of a new D-A dyad based on a PTM radical linked to a TTF moiety through a π-phenyl-pyrrole bridge. The crystal structure showed an interesting supramolecular arrangement with segregated donor and acceptor units. Moreover, we reported the appearance of conductivity in single crystals of the same system when increasing the pressure. The semiconducting behavior at high pressures has been attributed to the enhanced intermolecular interactions and charge delocalization due to incorporation of TTF units which force the formation of close packed stacks of molecules.

Finally in the last part of the Thesis, we have reported a new TTF-PTM dyad that was functionalized with a disulfide group in order to prepare self-assembled monolayers (SAMs) on gold. These SAMs were fully characterized by different spectroscopic techniques in order to study the electronic structure of the system. Moreover, charge transport measurements through the SAMs were performed in order to evaluate the possible rectification behavior.

Table of contents

Chapter 1

Introduction and objectives

1. Introduction

1.1. Multifunctional molecular materials

During the last decades the molecular approach to materials science has become a very promising research field for the near-future generation of electronic devices and information-processing systems at the nanoscale level because of their chemical and physical peculiarities. Indeed, molecular materials that can mimic the properties of classic technologically relevant materials have been already reported in different fields, with special relevance in magnetic, electrical and optical materials, such as organic light emitting diodes or organic solar cells.[1] The relevance of these materials, that are based on purely-organic or metal-organic building blocks, is mainly due to the almost infinite tuning of their physical properties by conventional chemical synthetic methods through soft routes such organic chemistry, coordination chemistry and supramolecular chemistry. Owing to important perspectives in both fundamental sciences and applications in, for example, nanotechnology or molecular electronics, considerable efforts have been made to design new multifunctional molecular materials which involve coexistence or interplay between multiple physical properties (i.e. electrical, optical, and magnetic properties) (Figure 1.1).[2]

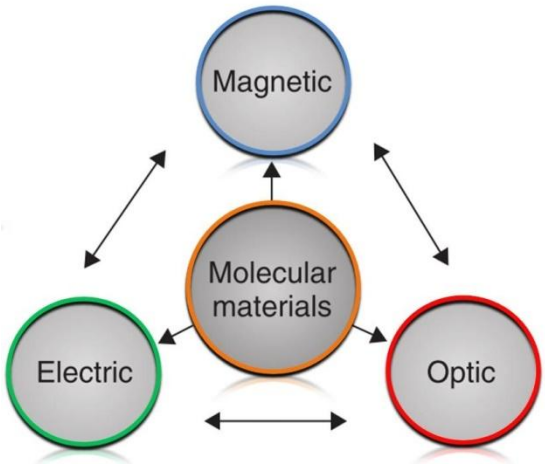

Figure 1.1. Interplay between different physical properties shown by multifunctional molecular materials.

Thus, tunability and versatility of molecular chemistry offers a unique opportunity to design new functional molecular materials or devices showing two or more functions at the same time. This kind of materials can exhibit different combinations of properties such as magnetism/conductivity, conductivity/optical or magnetism/nonlinear optical properties. The coexistence of two or more functional properties in the same molecule can be achieved thanks to the synergism between them and to new related physical phenomena that will give rise to new applications that are unusual in conventional inorganic solids.[3] On the other hand, the design of new multifunctional molecular materials can be even more interesting if they are able to tune their physical properties by applying an external stimulus such temperature, pressure or electric field due to their potential applications as molecular switches in nanotechnology.

1.2. Organic Donor-Acceptor dyads

Organic molecules formed by an electron donor (D) and an electron acceptor (A) units covalently linked by a π-conjugated bridge (D-π-A) (Figure 1.2) are an interesting family of molecules widely investigated for several applications, ranging from organic light-emitting devices,[4] nonlinear optics,[5] molecular electronics[6] and photonics.[7] Moreover, D-A dyads are also very interesting materials due to the possibility of switching between different electronic states through variation of an external stimulus such as temperature, light or pressure. Indeed, when the appropriate external stimulus is applied, an intramolecular electron transfer (IET) can be induced with the movement of an electron from the donor to the acceptor to form the charge-separated (zwitterionic) state that will show different physical properties (i.e. electrical, optical or magnetic properties) (Figure 1.2). Thus, donor-acceptor systems can be potentially used as molecular switches due to the related bistability phenomenon.[8]

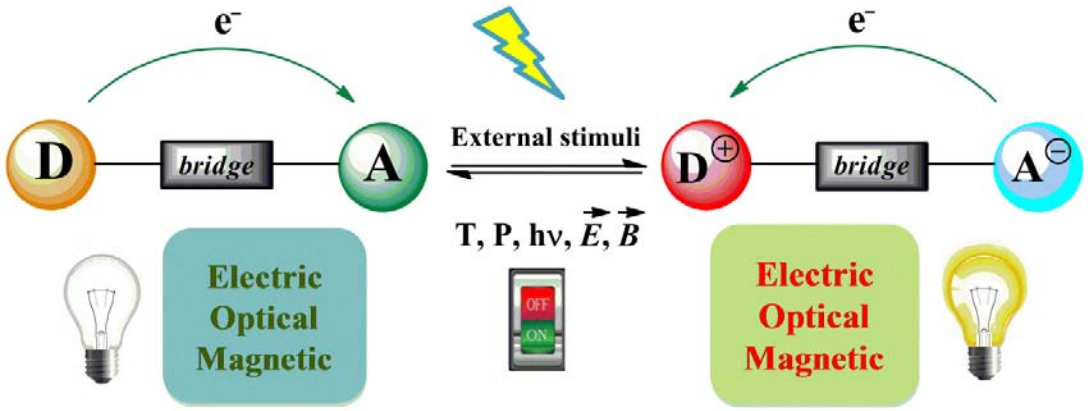

Figure 1.2. Schematic drawing of a D-A dyad and associated bistability phenomenon when an external stimulus (T, P or light) is applied forming the zwitterionic state with different physical properties.

On the other hand, organic donor-acceptor dyads (also known as *push-pull* systems) having conjugated bridges can exhibit large nonlinear (NLO) optical responses due to the dipolar nature. Indeed, π-conjugated and highly-polarizable D-A chromophores showing charge transfer between the donor and acceptor units are optimal candidates for presenting NLO properties with large β hyperpolarizabilities. For example, the *push-pull* 4-dimethylamino-4'-nitrostilbene (DANS) chromophore and its derivatives has been extensively investigated for such purpose for a long time (Figure 1.3).[9,10]

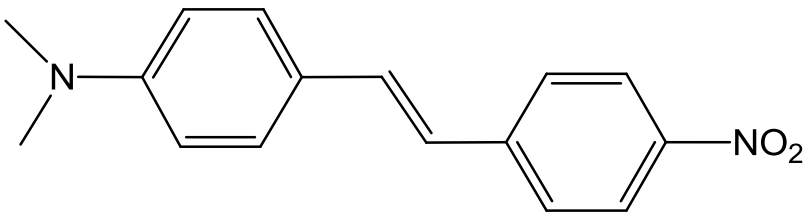

Figure 1.3. Molecular structure of 4-dimethylamino-4'-nitrostilbene (DANS) that has been widely studied for NLO applications.

Moreover, D-A dyads can also be very interesting if they exhibit a molecular packing in the solid state with complete segregation of donor and acceptor fragments as it is a prerequisite for obtaining organic conductors, semiconductors or organic field-effect transistors (OFETs) that could exhibit ambipolar characteristics.[11,12] For example, Geng *et al.* have recently reported a fused D-A system based on tetrathiafulvalene (TTF) and benzothiadiazole (BDT) units that has been explored as active material with OFET characteristics (Figure 1.4a).[13] Moreover, the partially oxidation of the system with iodine gave rise to a columnar π-stack of molecules that are aligned in a head-to-tail manner exhibiting good electrical conductivity at room temperature (Figure 1.4b).

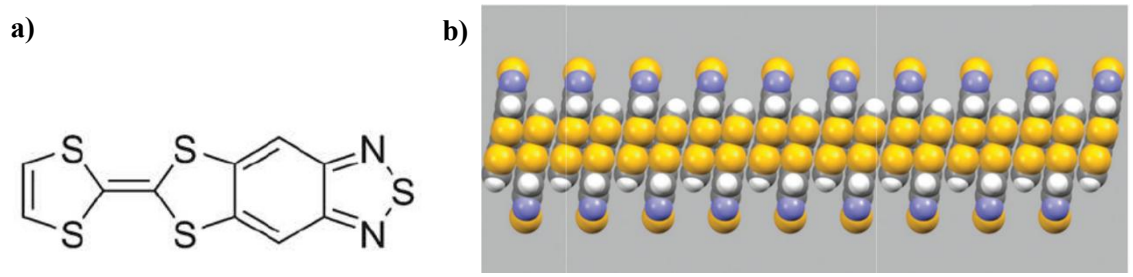

Figure 1.4. a) Molecular structure of TTF-DBT and b) the partially oxidized TTF–BTD molecules with π-stacked orientation in the crystalline $\{(TTF–BTD)_2I_3\}$ salt.

Among its many applications, D-A dyads are also very interesting in the field of molecular electronics as unimolecular rectifiers.[14,15] Indeed, when a dyad is connected between two electrodes the electron flow can be favored from one direction rather than the other. It was in 1974 when Aviram and Ratner proposed the first molecular rectifier consisting on a donor-acceptor (D-A) dyad based on the electron-donor tetrathiafulvalene (TTF) unit linked to the electron-acceptor tetracyanoquinodimethane (TNCQ) linked through a non-conjugated bridge (TTF-σ-TCNQ) (Figure 1.5), which was never synthesized in spite of much effort.[16] Since then several unimolecular rectifiers based on conjugated or non-conjugated D-A dyads have been investigated as candidates for molecular rectifiers. Normally, these D-A molecules can be deposited on surfaces as Langmuir-Blodgett (LB) films or chemically anchored as self-assembled monolayers (SAMs).

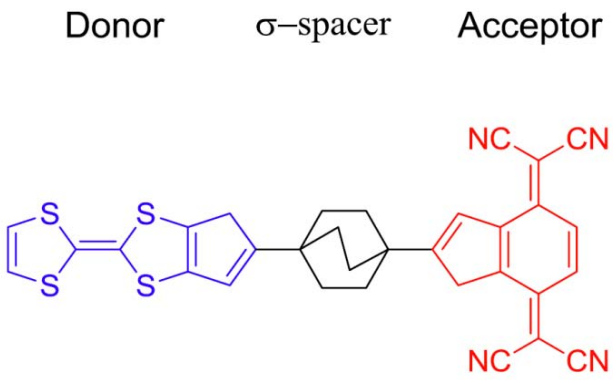

Figure 1.5. Molecular structure of the TTF-σ-TCNQ dyad proposed by Aviram and Ratner.

1.3. Building blocks of the studied dyads

Tetrathiafulvalenes (TTF) and polycholotriphenylmethyl (PTM) radical molecules are very good examples of molecular building blocks for obtaining multifunctional molecular materials, since they permit to combine magnetic, optical, conducting and electrochemical properties.

1.3.1. Electron-donor: Tetrathiafulvalene (TTF)

Tetrathiafulvalene (TTF) and its derivatives are among the most versatile and well known molecules which exhibit outstanding redox properties and remarkable electron donor character.[17,18] The first synthesis of TTF was reported in by Wudl 1970[19] and since then this sulfur-containing molecule and its derivatives became of high interest due to their potential application in molecular electronics as semiconductors, superconductors and organic metals.[20] Indeed, the first organic metal, discovered in 1972, was based on TTF and TCNQ molecules[21] and in 1979 Bechgaard *et al.* reported the superconductor salts based on selenium-containing TTF analogues.[22] During the next decades a huge amount of work was carried out to enhance the electron-donor strength of TTFs and improve conductivities in the salts and charge-transfer (CT) complexes. However, during the past years, TTF and its derivatives have also been widely used as building block in molecular and supramolecular structures, in switchable processes,[23] or as electron-donor unit in D-A systems with application in NLO properties[24] or for the preparation of unimolecular rectifiers on surfaces.[25]

Tetrathiafulvalene is a non-aromatic 14-π-electron system in which oxidation to the radical cation and dication species occurs sequentially and reversibly at very low oxidation potentials ($E_{1/2}^{1}$ = 0.37 V and $E_{1/2}^{2}$ = 0.67 V in CH_2Cl_2) (Figure 1.6). In contrast to the neutral TTF molecule, both the radical cation and dication species are aromatic in the Hückel sense due to the 6π-electron heteroaromaticity of the 1,3-dithiolium cation and, therefore, while $TTF^{+\bullet}$ exhibits a planar D_{2h} symmetry, TTF^{2+} is not planar and has a D_2 symmetry, whereas neutral TTF shows a slightly boat-like structure with C_{2v} symmetry.[18]

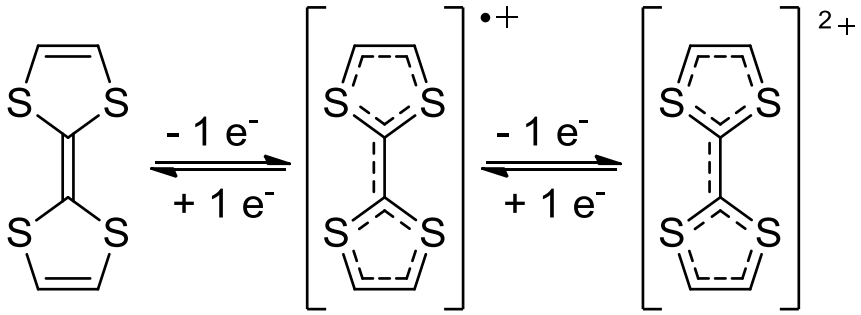

Figure 1.6. TTF and its radical cation and dication species.

1.3.2. Electron-acceptor: Polychlorotriphenylmethyl (PTM) radicals

Polychlorotriphenylmethyl (PTM) radicals are neutral open-shell organic molecules with a net magnetic moment which are characterized by extremely high persistence and stability. They are composed of three totally or partially chlorinated phenyl rings connected to a central carbon with a sp^2 hybridization exhibiting a large chemical and thermal stability. The large persistence of these radicals is mainly due to the presence of bulky chlorine atoms located in *ortho* position providing a source of steric protection for the central carbon where the spin density is mainly localized (Figure 1.7).[3,8] Indeed, in solution PTM radicals remain perfectly inert to oxygen and only decompose in presence of light whereas in solid state only decompose with high melting points, usually near 300ºC.

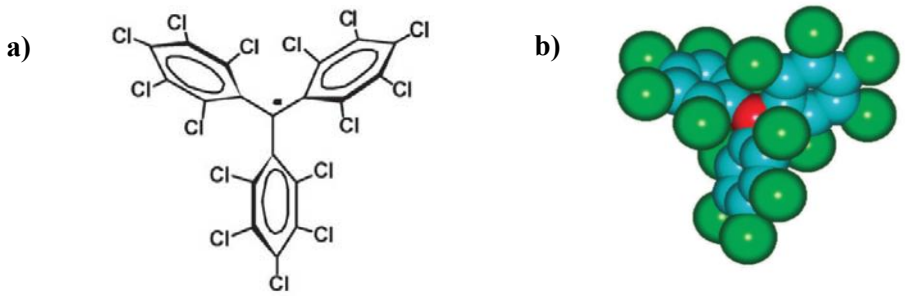

Figure 1.7. a) Molecular structure and b) molecular model of PTM radical showing the high steric shielding of the central carbon atom (in red) surrounded by six bulky chlorine atoms (in green) at the *ortho* positions.

On the other hand, PTM radicals are also interesting because they are electroactive species that can be oxidized to polychlorotriphenylcarbonium ion or reduced to polychlorotriphenylmethyl-carbanion (Figure 1.8). The steric protection by the chlorine atoms also confers stability to the corresponding carbanionic and carbocationic species which have good stability toward oxygen. The reduction of PTM radicals usually occurs at very low potentials (-0.19 V in CH_2Cl_2) and it is more feasible than the corresponding oxidation that requires high potentials (1.61 V in CH_2Cl_2). Such evidence makes this type of radicals optimal electron-acceptor units in D-A systems with NLO properties or to study intramolecular electron transfer for making switchable multifunctional molecular materials since the magnetic, optical and electronic properties of these open-shell molecules can be switched on and off with an external electrochemical stimuli.[8]

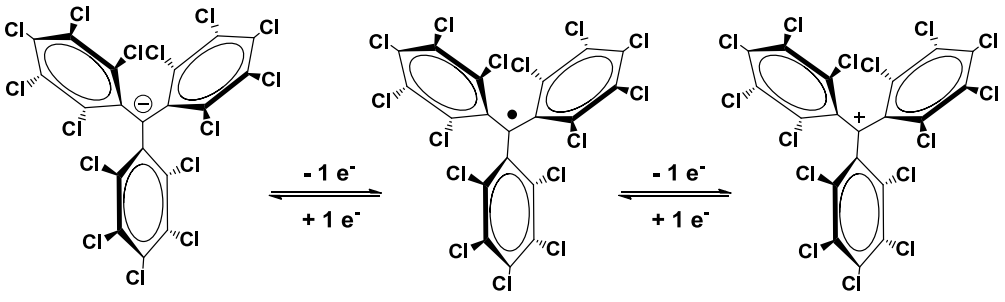

Figure 1.8. Reversible redox processes of the PTM radical and its ionic species.

1.4. Objectives

The main objectives of the present Thesis are the design, synthesis and study of new multifunctional molecular materials based on donor-acceptor (D-A) dyads formed by the electron-donor TTF unit linked to the electron-acceptor PTM moiety through different conjugated π-bridges (Figures 1.9).

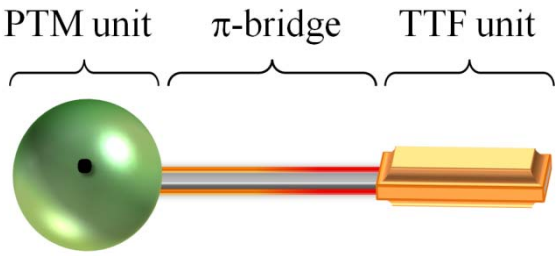

Figure 1.9. Schematic representation of a TTF-π-PTM dyad.

In this Thesis, we will report the synthesis and characterization of a new family of TTF-π-PTM derivatives (Figure 1.10). Moreover, we will study different physical properties of these compounds such as bistability and nonlinear optical (NLO) properties in solution, conductivity in the solid state or charge transport through the molecules when anchored on surfaces.

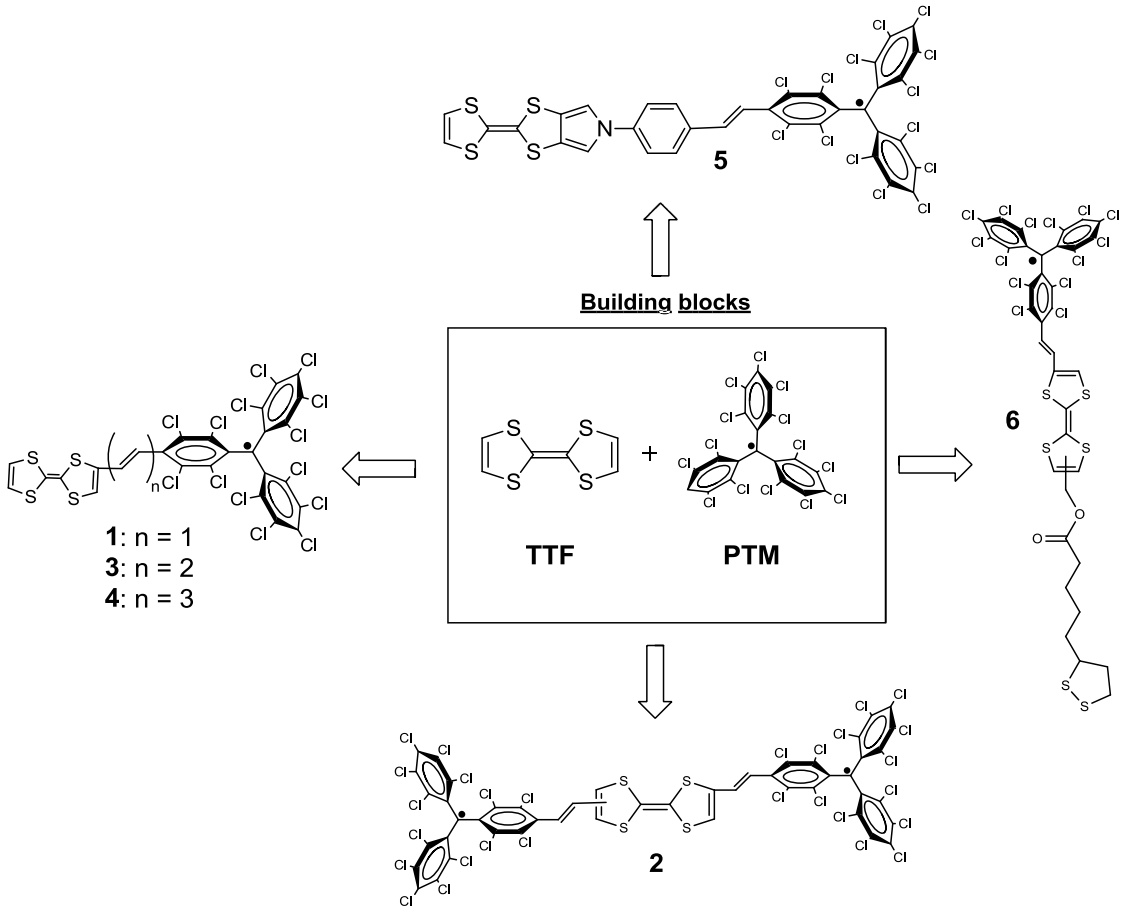

Figure 1.10. Overview of all the studied TTF-π-PTM systems (**1-6**) in the Thesis.

Specifically, we will focus our attention on the following four objectives: 1) The bistability and tristability phenomena in solution of dyad **1** and triad **2**, respectively, in which the application of an external stimulus could give rise to different electronic states exhibiting different optical and magnetic properties in a reversible way. 2) The study of the influence of the bridge length and the open-shell character on the nonlinear (NLO) properties of dyads **1**, **3** and **4** in solution. 3) The study of the supramolecular assemblies of dyad **5** in the solid state and the possible conducting properties of the single crystal. 4) The nanostructuration of dyad **6** on gold surface and the study of its possible electrical rectification behavior.

1.4.1. Study of TTF-PTM dyads as molecular switches in solution

In the first Section of Chapter 2 (Publication #1) we will study the reversible temperature-induced switching process that exhibits radical dyad **1** in DMF solution between diamagnetic dimers, observed at room temperature, and paramagnetic monomers at high temperature (Figure 1.11). We will study the possible different optical and magnetic properties for the two different states of this supramolecular switch when using the temperature as external input.

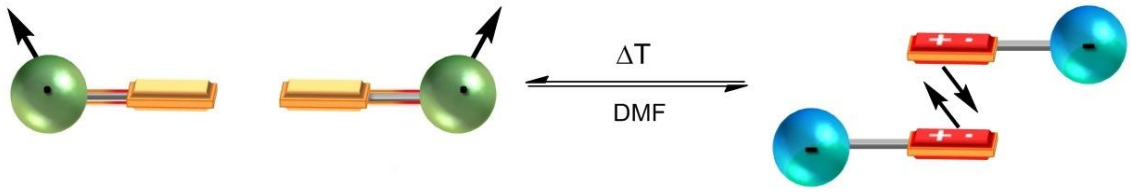

Figure 1.11. Schematic representation of the reversible temperature-induced supramolecular switching of dyad **1** in DMF solution between diamagnetic dimers at low temperature and paramagnetic monomers at high temperature.

In the second Section of Chapter 2 (Publication #2), we will study another example of molecular switch based on the acceptor-donor-acceptor (A-D-A) diradical triad **2** based on two PTM units linked through a TTF-vinylene bridge. Thus, we will analyze the electrochemical reversible switching in CH_2Cl_2 solution by one-electron reduction and oxidation and evaluate the modification of its optical and magnetic properties (Figure 1.12). Thus, we will study the possible modification of the magnetic and optical properties of the mixed-valence radical anion and triradical cation species obtained upon electrochemical reduction or oxidation, respectively. Moreover, the possible changes will be rationalized by theoretical calculations.

Figure 1.12. Schematic representation of the reversible switching of triad **2** in CH_2Cl_2 solution upon electrochemical reduction and oxidation exhibiting three different electronic states.

1.4.2. Study of TTF-PTM dyads as NLO-phores in solution

In Chapter 3 (Publication #3), we will report the synthesis and characterization of a new family of TTF-π-PTM radical derivatives (**1, 3** and **4**) and their non-radical analogues (**1-H**, **3-H** and **4-H**) increasing the number of vinylene units between the D and A units (Figure 1.13). We will provide a detailed study of the intramolecular charge transfer dependence on the open-shell structure and bridge length of this family of compounds that will be rationalized by theoretical calculations. Moreover, nonlinear (NLO) properties of such dyads will be evaluated by means of the Hyper-Rayleigh Scattering (HRS) technique.

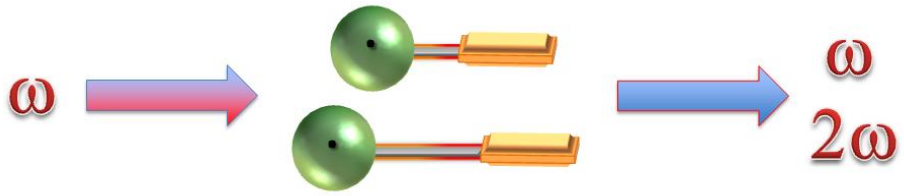

Figure 1.13. Schematic representation of the TTF-PTM dyads (**1**, **3** and **4**) exhibiting NLO properties.

1.4.3. Study of TTF-PTM dyad as single-component conductors in solid state

In the first Section of Chapter 4 (Publication #4), we will study the synthesis and characterization of radical dyad **5** evaluating the intramolecular electron transfer by different spectroscopic techniques in solution as well in solid state. Moreover, we will analyze in detail the crystal structure of such dyad which could reveal an interesting self-assembly architecture with segregated donor and acceptor units (Figure 1.14).

On the other hand, in the second part of Chapter 4 (Publication #5), we will study the conducting properties of single crystals of the same radical dyad **5** and the influence of the pressure on the conductivity. We will rationalize the influence of the charge delocalization and the intermolecular interactions between the molecules. Moreover, we will provide band structures and charge transfer calculations at different pressures in order to understand the origin of such behavior.

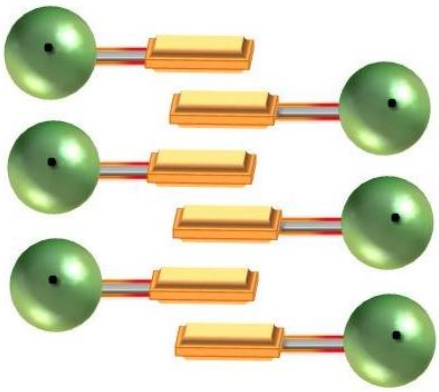

Figure 1.14. Schematic representation of the crystal packing of radical dyad **5**.

1.4.4. Study of nanostructured TTF-PTM dyads as molecular rectifiers

Finally, in the last Chapter 5 (Publication #6), we will study the synthesis and characterization of dyad **6** which contains a disulfide group in order to anchor it on gold surface forming self-assembled monolayers (SAMs) (Figure 1.15). We will characterize the formed SAMs by multiple spectroscopic techniques in order to study the electronic structure of the system and stability of the SAMs. Finally we will analyze the electron transport through the SAMs and discuss its possible rectification behavior.

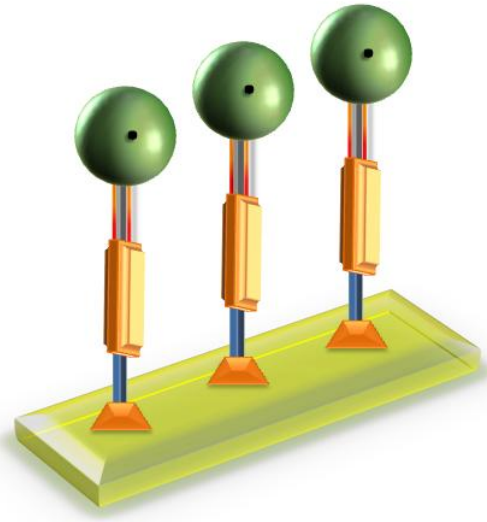

Figure 1.15. Schematic representation of self-assembled monolayers (SAMs) of radical dyad **6** on gold.

1.5. References

1. Coronado, E., Nuez, A. & Romero, F. M. Multifunctional molecular materials. *Solid State Sci.* **5,** 917–924 (2003).

2. Ouahab, L. *Multifunctional Molecular Materials*. (CRC Press, 2013).

3. Veciana, J. & Ratera, I. *Radicals : Towards Multifunctional Molecular Materials*. (Wiley, 2010).

4. Yao, L. *et al.* Highly Efficient Near-Infrared Organic Light-Emitting Diode Based on a Butterfly-Shaped Donor–Acceptor Chromophore. *Angew. Chemie - Int. Ed.* **53,** 2119–2123 (2014).

5. Bures, F. Fundamental aspects of property tuning in push–pull molecules. *RSC Adv.* **4,** 58826–58851 (2014).

6. Metzger, R. M. Unimolecular Electronics. *Chem. Rev.* **115,** 5056–5115 (2015).

7. Gorshelev, A. A. *et al.* Ortho-Dichlorobenzene Doped with Terrylene- A Highly Photo-Stable Single-Molecule System Promising for Photonics Applications. *Chem. Phys. Chem.* **11,** 182–187 (2010).

8. Ratera, I. & Veciana, J. Playing with organic radicals as building blocks for functional molecular materials. *Chem. Soc. Rev.* **41,** 303 (2012).

9. Albert, I. D. L., Marks, T. J. & Ratner, M. A. Large Molecular Hyperpolarizabilities. Quantitative Analysis of Aromaticity and Auxiliary Donor - Acceptor Effects. *J. Am. Chem. Soc.* **119,** 6575–6582 (1997).

10. Marder, S. R. *et al.* Large First Hyperpolarizabilities in Push-Pull Polyenes by Tuning of the Bond Length Alternation and Aromaticity. *Science* **263,** 511–514 (1994).

11. Yamashita, Y. & Tomura, M. Highly polarized electron donors, acceptors and donor–acceptor compounds for organic conductors. *J. Mater. Chem.* **8,** 1933–1944 (1998).

12. Bergkamp, J. J., Decurtins, S. & Liu, S.-X. Current advances in fused tetrathiafulvalene donor-acceptor systems. *Chem. Soc. Rev.* **44,** 863–874 (2015).

13. Geng, Y. *et al.* A Compact Tetrathiafulvalene – Benzothiadiazole Dyad and Its Highly Symmetrical Charge-Transfer Salt : Ordered Donor π-Stacks Closely Bound to Their Acceptors. *Chem. Eur. J.* **20,** 7136–7143 (2014).

14. Metzger, R. M. Unimolecular electrical rectifiers. *Chem. Rev.* **103,** 3803–3834 (2003).

15. Metzger, R. M. Unimolecular electronics and rectifiers. *Synth. Met.* **159,** 2277–2281 (2009).

16. Aviram, A. & Ratner, M. A. Molecular rectifiers. *Chem. Phys. Lett.* **29,** 277–283 (1974).

17. Segura, J. L. & Martín, N. New concepts in tetrathiafulvalene chemistry. *Angew. Chemie - Int. Ed.* **40,** 1372–1409 (2001).

18. Martín, N. Tetrathiafulvalene: the advent of organic metals. *Chem. Commun.* **49,** 7025–7 (2013).

19. Wudl, F., Smith, G. M. & Hufnagel, E. J. Bis- 1,3=dithiolium Chloride: an Unusually Stable Organic Radical Cation. *J. Chem. Soc., Chem. Commun.* 1453–1454 (1970).

20. Batail, P. Introduction: Molecular conductors. *Chem. Rev.* **104,** 4887–4890 (2004).

21. Wudl, F., Wobschall, D. & Hufnagel, E. J. Electrical conductivity by the bis (1,3-dithiole)-bis (1,3-dithiolium) system. *J. Am. Chem. Soc.* **94,** 670–672 (1972).

22. Bechgaard, K., Jacobsen, C. S., Mortensen, K., Pedersen, H. J. & Thorup, N. The properties of five conducting salts: $(TMTSF)_2X$, derived from tetramethyletraselecafulvalene (TMTSF). *Solid State Commun.* **33,** 119–1125 (1980).

23. Canevet, D., Sallé, M., Zhang, G., Zhang, D. & Zhu, D. Tetrathiafulvalene (TTF) derivatives: key building-blocks for switchable processes. *Chem. Commun.* **7345,** 2245–2269 (2009).

24. González, M. *et al.* Tetrathiafulvalene Derivatives as NLO-phores : Synthesis, Electrochemistry, Raman Spectroscopy, Theoretical Calculations, and NLO Properties of Novel TTF-Derived Donor- π -Acceptor Dyads. *J. Org. Chem.* **66,** 8872–8882 (2001).

25. Ho, G. *et al.* The first studies of a tetrathiafulvalene-σ-acceptor molecular rectifier. *Chem. - A Eur. J.* **11,** 2914–2922 (2005).

Chapter 2

Molecular switches in solution

2.1. Introduction

Switching a molecular material between two or more states that can exhibit different physical properties, for example optical, magnetic or electrical properties, upon the application of external stimuli such as temperature,[1] pressure,[2] light[3] or electric field,[4] is an interesting phenomenon mainly due to their potential application as molecular switches and memories.[5,6] Molecular bistability or multistability, which is the property of a molecular system able to evolve from a stable state to other stable states in a reversible and detectable manner when applying an appropriate and controllable perturbation,[7] can be achieved due to intramolecular processes inherent to the molecule and/or to intermolecular interactions between molecules at the supramolecular level.

2.1.1. Classes of molecular switchable materials

Depending on the way that the bistability takes place, we can categorize switchable materials in two types: those in which bistability is originated in a single molecule (molecular bistability) or those requiring two or more molecules (supramolecular bistability).

a) Molecular bistability

There are four main classes of molecular switchable materials that can exhibit bistability as a function of temperature, pressure or other external stimuli: Spin-crossover (SC), valence-tautomeric (VT), mixed-valence (MV), and donor-acceptor (D-A) systems.

Spin-crossover (SC) compounds present d^n (n=4-7) first-row transition-metal ions in octahedral environments that can be switched between two molecular spin states, the so-called high spin (HS) and low spin (LS), by using external perturbations as temperature (Figure 2.1a).[8–11] During the last decades several hundreds of spin crossover complexes have been synthesized and characterized as bulk (powder or single crystal) or diluted materials. On the other hand, valence-tautomeric (VT) compounds exhibit reversible interconversion between two or more isomers that not only present different spin multiplicity but also oxidation state.[12–14] For example, Buchanan and Pierpont reported that the Co compound $[Co^{II\text{-}HS}(3,5\text{-dbsq})_2(bpy)]$ shows thermally induced charge transfer between the Co center and the semiquinone in solution (Figure 2.1b).[15]

a)

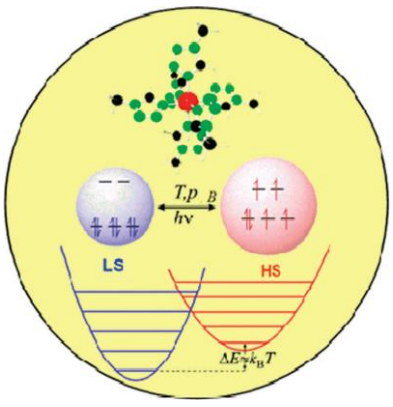

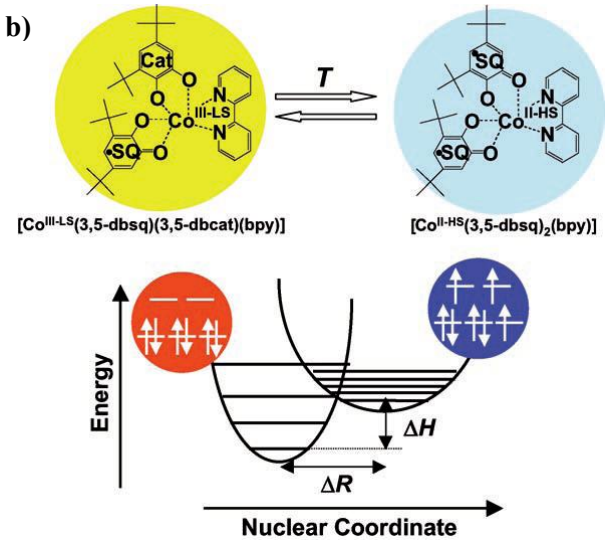

Figure 2.1. LS and HS potential energy wells and 3d electron configurations for a) an Fe(II) spin crossover system[10] and b) valence tautomerism of $[Co^{II\text{-}HS}(3,5\text{-dbsq})_2(bpy)]$ complex.[12]

Mixed-valence (MV) systems are formed by at least two equal redox sites with different oxidation states linked by a bridge that mediates the electron from one site to the other.[16,17] MV compounds have been classified by Robin and Day in three different groups depending on the electron transfer process between the two redox sites. In Class I, there is no interaction between the redox centers. Class III systems have an intense electronic interaction and the electron is completely delocalized all over the molecule. Finally, in Class II this electronic interaction is moderate and the electron is vibrationally localized in one of the redox centers due to the presence of an activation energy barrier (ΔG). However, this barrier can be overcome by an external optical or thermal stimulus and promote an IET process which can give place to bistability.[18]

Donor-acceptor (D-A) systems are formed by an electron donor (D) unit covalently linked to an electron acceptor (A) unit through a bridge. When an external stimulus is applied an intramolecular electron transfer (IET) process can be induced with the movement of one electron from the donor to the acceptor through the bridge giving place to almost two degenerated electronic states of the molecules that can present different chemical and physical properties. These materials can show interconversion between the two localized electronic states (neutral and ziwtterionic) in a reversible manner under specific conditions (Figure 2.2).

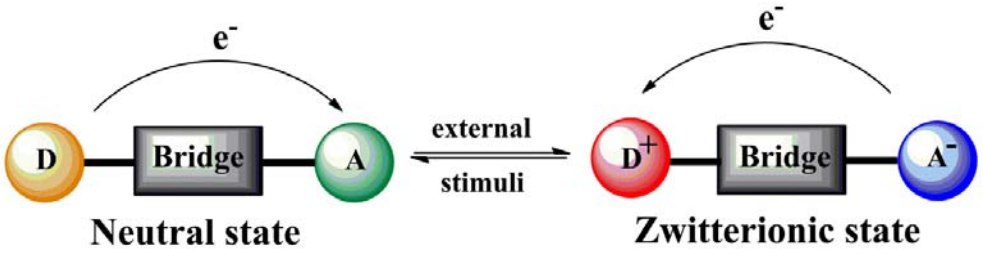

Figure 2.2. Schematic drawing of a dyad formed by an electron donor (D) linked to an electron acceptor (A) by a conjugated bridge.

b) Supramolecular bistability

Organic radicals have received less attention in the context of bistability mainly due to their high reactivity. However, there are some stable radicals that can exhibit a reversible dimerization in response to external stimuli, with monomers and dimers coexisting at the equilibrium in solution[19] and may produce bistable systems in the solid state.[20–22] Spirobisphenalenyl[23,24] and thiazyl[25,26] radicals are good examples of such materials. These radicals are able to switch between a monomeric radical form at high temperature and dimeric form at lower temperature that mainly arises from the π-π intermolecular interactions within the dimers. Furthermore, some of them can present thermal hysteresis with a diamagnetic-to-paramagnetic transition occurring at different temperature than the reverse transition showing a finite temperature regime within which the form of the radical depends on its history (Figure 2.3).

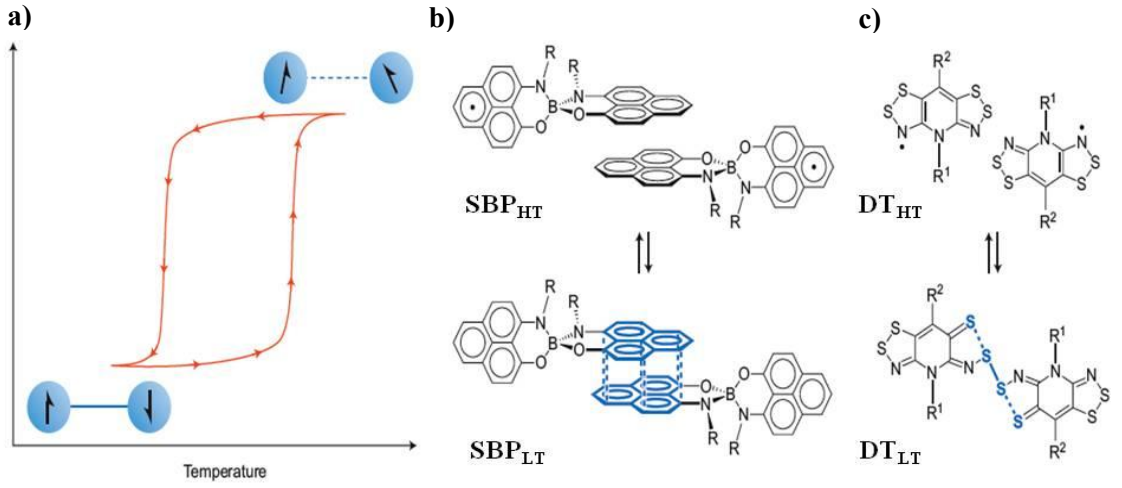

Figure 2.3. a) Schematic diagram of thermal hysteresis arising from the transition between monomeric organic radicals at high temperature and diamagnetic dimers at low temperatures. b) High-temperature form (**SBP$_{HT}$**) and low-temperature form (**SBP$_{LT}$**) of Haddon and co-workers' spirobis(phenalenyl) radical (**SBP**) (R = *n*-Bu). c) High-temperature form (**DT$_{HT}$**) and low-temperature form (**DT$_{LT}$**) of Oakley and co-workers' *bis*(1,2,3-dithiazolyl) radical (**DT**) (R^1 = Et, R^2 = F).[22]

On the other hand, tetrathiafulvalenes (TTF) and their radical cation ($TTF^{+\bullet}$) derivatives have received a great deal of attention due to their unique electrical properties and synthetic versatility.[27–29] These molecules are among the most widely used compounds for the development of organic metals due to their tendency to form self-assembled stacks of neutral TTFs and their mono-oxidized radical-cation ($TTF^{+\bullet}$) that originate partially filled bands and conductivity in the solid state.[30,31] Likewise, $TTF^{+\bullet}$ pairs can form strong π-interactions and form diamagnetic dimers exhibiting insulator behavior. Besides a traditional use for the development of organic conducting materials, TTF derivatives have been extensively used in the last years as building blocks for the development of molecular and supramolecular switchable materials exploiting their redox properties to produce systems whose structure can be varied through an external stimulus.[32] Indeed, during the last years there has been a lot of examples of TTF-based molecules that have been used for the preparation of interlocked compounds such as catenanes and rotaxanes.[33–36]

However, whereas a large number of studies are available on the self-assembling of TTF derivatives in solid state, little is known in solution because of the weakness of non-covalent interactions in this media. Rosokha and Kochi reported in 2007 an exhaustive study of the self-assembling of the $TTF^{+\bullet}$ cation radical in solution at room temperature using high concentrations of its salts.[37] The authors studied the formation of diamagnetic $[TTF^{+\bullet}]_2$ dimers in solution as well as the mixed-valence dimerization of the $TTF^{+\bullet}$ cation with its parent neutral TTF donor (Figure 2.4). Nevertheless, the observation of these mixed-valence $[(TTF)_2]^{+\bullet}$ and radical cation $[TTF^{+\bullet}]_2$ dimers in solution is still a challenging task unless suitable hosts[38] or self-assembled molecular cages[39] are used to bridge TTF units non-covalently.[40–43]

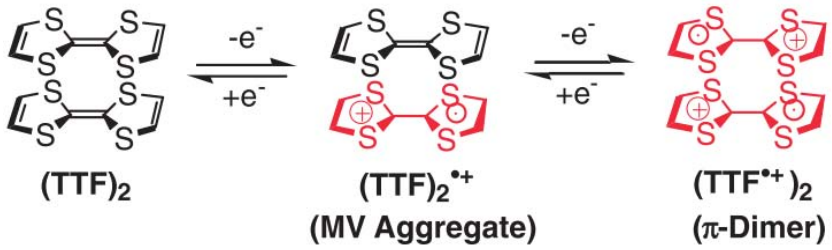

Figure 2.4. Interactions between TTFs in a face-to-face manner.[42]

2.1.2. Acceptor-Donor-Acceptor triads

In the last few years there has been a lot of interest in the design of new organic molecules containing different radical centers linked through ferromagnetic coupling units in order to study the interaction between the radical units.[44–46] For example, some years ago it was reported a diradical PTM-Fc-PTM triad based on two PTM radical units connected by a ferrocene-vinylene (Fc) bridge that acted as a ferromagnetic coupler between the radicals (Figure 2.5a).[45] Also organics A-D-A triads incorporating the TTF units as donors are very interesting materials in order to study the intramolecular electron transfer (IET) processes that can occur in the generated mixed-valence system.[47–50] For example, it has been reported the study of the IET process of the mixed-valence (MV) species derived from the fused TCNQ-TTF-TCNQ triad (Figure 2.5b) in solution.[49]

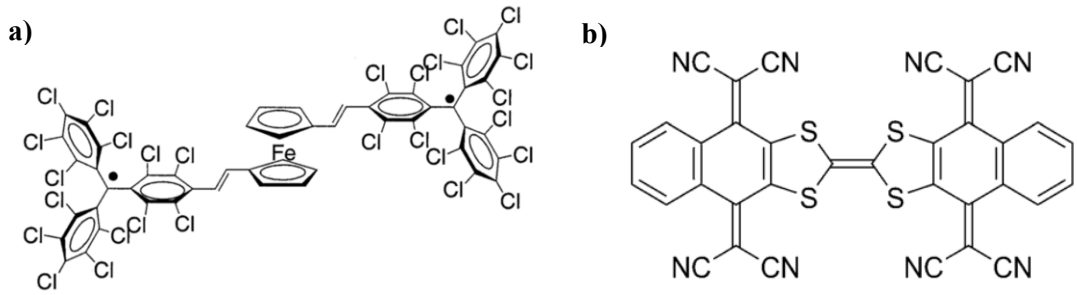

Figure 2.5. Molecular structures of a) PTM-Fc-PTM diradical and b) TCNQ-TTF-TCNQ triads.

2.1.3. Donor-Acceptor (D-A) radical dyads

Organic molecules that contain electron donor and electron acceptor units linked by π-conjugated bridges (D-π-A dyads) are very promising molecular materials for the development of molecular switches and memory devices.[51] For example, during the last years in the framework of our group, it has been reported different D-A systems based on the electron-acceptor polychlorotriphenylmethyl (PTM) radical linked to ferrocene (Fc) derivatives that can be switched from the neutral (N) to the zwitterionic (Z) state by changing the polarity of the solvent or by tuning the temperature in the solid state (Figure 2.6).[52–57]

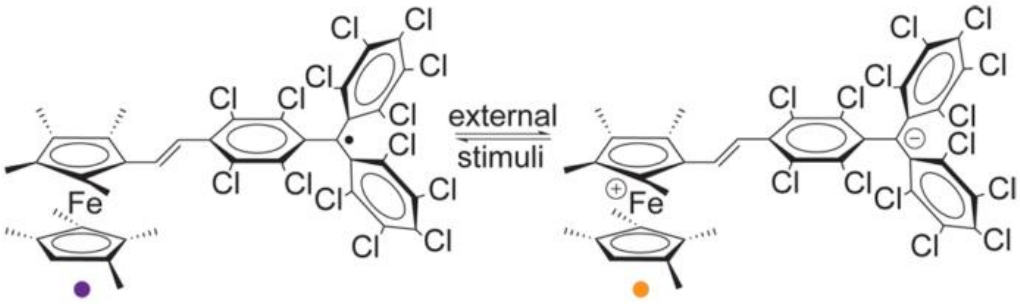

Figure 2.6. Molecular structures relevant to the neutral DA (purple, ●) and zwitterionic D^+A^- (orange, ●) states of Me_8Fc-PTM.[56]

Otherwise, D-A radical dyads using a TTF molecule as electron-donor unit are very interesting compounds due to their IET process and their possible application in areas such as solar cells, molecular wires and optoelectronics.[58] For example, Nishida *et al.* proposed a TTF-based dyad which exhibits bistability in solution originated by an IET process between a TTF electron-donor linked to the electron-acceptor di-*tert*-butyl-6-oxophenalenoxyl (6OP) organic radical (Figure 2.7a).[59] Such bistability can be induced by changes in temperature and in the polarity of the solvent. This phenomenon was followed by UV-vis-NIR spectroscopy observing the neutral state in CH_2Cl_2 whereas the zwitterionic state of the molecule was obtained in the polar CF_3CH_2OH solvent. Moreover, the ESR spectrum in toluene showed the presence of the neutral state whereas the zwitterionic species was identified when using the polar CF_3CH_2OH solvent. Interestingly, T-dependent ESR spectra in a mixture of CH_2Cl_2:CF_3CH_2OH (199:1) solvent show that the neutral state is only present at 293 K whereas the zwitterionic state is stabilized at 243 K (Figure 2.7b).

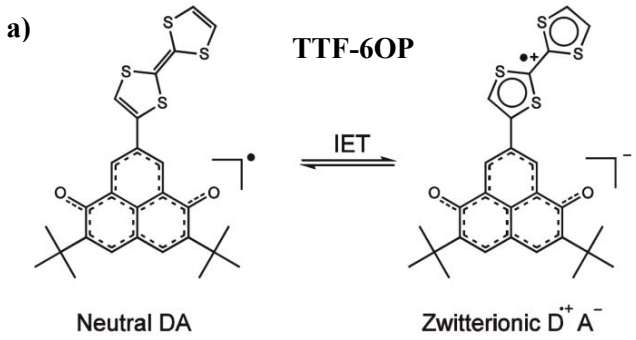

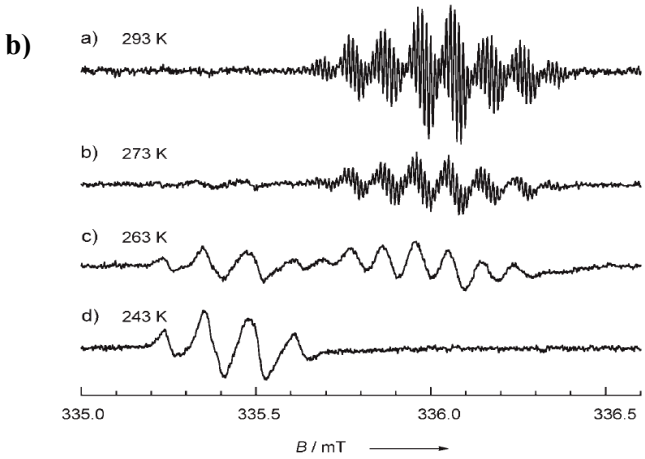

Figure 2.7. a) The two possible states (neutral and zwitterinic) of the TTF-6OP dyad. b) Temperature-dependence ESR spectra of a solution of the dyad in CH_2Cl_2:CF_3CH_2OH (199:1). The neutral state is observed at 293 K whereas the zwitterionic is present at 243 K.

In a similar approach to the last example, in our group we have recently reported a D-A dyad that consists on the electron-acceptor polychlorotriphenylmethyl (PTM) radical linked to a tetrathiafulvalene (TTF) through a vinylene bridge (**1**).[60] This neutral organic D-A radical dyad exhibits a reversible switching from its neutral to its zwitterionic state that can occur through an IET from the TTF to the PTM radical simply by the modification of the solvent polarity (Figure 2.8). For example, in the non-polar CH_2Cl_2 solvent only the neutral (N) species is present whereas in the polar DMF solvent an IET process is promoted and the zwitterionic (Z) species is formed.

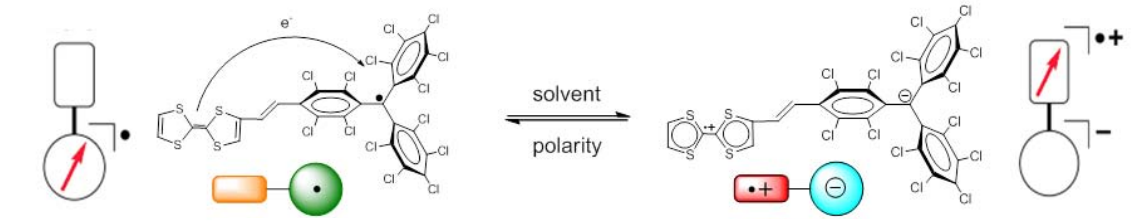

λ_{max} = 387 nm **CH_2Cl_2 (N)** **DMF (Z)** **λ_{max} = 512 nm**

Figure 2.8. Schematic representation of the reversible switching of the radical dyad TTF-PTM (**1**) between the neutral (N) and zwitterionic (Z) states through an IET process.

This phenomenon was followed by UV-vis-NIR spectroscopy where the absorption spectrum in CH_2Cl_2 shows an intense peak at 387 nm attributed to the radical chromophore of the PTM subunit whereas the spectrum in DMF presents an intense band at 512 nm that corresponds to the anionic form of the PTM moiety (Figure 2.9a). Moreover, it was demonstrated that the IET process can induce the self-assembly of the zwitterionic dyads to form diamagnetic dimers in DMF at room temperature. Indeed, the ESR spectrum of TTF-PTM dyad in CH_2Cl_2 presents the typical signal for the PTM radical in agreement with the presence of neutral species whereas the spectrum in DMF do not give any signal (Figure 2.9b). The lack of signal related to the $TTF^{+\cdot}$ cation radical suggests that zwitterionic species can aggregate forming diamagnetic dimers (π-dimer) that are ESR silent.[60]

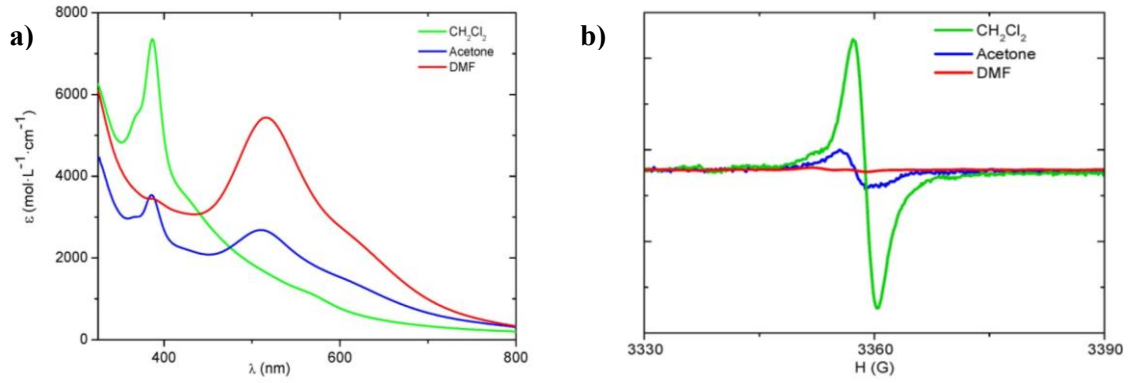

Figure 2.9. a) UV-vis spectra of TTF-PTM (**1**) dyad in CH_2Cl_2 (green line), acetone (blue line) and DMF (red line). b) ESR spectra of TTF-PTM in CH_2Cl_2 (green line), acetone (blue line) and DMF (red line).[60]

Moreover, in order to investigate the origin of such aggregation phenomenon, temperature-dependent optical an ESR spectroscopy studies in CH_2Cl_2 were performed for a family of TTF-PTM dyads bearing different number of electrons and/or with hydrogenated PTM residue giving information on the formation of homo- and mixed-valence dimers.[61] Analysis of the equilibrium constants and thermodynamic parameters showed that dimers formed by radical dyads are much more stable due to the contribution of the intramolecular electron transfer that delocalizes the electrons along the vinylene bridge and the PTM subunit. Moreover, a theoretical model, merging a Hubbard-like description of the intermolecular CT interaction with an essential-state description of the IET, was proposed in order to rationalize the subtle interplay between the IET within a dyad and the intermolecular charge transfer (CT) occurring in a dimer between the TTF residues (Figure 2.10).

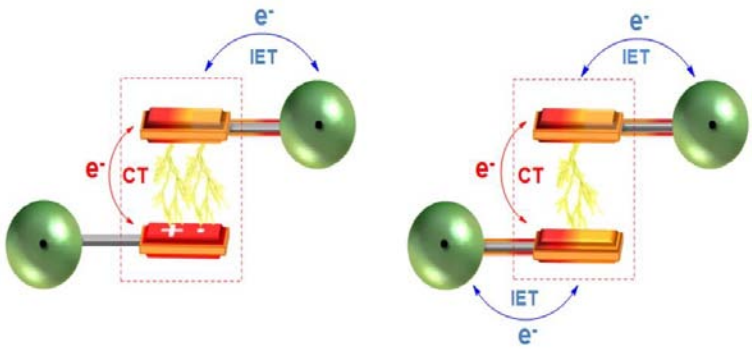

Figure 2.10. Schematic representation of the interplay between the IET within a TTF-PTM radical dyad with the intermolecular CT occurring between the two TTF units in each supramolecular aggregate.

2.2. Results and discussion

In order to get more insight on the dimerization in solution of compounds having TTF units linked to PTM units and their related bistability phenomena, we decided to investigate such processes in a TTF-PTM radical dyad (**1**) and in a PTM-TTF-PTM diradical triad (**2**).

2.2.1. Thermomagnetic molecular switch based on a TTF-PTM radical dyad

In this section we present the study of the reversible temperature-induced switching that exhibits dyad TTF-PTM (**1**) radical in DMF solution between diamagnetic dimers, observed at room temperature, and paramagnetic monomers at high temperature (see Publication #1) (Figure 2.11).[62] This temperature-induced process was followed by different spectroscopic techniques such as UV-vis-NIR, ESR, Raman, ^{1}H-NMR and cyclic voltammetry and the reversibility of the system was confirmed. Moreover, the dimerization process was rationalized by a theoretical model that combines the Hubbard model description of TTF-based dimers with an essential state model relevant to D-A dyads.

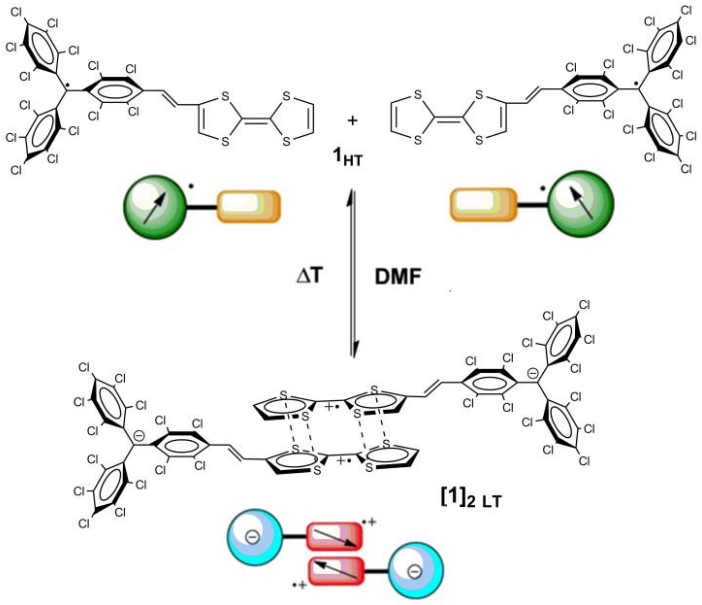

Figure 2.11. Schematic representation of the reversible temperature-induced supramolecular switching of TTF-PTM (**1**) between diamagnetic dimers at low temperature ($\mathbf{1}_{LT}$) and paramagnetic monomers at high temperature ($\mathbf{1}_{HT}$).

Regarding the optical properties, UV-vis-NIR spectra of dyad **1** in DMF were recorded at different temperatures in the 300-375 K range in order to follow the dimerization process (Figure 2.12a) observing a clear color change. At 300 K the spectrum exhibited an intense band at 512 nm with a shoulder at 605 nm assigned to the PTM subunit in its anionic form indicating that **1** is only present in the zwitterionic $D^{+}A^{-}$ state. When the solution was heated the band associated to the PTM anion weakens whereas the band related to the PTM neutral radical (387 nm) acquires intensity together with the appearance of a weak band at 950 nm that is most probably associated to the IET process of **1** in the neutral D-A form.

On the other hand, ESR measurements were performed at different temperatures (Figure 2.12b). Whereas the strong antiferromagnetic coupling of TTF-radical spins in the $\mathbf{[1]_{2\ LT}}$ dimers is responsible for the lack of ESR signal at room temperature, heating the solution at 375 K, a broad line appears at a *g*-value of 2.0025. This signal is typical of PTM radicals, indicating the formation of paramagnetic species that we identify as the $\mathbf{1_{HT}}$ monomer in the neutral D-A form. Cooling down the solution to room temperature, it gradually becomes ESR silent again, exhibiting a completely reversible behavior from 375 K to 300 K. Moreover, to demonstrate the complete reversibility of the system, several and consecutive ESR and UV-vis cycles at 300 and 375 K were performed without showing any sign of deterioration.

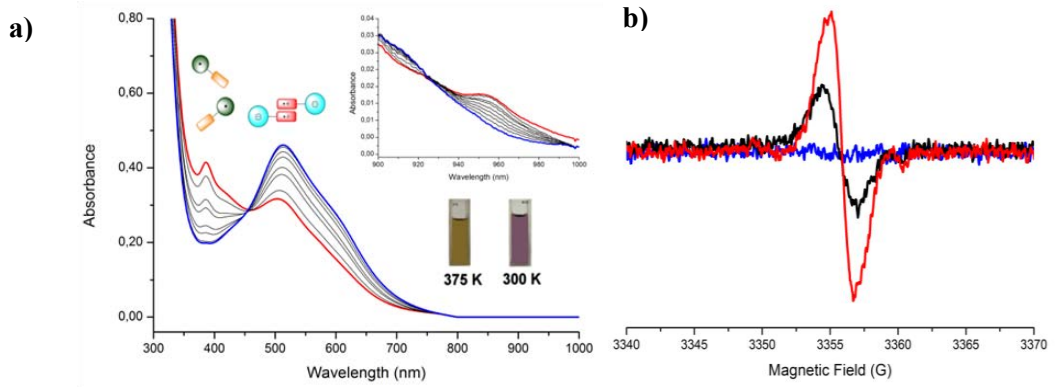

Figure 2.12. a) UV-Vis spectra of dyad **1** in DMF (0.1 mM) at 375 (red line), 365, 355, 350, 345, 340, 330, 320 and 300 K (blue line). b) ESR spectra of **1** in DMF (0.1 mM) at 375 (red line), 365 (black line) and 300 (blue line) K.

Moreover, a theoretical model was used to rationalize this interesting behavior. Figure 2.13 shows the evolution of the ground state and of the lowest triplet state for a monomer $\mathbf{1}_{HT}$ species (left) and a dimer $[\mathbf{1}]_{2LT}$ (right). Top and bottom panels refer to a low-polarity solvent and a strongly polar solvent, respectively. Interestingly, in the polar solvent (DMF), the monomer has a bistable behavior with two minima; the lowest-energy minimum corresponds to a neutral state and is separated by a large energy gap from the zwitterionic state, so that only neutral monomers are observed in solution. On the other hand, dimeric species are only stable as dimers of zwitterions, with the PTM moiety bearing a -0.9 charge.

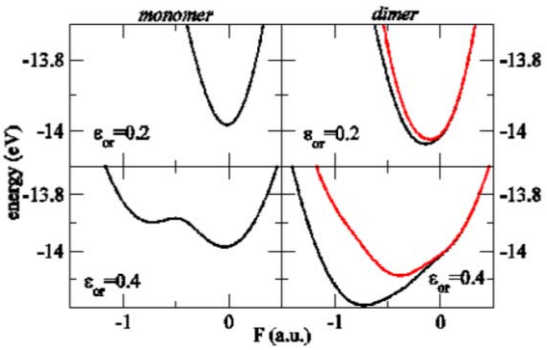

Figure 2.13. Evolution of the ground-state energy (black lines) as a function of the solvent reaction field F, plotted for ε_{or} = 0.2 and 0.4 eV (top and bottom panels) for the monomer **1** (left panels) and the dimer $[\mathbf{1}]_{2LT}$ (right panels). The red lines in the right panels show the energy of the lowest triplet state.

2.2.2. Three-state molecular switch based on a PTM-TTF-PTM diradical triad

As we have seen in the Introduction of this Chapter, there is a high interest in the design of new organic acceptor-donor-acceptor (A-D-A) diradical triads. In view of the interesting properties of such triads, we have designed and synthesized the A-D-A diradical triad based on two PTM radicals connected through a TTF-vinylene bridge (**2**). This molecule can exhibit an electrochemical reversible switching by one-electron reduction and oxidation modifying its optical, magnetic and electronic properties (Figure 2.14). In this section, we will also study the generation of the mixed-valence radical anion $\mathbf{2}^{\bullet -}$ and triradical cation $\mathbf{2}^{\bullet\bullet\bullet +}$ species obtained upon electrochemical reduction or oxidation, respectively, that was monitored by optical and ESR spectroscopy. Interestingly, the modification of electron delocalization and magnetic coupling was observed when the charged species were generated and the changes have been rationalized by theoretical calculations. This system behaves as a molecular switch in which an electrical input can tune their physical properties in a reversible way (see Publication #2).

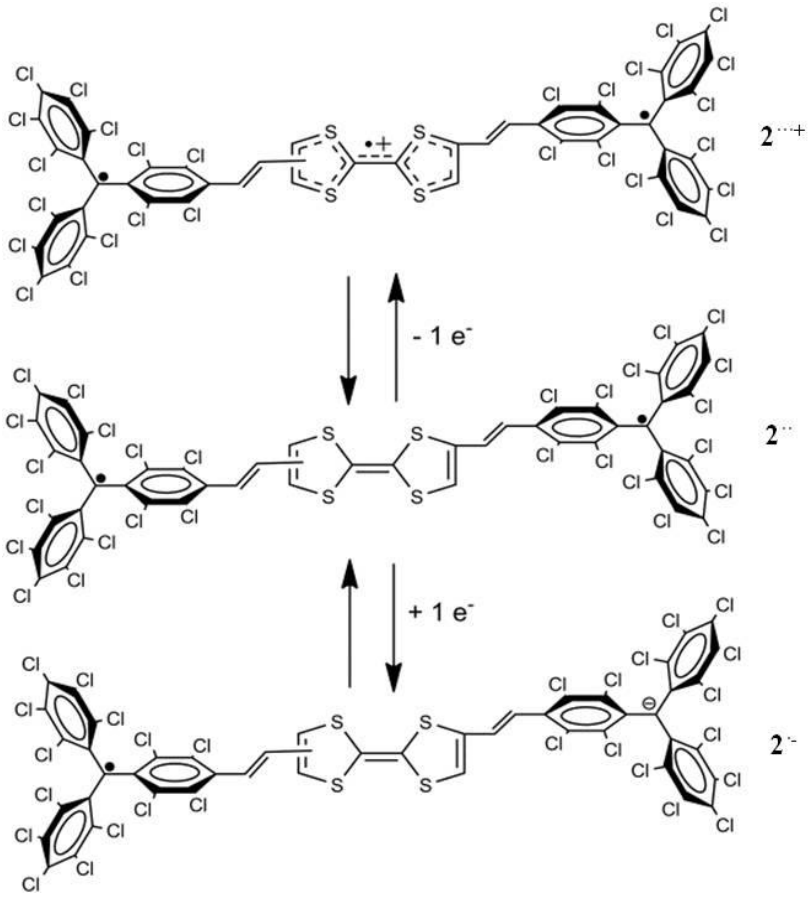

Figure 2.14. Molecular structures of diradical **2**, mixed-valence $\mathbf{2}^{\bullet -}$ and triradical cation $\mathbf{2}^{\bullet\bullet +}$.

Regarding the optical properties, UV-vis-NIR spectrum of diradical $\mathbf{2}^{\cdot\cdot}$ was obtained in CH_2Cl_2 at 300 K (Figure 2.15) showing an intense band at 385 nm, characteristic of PTM radical chromophores, and shoulders around 420 and 540 nm which are attributed to the electronic conjugation of the unpaired electron into the π-framework. Regarding the low-energy spectral region, the weak broad band that appears around 900 nm is assigned to the intramolecular charge transfer process from the electron-donor TTF bridge to the two electron-acceptor PTM radical subunits. On the other hand, the mixed-valence species $\mathbf{2}^{\cdot-}$ showed the decreasing of the band at 385 nm, characteristic of the PTM radical chromophore, and the appearance of two new intense bands at 520 and 604 nm attributed to the PTM anion chromophore. Finally, triradical cation $\mathbf{2}^{\cdot\cdot\cdot+}$ showed a decreasing in intensity of the shoulders at 420 and 540 nm and the appearance of two new bands at 550 and 690 nm associated with the formation of $TTF^{\cdot+}$ species.

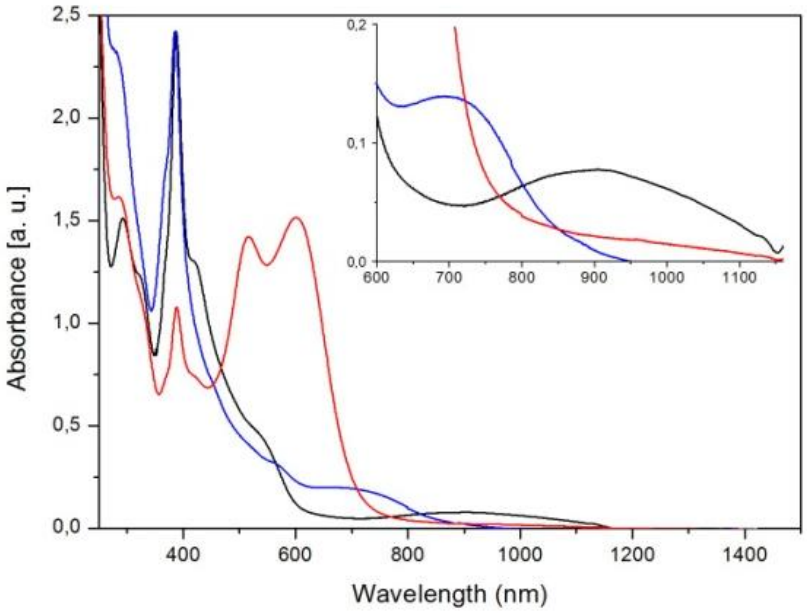

Figure 2.15. UV-Vis-NIR spectra of a solution 0.05 mM of diradical $\mathbf{2}^{\cdot\cdot}$ (black line), mixed-valence species $\mathbf{2}^{\cdot-}$ (red line) and triradical cation $\mathbf{2}^{\cdot\cdot\cdot+}$ (blue line) in CH_2Cl_2. Inset shows the low-energy range of the absorption spectra.

Regarding the magnetic properties, ESR experiments of the three species can give us information about the electron delocalization in the system (Figure 2.16). Interestingly, the presence of three symmetrical lines in the ESR spectrum of $\mathbf{2}^{\cdot\cdot}$ indicates that the magnetic interaction of the two electrons of the PTM radicals have a magnetic exchange coupling constant, *J,* that fulfils the condition $|J| >> |a_i|$, as it has been already observed for other PTM diradicals.[56,57] On the other hand, only two lines were observed for $\mathbf{2}^{\cdot-}$ and $\mathbf{2}^{\cdot\cdot\cdot+}$ indicating that the unpaired electrons on the PTM units remains localized. In the case of $\mathbf{2}^{\cdot\cdot\cdot+}$, the 5-lines signals are attributed to the coupling of the unpaired electron of the $TTF^{\cdot+}$ moiety with four protons and appear separated from the PTM lines indicating that electrons at the two terminal PTM radical subunits remain localized at the ESR time scale.

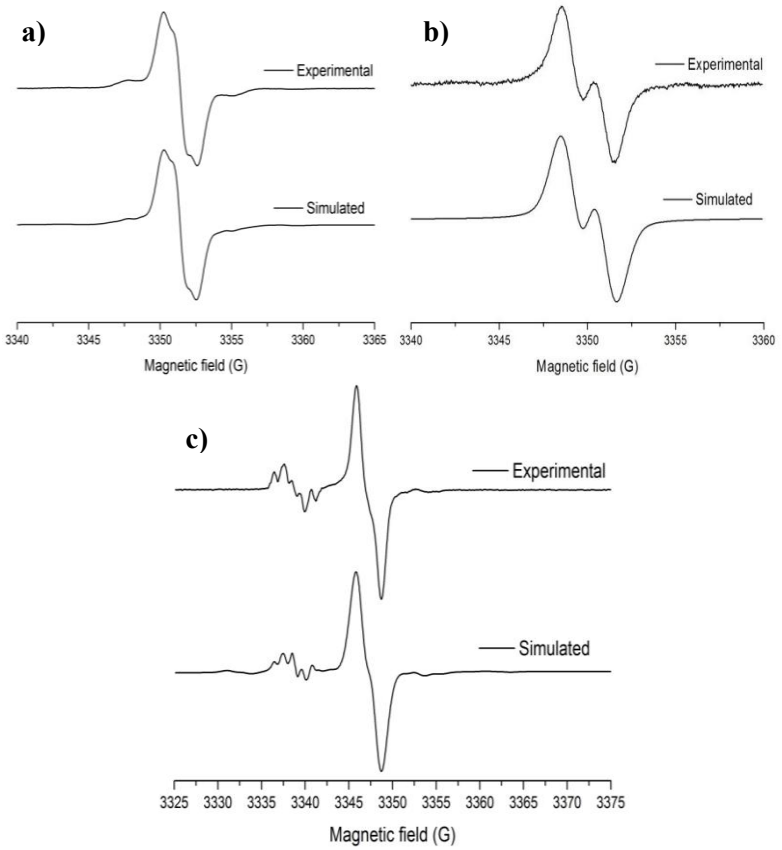

Figure 2.16. Experimental and simulated ESR spectra of 0.05 mM solution of a) diradical **2**$^{\bullet\bullet}$, b) mixed-valence species **2**$^{\bullet-}$ and c) triradical cation **2**$^{\bullet\bullet\bullet+}$ in CH_2Cl_2 at 240 K.

In order to demonstrate the reversibility of the system, we have carried out electrochemical redox reactions starting from **2**$^{\bullet\bullet}$ that is oxidized to **2**$^{\bullet\bullet\bullet+}$, then reduced to **2**$^{\bullet-}$ and oxidized back to the diradical species using CH_2Cl_2 with [(n-Bu)$_4$N] PF_6 (0.1 M) as supporting electrolyte, Pt wire as a working electrode, and Ag/Ag+ as the reference electrode (Figure 2.17). We performed several cycles and the electrochemical oxidation and reduction processes were monitored by UV-vis spectroscopy at the wavelength of 650 nm showing that the absorbance intensity is completely recovered after each step demonstrating the high reversibility and stability of the resulted species.

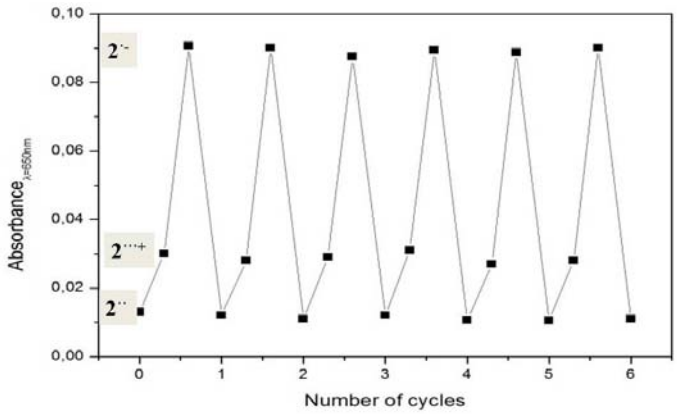

Figure 2.17. Evolution of the UV-Vis intensity at 650 nm recorded during the stepwise oxidation and reduction cycles of **2**$^{\bullet\bullet}$.

2.3. Summary

In this Chapter, two different organic radical compounds acting as molecular switches in solution have been presented. Both systems are formed using the electron-acceptor PTM radical and the electron-donor TTF moieties connected through different linkers. These two molecular systems can exhibit bistability or even tristability through the application of external stimuli such as temperature or electric field.

The first example consists on a D-A system formed by a PTM radical unit connected to a TTF unit through a vinylene bridge (**1**). This compound exhibited bistability in solution through an IET process that was driven by the change in solvent polarity. Specifically, it was observed that the zwitterionic state of this dyad, stabilized in polar solvents such DMF, induced the dimerization of the TTF subunits forming diamagnetic dimers of the zwitterions at room temperature. This study is detailed in **Publication #1** where the reversible temperature-induced switching between diamagnetic dimers $\mathbf{[1]_{2\ LT}}$, observed at room temperature, and paramagnetic monomers $\mathbf{1_{HT}}$ at high temperature was investigated. Different optical and magnetic properties were observed for the two different states of this supramolecular switch when using the temperature as external input. Temperature-dependent UV-vis-NIR, ESR, ^{1}H-NMR, Raman and CV experiments were performed in order to study the change on these optical, magnetic and supramolecular properties of the two states. Moreover, a theoretical model was proposed to rationalize in a proper way this interesting phenomenon. In summary, a new molecular reversible switch based on a TTF-PTM radical dyad that exhibited changes in its optical, magnetic, and supramolecular properties when using temperature as an external input was reported. Such changes are due to the subtle interplay of intra- and intermolecular CT processes occurring between the subunits of the involved species.

On the other hand, the second example of molecular switch is reported in **Publication #2** and consists on an A-D-A diradical triad ($\mathbf{2^{\cdot\cdot}}$), composed by two PTM radical subunits connected through a TTF-vinylene bridge. This system can modulate the optical, electronic and magnetic properties by one-electron reduction and oxidation processes in a reversible way. Interestingly, the suppression of the electron delocalization was observed when passing from the diradical $\mathbf{2^{\cdot\cdot}}$ to the anion radical mixed-valence $\mathbf{2^{\cdot-}}$ species indicating the preferable localization of the unpaired electron on only one of the two PTM radical moieties. On the other hand, the switching from an almost negligible ferromagnetic (FM) magnetic interaction to a moderate-strong antiferromagnetic (AFM) interaction between TTF and PTM moieties was observed when the TTF bridge was oxidized in $\mathbf{2^{\cdot\cdot\cdot+}}$ triradical cation. Finally, the system was found to be highly reversible and can be proposed as a promising building block for the development of molecular switches.

2.4. References

1. Poneti, G. *et al.* Soft-X-ray-induced redox isomerism in a cobalt dioxolene complex. *Angew. Chemie - Int. Ed.* **49,** 1954–1957 (2010).

2. Wang, Y. *et al.* Dynamic Behavior of Molecular Switches in Crystal under Pressure and Its Reflection on Tactile Sensing. *J. Am. Chem. Soc.* **137,** 931–939 (2015).

3. Bléger, D. & Hecht, S. Visible-Light-Activated Molecular Switches. *Angew. Chem. Int. Ed. Engl.* 2–14 (2015).

4. Droghetti, a. & Sanvito, S. Electric field control of valence tautomeric interconversion in cobalt dioxolene. *Phys. Rev. Lett.* **107,** 2–5 (2011).

5. Feringa, L.; Browne, W. R. *Molecular Switches*. (Wiley, 2011).

6. Zhang, J. L. *et al.* Towards single molecule switches. *Chem. Soc. Rev.* **44,** 2998–3022 (2015).

7. Kahn, O. & Launay, J. P. Molecular bistability; an overview. *Chemtronics* **3,** 140–151 (1988).

8. Halcrow, M. A. *Spin-Crossover Materials: Properties and Applications*. (Wiley, 2013).

9. Ohkoshi, S.-I., Imoto, K., Tsunobuchi, Y., Takano, S. & Tokoro, H. Light-induced spin-crossover magnet. *Nat. Chem.* **3,** 564–569 (2011).

10. Bousseksou, A., Molnár, G., Salmon, L. & Nicolazzi, W. Molecular spin crossover phenomenon: recent achievements and prospects. *Chem. Soc. Rev.* **40,** 3313–3335 (2011).

11. Schweinfurth, D. *et al.* Spin crossover in Fe(II) and Co(II) complexes with the same click-derived tripodal ligand. *Inorg. Chem.* **53,** 8203–12 (2014).

12. Sato, O., Tao, J. & Zhang, Y.-Z. Z. Control of magnetic properties through external stimuli. *Angew. Chemie - Int. Ed.* **46,** 2152–2187 (2007).

13. Poneti, G. *et al.* Magnetic and spectroscopic investigation of thermally and optically driven valence tautomerism in thioether-bridged dinuclear cobalt-dioxolene complexes. *Inorg. Chem.* **52,** 11798–11805 (2013).

14. Li, B., Chen, L. Q., Tao, J., Huang, R. Bin & Zheng, L. S. Unidirectional charge transfer in Di-cobalt valence tautomeric compound finely tuned by ancillary ligand. *Inorg. Chem.* **52,** 4136–4138 (2013).

15. Buchanan, R. M. & Pierpont, C. G. Tautomeric catecholate-semiquinone interconversion via metal-ligand electron transfer. Structural, spectral, and magnetic properties of (3, 5-di-tert-butylcatecholato). *J. Am. Chem. Soc.* **102,** 4951–4957 (1980).

16. Heckmann, A. & Lambert, C. Organic mixed-valence compounds: A playground for electrons and holes. *Angew. Chemie - Int. Ed.* **51,** 326–392 (2012).

17. Hankache, J. & Wenger, O. S. Organic mixed valence. *Chem. Rev.* **111,** 5138–5178 (2011).

18. Robin, M. B. & Day, P. Mixed Valence Chemistry-A Survey and Classification. *Adv. Inorg. Chem. Rad.* **10,** 247–422 (1967).

19. Small, D. *et al.* Intermolecular π-to-π bonding between stacked aromatic dyads. Experimental and theoretical binding energies and near-IR optical transitions for phenalenyl radical/radical versus radical/cation dimerizations. *J. Am. Chem. Soc.* **126,** 13850–13858 (2004).

20. Morita, Y. *et al.* Thermochromism in an organic crystal based on the coexistence of sigma- and pi-dimers. *Nat. Mater.* **7,** 48–51 (2008).

21. Morita, Y., Suzuki, S., Sato, K. & Takui, T. Synthetic organic spin chemistry for structurally well-defined open-shell graphene fragments. *Nat. Chem.* **3,** 197–204 (2011).

22. Hicks, R. G. Switchable materials: A new spin on bistability. *Nat. Chem.* **3,** 189–191 (2011).

23. Itkis, M. E., Chi, X., Cordes, A. W. & Haddon, R. C. Magneto-Opto-Electronic Bistability in a Phenalenyl-Based Neutral Radical. *Science* **296,** 1443–1445 (2002).

24. Pal, S. K. *et al.* Hysteretic spin and charge delocalization in a phenalenyl-based molecular conductor. *J. Am. Chem. Soc.* **132,** 17258–17264 (2010).

25. Rawson, J. M. & Palacio, F. Magnetic Properties of Thiazyl Radicals. *Structure* **100,** 94–108 (2001).

26. Brusso, J. L. *et al.* Bistabilities in 1, 3, 2-Dithiazolyl Radicals. *J. Am. Chem. Soc.* **126,** 8256–8265 (2004).

27. Díaz, M. C. *et al.* Highly Conjugated p-Quinonoid π-Extended Tetrathiafulvalene Derivatives: A Class of Highly Distorted Electron Donors. *Chem. - A Eur. J.* **10,** 2067–2077 (2004).

28. Bryce, M. R. Functionalised tetrathiafulvalenes: new applications as versatile π-electron systems in materials chemistry. *J. Mater. Chem.* **10,** 589–598 (2000).

29. Segura, J. L. & Martín, N. New concepts in tetrathiafulvalene chemistry. *Angew. Chemie - Int. Ed.* **40,** 1372–1409 (2001).

30. Yamada, J. *TTF Chemistry: Fundamentals and Applications of Tetrathiafulvalene*. (Springer, 2004).

31. Batail, P. Introduction: Molecular conductors. *Chem. Rev.* **104,** 4887–4890 (2004).

32. Canevet, D., Sallé, M., Zhang, G., Zhang, D. & Zhu, D. Tetrathiafulvalene (TTF) derivatives: key building-blocks for switchable processes. *Chem. Commun.* **7345,** 2245–2269 (2009).

33. Feng, M. *et al.* Stable, reproducible nanorecording on rotaxane thin films. *J. Am. Chem. Soc.* **127,** 15338–9 (2005).

34. Yoon, I., Miljanic, O. S., Benitez, D., Khan, S. I. & Stoddart, J. F. An interdigitated functionally rigid [2]rotaxane. *Chem Commun* 4561–4563 (2008).

35. Spruell, J. M. *et al.* Highly stable tetrathiafulvalene radical dimers in [3]catenanes. *Nat. Chem.* **2,** 870–879 (2010).

36. Coskun, A. *et al.* Mechanically stabilized tetrathiafulvalene radical dimers. *J. Am. Chem. Soc.* **133,** 4538–4547 (2011).

37. Rosokha, S. V. & Kochi, J. K. Molecular and electronic structures of the long-bonded π-dimers of tetrathiafulvalene cation-radical in intermolecular electron transfer and in (solid-state) conductivity. *J. Am. Chem. Soc.* **129,** 828–838 (2007).

38. Ziganshina, A. Y., Ko, Y. H., Jeon, W. S. & Kim, K. Stable π-dimer of a tetrathiafulvalene cation radical encapsulated in the cavity of cucurbit [8] uril. 806–807 (2004).

39. Yoshizawa, M., Kumazawa, K. & Fujita, M. Room-temperature and solution-state observation of the mixed-valence cation radical dimer of tetrathiafulvalene, $[(TTF)_2]^{+\cdot}$, within a self-assembled cage. *J. Am. Chem. Soc.* **127,** 13456–13457 (2005).

40. Chiang, P. T., Chen, N. C., Lai, C. C. & Chiu, S. H. Direct observation of mixed-valence and radical cation dimer states of tetrathiafulvalene in solution at room temperature: association and dissociation of molecular clip dimers under oxidative control. *Chem. A Eur. J.* **14,** 6546–6552 (2008).

41. Khodorkovsky, V. *et al.* Do π-dimers of tetrathiafulvalene cation radicals really exist at room temperature? *Chem. Commun.* 2736–2737 (2001).

42. Hasegawa, M., Da, K. & Hash, K. Face-to-Face Dimeric Tetrathiafulvalenes and Their Cation Radical and Dication Species as Models of Mixed Valence and Dimer States. *Bull. Chem. Soc. Jpn.* **85,** 51–60 (2012).

43. Fumanal, M., Capdevila-Cortada, M., Miller, J. S. & Novoa, J. J. Keys for the existence of stable dimers of bis-tetrathiafulvalene (bis-TTF)-functionalized molecular clips presenting $[TTF]^{\bullet+}\cdots[TTF]^{\bullet+}$ long, multicenter bonds at room temperature. *J. Am. Chem. Soc.* **135,** 13814–13826 (2013).

44. Elsner, O., Ruiz-Molina, D., Vidal-Gancedo, J., Rovira, C. & Veciana, J. Ferromagnetic interactions between triphenylmethyl radicals through an organometallic coupler. *Chem. Commun.* 579–580 (1999).

45. Elsner, O. *et al.* Ferrocene as a ferromagnetic coupler. Synthesis and characterization of a ferrocene bridged polychlorotriphenylmethyl diradical. *J. Organomet. Chem.* **637,** 251–257 (2001).

46. Ito, A., Nakano, Y., Urabe, M., Kato, T. & Tanaka, K. Triradical cation of p-phenylenediamine having two nitroxide radical groups: spin alignment mediated by delocalized spin. *J. Am. Chem. Soc.* **128,** 2948–53 (2006).

47. Gautier, N., Dumur, F., Lloveras, V., Vidal-Gancedo, J., Veciana, J., Rovira, C. & Hudhomme, P. Intramolecular Electron Transfer Mediated by a Tetrathiafulvalene Bridge in a Purely Organic Mixed-Valence System. *Angew. Chemie* **115,** 2871–2874 (2003).

48. Dumur, F. *et al.* Novel Fused D-A Dyad and A-D-A Triad Incorporating Tetrathiafulvalene and p-Benzoquinone. *J. Org. Chem.* **69,** 2164–2177 (2004).

49. Otón, F. *et al.* Coupling tetracyanoquinodimethane to tetrathiafulvalene: A fused TCNQ-TTF-TCNQ triad. *Angew. Chemie - Int. Ed.* **50,** 10902–10906 (2011).

50. Calbo, J. *et al.* Tetrathiafulvalene-based mixed-valence acceptor-donor-acceptor triads: A joint theoretical and experimental approach. *Chem. - A Eur. J.* **19,** 16656–16664 (2013).

51. Chu, C. W., Ouyang, J., Tseng, J. H. & Yang, Y. Organic donor-acceptor system exhibiting electrical bistability for use in memory devices. *Adv. Mater.* **17,** 1440–1443 (2005).

52. Ratera, I. *et al.* A new valence tautomerism example in an electroactive ferrocene substituted triphenylmethyl radical. *J. Am. Chem. Soc.* **125,** 1462–1463 (2003).

53. Ratera, I. *et al.* Solvent tuning from normal to inverted marcus region of intramolecular electron transfer in ferrocene-based organic radicals. *J. Am. Chem. Soc.* **129,** 6117–6129 (2007).

54. D'Avino, G. *et al.* Bistability in Fc-PTM crystals: The role of intermodular electrostatic interactions. *J. Am. Chem. Soc.* **130,** 12064–12072 (2008).

55. Grisanti, L. *et al.* Essential state models for solvatochromism in donor-acceptor molecules: The role of the Bridge. *J. Phys. Chem. B* **113,** 4718–4725 (2009).

56. Guasch, J. *et al.* Bistability of Fc-PTM-Based dyads: The role of the donor strength. *Chem. Mater.* **25,** 808–814 (2013).

57. Souto, M. *et al.* Intramolecular electron transfer and charge delocalization in bistable donor-acceptor systems based on perchlorotriphenylmethyl radicals linked to ferrocene and tetrathiafulvalene units. *J. Phys. Org. Chem.* **27,** 465–469 (2014).

58. Bergkamp, J. J., Decurtins, S. & Liu, S.-X. Current advances in fused tetrathiafulvalene donor-acceptor systems. *Chem. Soc. Rev.* **44,** 863–874 (2015).

59. Shinsuke Nishida, Y. M. K. F. K. S. D. S. T. T. K. N. Spin Transfer and Solvato-/Thermochromism Induced by Intramolecular Electron Transfer in a Purely Organic Open-Shell System. *Angew. Chemie Int. Ed.* **44,** 7277–7280 (2005).

60. Guasch, J. *et al.* Induced self-assembly of a tetrathiafulvalene-based open-shell dyad through intramolecular electron transfer. *Angew. Chemie - Int. Ed.* **51,** 11024–11028 (2012).

61. Guasch, J. *et al.* Intra- and Inter-Molecular Charge-Transfer in Aggregates of Tetrathiafulvalene - Triphenylmethyl Radical Derivatives in Solution. *J Am Chem Soc* **135,** 6958–6967 (2013).

62. Souto, M. *et al.* Thermomagnetic molecular system based on TTF-PTM radical: Switching the spin and charge delocalization. *J. Phys. Chem. Lett.* **4,** 2721–2726 (2013).

Publication #1

Title: Thermomagnetic Molecular Switch based on TTF-PTM Radical: Switching the Spin and Charge Delocalization

Authors: an uel o uto, udith Guasch, e a loveras, au la ay or a, uan . pe avarrete, Juan Casado, Imma Ratera, Concepció Rovira, Anna Painelli, and Jaume Veciana

Publication: *J. Phys. Chem. Lett.* 2013, 4, 2721−2726

Thermomagnetic Molecular System Based on TTF-PTM Radical: Switching the Spin and Charge Delocalization

Manuel Souto,[†] Judith Guasch,[†,⊥] Vega Lloveras,[†] Paula Mayorga,[‡] Juan T. López Navarrete,[‡] Juan Casado, [‡] Imma Ratera,[†,*] Concepció Rovira,[†] Anna Painelli,[§] and Jaume Veciana[†,*]

[†] Institut de Ciència de Materials de Barcelona (ICMAB-CSIC)/CIBER-BBN, Campus Universitari de Bellaterra, 08193 Cerdanyola del Vallès (Barcelona), Spain

[‡] Departamento de Química Física, Universidad de Málaga, 29071-Málaga, Spain.

[§] Dipartimento Chimica, GIAF, Parma University/INSTM-UdR, I-4310 Parma, Italy

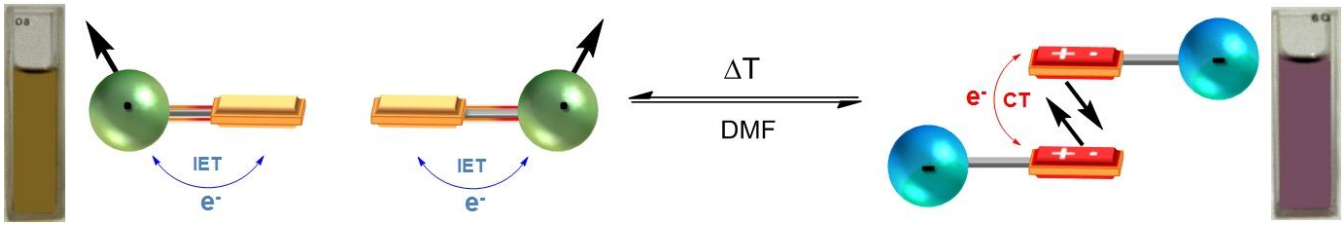

ABSTRACT: The electron donor-acceptor dyad 1, based on a polychlorotriphenylmethyl radical subunit linked to a tetrathiafulvalene moiety, shows in DMF solution a reversible temperature-induced switching between diamagnetic dimers, observed at room temperature, and paramagnetic monomers at high temperature. Different optical and magnetic properties are observed for the two states of this supramolecular switch, related to the subtle interplay between intramolecular electron transfer and intermolecular charge transfer processes.

SECTION: Bistability, tetrathiafulvalene, intramolecular charge-transfer, and Raman spectroscopy

Molecules that can be switched between two or more states through the application of an external stimulus (for example, temperature, pressure or light) have attracted a great deal of attention for their possible application in information technology.[1-10] In particular, paramagnetic transition metal compounds showing molecular bistability, such as spin-crossover and valence tautomeric systems, have been widely investigated.[2] Magnetic bistability has been discussed either for bulk materials or for isolated molecules. In the latter case, bistability is only observed at very low temperatures: examples of magnetic bistability in isolated molecules at technologically relevant temperatures[11-12] are still missing.

Paramagnetic organic molecules (radicals) have received less attention in the context of bistability, possibly due to their high reactivity. However, few stable radicals are known that show a reversible dimerization in response to external stimuli, with monomers and dimers coexisting at the equilibrium in solution.[4] Spirobiphenalenyl and thiazyl radicals are good examples of such materials.[13-21] The ability of tetrathiafulvalene (TTF) cations to readily self-assemble in columnar structures is of great interest for the bottom-up building of supramolecular structures.[22-24] A large number of studies are available on the self-assembly of TTF molecules in the solid state, but solution studies are hindered by the weakness of non-covalent interactions. Several studies report the formation of diamagnetic [$TTF^{+\cdot}\cdots TTF^{+\cdot}$] and mixed valence [$TTF^{+\cdot}\cdots TTF$] dimers generated by chemical oxidation[25-36] of TTF solutions, but very few examples are known of systems where TTF-dimerization is activated by an intramolecular electron transfer (IET) on neutral TTF derivatives. Recently, it has been reported that the electron donor-acceptor (DA) dyad **1**, based on a TTF electron π-donor connected to the polychlorotriphenylmethyl (PTM) radical, exhibits a reversible switching between a neutral and a zwiterionic state. The switching, occurring through an IET process, is driven by a change in solvent polarity.[37-38] Specifically, it has been observed that the zwitterionic state, stabilized in polar solvents, like DMF, drives the dimerization of the TTF subunits at room temperature.

In this paper, we study the reversible switching of dyad **1** induced in polar solvents by temperature changes. Indeed, dyad **1** exists in DMF solution at room temperature in the form of diamagnetic dimers $\mathbf{[1]_{2\,LT}}$ but upon increasing temperature the dimers dissociate into paramagnetic monomers $\mathbf{1_{HT}}$ (Scheme 1). To the best of our knowledge, this is the first time that a TTF-based radical exhibits a temperature-controlled switchable supramolecular architecture. Understanding this phenomenon is of fundamental interest for the design of new supramolecular switches and logic gates as well as for the comprehension of spin operative molecular technologies.

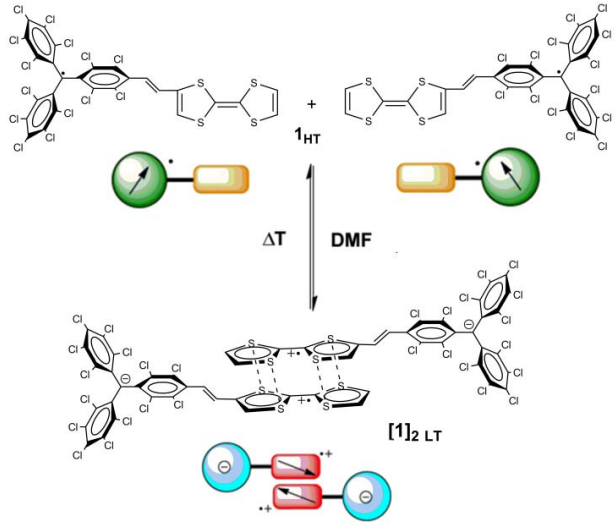

Scheme 1. Reversible temperature-induced supramolecular switching of **1** in DMF solution.

UV-Vis spectra of dyad **1** in DMF were obtained at different temperatures in the 300-375 K range (Figure 1). At 300 K the spectrum exhibits an intense band at 512 nm with a shoulder at 605 nm assigned to the PTM subunit in its anionic form indicating that **1** is only present in the zwitterionic D^+A^- state. The lack of ESR signal in these conditions (see below and ref. 31) suggests the quantitative formation of diamagnetic dimers.[38] When the solution is heated the band associated to the PTM anion weakens whereas the band related to the PTM neutral radical (387 nm) acquires intensity together with the appearance of a weak band at 950 nm that is most probably associated to the IET process of **1** in the neutral DA form. Two isosbestic points are observed. These spectral changes suggest that the $\mathbf{[1]_{2\ LT}}$ dimers observed at low temperature in DMF break down upon increasing temperature into paramagnetic monomers $\mathbf{1_{HT}}$ corresponding to the neutral form of dyad **1**.

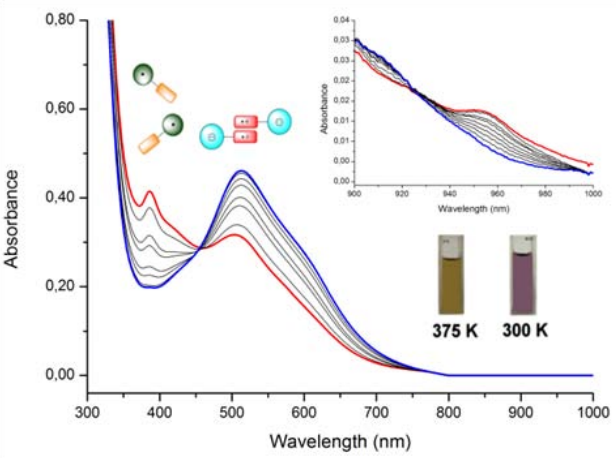

Figure 1. UV-Vis spectra of dyad **1** in DMF (0.1 mM) at 375 (red line), 365, 355, 350, 345, 340, 330, 320 and 300 K (blue line). Inset: Low-energy range of the absorption spectra and colour changes at 375 K and 300 K.

Upon cooling the solution from 375 K to room temperature the band associated to the zwitterionic form increases again whereas the band assigned to the PTM radical subunit disappears in a fully reversible process (see SI). Interestingly, dyad **1** in DMF exhibits marked thermochromism as shown in the inset of Figure 1 by the variation of the colour of solutions at different temperature. While the spectra in Figure 1 nicely support the presence of a monomer-dimer equilibrium, with the monomer species favoured at high temperature (as expected on physical basis), a quantitative estimate of relevant equilibrium constants is hindered by the superposition of the monomer and dimer bands with the intense tail of absorption bands located for TTF and PTM species in the UV region.

Variable temperature ESR experiments give independent information on the monomer-dimer equilibrium and the magnetic properties of the two involved species (Figure 2). The strong antiferromagnetic coupling of TTF-radical spins in the $\mathbf{[1]_{2\ LT}}$ dimers is responsible for the lack of ESR signal at room temperature, supporting the quantitative formation of dimers.[37-38] By contrast, heating the solution at 375 K, a broad line appears at a *g*-value of 2.0025, typical of PTM radicals, indicating the formation of a paramagnetic species that we identify as the $\mathbf{1_{HT}}$ monomer in the neutral DA form, to justify the ESR signal associated with the PTM radical. Cooling down the solution to room temperature, it gradually becomes ESR silent again, exhibiting a completely reversible behaviour from 375 K to 300 K. The signal is flat at room temperature, in line with a fully dimerized system and increases with T, never reaching however the saturation. Figure S7 shows the T-dependence of the doubly-integrated ESR signal (proportional to the monomer concentration) in the relevant region: a sizable fraction of dimers survives even at the highest experimentally accessible temperature. This result, in line with data in Figure 1 showing a sizable signal due to the zwitterionic species also at the highest temperature, hinders the reliable estimate of equilibrium constants for the monomer-dimer equilibrium. However, the quantitative dimerization supported at room temperature by ESR data, suggest a dimerization tendency for **1** much larger than that typically observed for TTF and its cation.

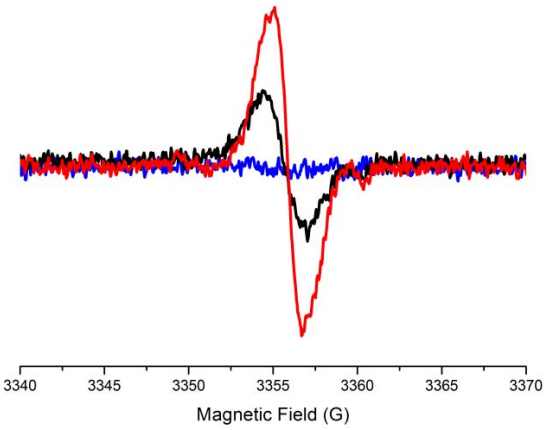

Figure 2. ESR spectra of **1** in DMF (0.1 mM) at 375 (red line), 365 (black line) and 300 (blue line) K.

To demonstrate the complete reversibility of the system, several ESR cycles at 300 and 375 K were performed without showing any sign of deterioration (Figure 3 and S9). Moreover, consecutive switching UV-Vis cycles at the same temperatures were also performed corroborating optically the reversible thermochromism of the dimerization process (Figure S8).

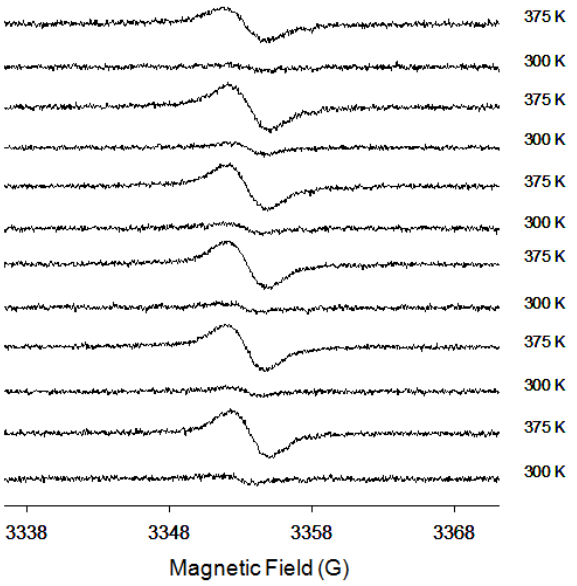

Figure 3. ESR spectra of dyad **1** (0.1 mM) in DMF during switching cycles at 300 and 375 K.

The temperature-induced dimerization of **1** in DMF is also confirmed by cyclic voltammetry (See Figure S4 and Table S1). The first oxidation potential of the TTF subunit in fact splits in two waves at 300 K suggesting that TTF moieties are in sufficiently close proximity to each other forming dimers.[30, 38-41] Increasing the temperature at 375 K this splitting is not observed.

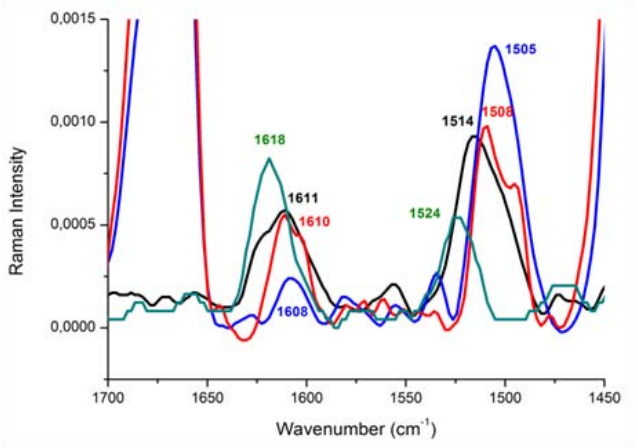

Figure 4. Raman spectra of **1-H** (0.1 M) in CH_2Cl_2 (green line) and **1** (0.1 M) in CH_2Cl_2 (black line) and in DMF at 300 K (blue line) and at 375 K (red line).

Several dimerization studies have been reported with infrared spectroscopy, [42] however, infrared studies are strongly conditioned by the infrared absorption bands of the solvent that make large spectral regions spectroscopically inaccessible. Raman spectroscopy can circumvent this problem. Although it can be used as a direct probe of dimerization in solid state,[43] in solution it offers reliable information about the impact on the molecular structure of the charge redistribution concomitant with the dimerization process.[44] Raman spectra of dyad **1** were obtained at different temperatures (300 and 375 K) in a low-polarity solvent, CH_2Cl_2, and in a strongly polar solvent, DMF. For reference, Figure 4 also shows the spectra collected for solutions of the protonated TTF-PTM derivative **1-H**. In general, Raman spectra of π-conjugated molecules show intense bands associated with vibrations strongly involved in the π-conjugation path, in our case the vinylene and TTF C=C stretches in the 1610 cm^{-1} and 1500-1525 cm^{-1} regions, respectively.[45] The similarity between frequencies and relative intensities of the spectra collected for **1** in CH_2Cl_2 at 300 K (black line) and in DMF at 375 K (red line) suggests that the same species are present in both cases, corresponding to the neutral dyad **1**. This assignment, in line with previous discussion, is also supported by Raman spectra collected for solutions of **1-H** in CH_2Cl_2 (green line). In **1-H** the IET is suppressed since the protonated PTM subunit is not a good electron-acceptor and the charge distribution on the TTF subunit in **1-H** is expected to be more similar to that of dyad **1** in its neutral form than to the zwitterionic dimer. As we have discussed above the dimeric species are very stable in DMF and they are only partly dissociated even at the highest temperature achieved. As a result, and in close similarity with UV-Vis spectra in Fig. 1, spectra in Fig. 4 collected at 375 K in DMF are the superposition of contributions of a fraction of the dimer of zwitterions together with another of dissociated neutral dyad. A large redistribution of intensities in the investigated spectral region, supports this view. In particular, the 1608 cm^{-1} band of the vinylene stretch decreases its intensity whereas that at 1505 cm^{-1} of the TTF unit in the spectrum of **1** in DMF at 300 K increases.[45-47] The comparison with spectra of **1** and its oxidized form, **1-H**$^+$ (solid state, Figure S5) suggests that this intensity redistribution is related to an increased concentration of neutral dyads in DMF solution upon increasing temperature. This increase of the relative intensity of the TTF Raman peak and the decrease in intensity of the C=C stretching Raman band is an indication of a preferential electron delocalization between the two TTF units, due to the dimer formation and inter-unit [$(TTF)_2^{2+}$] intermolecular (through space) charge delocalization. Simultaneously, the formation of the dimeric zwitterionic species limits intramolecular charge delocalization through the vinylene bridge which explains the rather small intensity of its stretching mode. This situation is progressively inverted when dimerization is suppressed.

^{1}H-NMR spectra of the dyad **1** and its protonated derivative **1-H** at different temperatures in DMF-d_7 were obtained to study the electronic structure of the dimers (see Figure S6). Data support the existence of a temperature-induced switching process (see SI). Indeed, the doublet signal attributed to the proton of the vinylene bridge closer to the TTF subunit in **1-H** (6.46 ppm, H_C) is shifted downfield (7.23 ppm) in dyad **1** due to the increased electron-withdrawing effect of the PTM radical unit. The doublet assigned to the other vinylene proton in **1-H** (7.26 ppm, H_B) is slightly shifted in **1** (7.28 ppm). The clearest evidence of the breaking of TTF π-dimers is the emergence of a signal at 6.75-6.80 ppm with the increasing of temperature, attributed to the two external protons of the TTF in the monomeric state (H_E) which are also present in **1-H**. On the other hand, at 370 and 375 K the compound exhibits ^{1}H-NMR unusual signal shifts and broadenings due to the presence in the media of paramagnetic radical species.

The interplay between intramolecular ET and intermolecular CT leads to a complex behaviour of dyad **1** in strongly polar solvents, where at room temperature dimers of the zwitterionic form of **1** are quantitatively formed. Upon increasing temperature the dimer dissociates releasing isolated **1**-dyads in the neutral form. To rationalize this complex behaviour we make resort to a model developed in Ref. 38, based on the detailed analysis of TTF-PTM based systems, and extended here to account for solvation effects.

The model combines the Hubbard model description of TTF-based dimers[48] with essential state models relevant to DA dyads.[49-51] Basically each DA dyad is described as a two-site system bearing 3 electrons overall. The electrons are delocalized on the two D and A sites, and more precisely over the HOMO of the D site and LUMO of the A site. The dimer then has 4 sites and 6 electrons.[37] Based on chemical intuition, we assign a large energy to states bearing positively charged PTM units. This not only reduces the number of relevant states, but also (and more importantly) reduces the number of relevant model parameters to only 4. Two of these four parameters, t and U, are the parameters of the Hubbard model relevant to the intermolecular CT, while the other two parameters, $2z$ and τ, fully define the two essential-state model relevant to dyad **1**. To account for polar solvation, in line with the standard treatment of DA dyads,[52-55] the Hamiltonian for each dyad acquires a new term accounting for the interaction of the molecular dipole moment, μ, with the solvent reaction field (F). The solvent polarity is then described in terms of a single additional parameter, the solvent relaxation energy, ε_{or}, that vanishes in non-polar solvents and increases with solvent polarity (more details can be found in the Supporting Information). Accordingly, Figure 5 shows the evolution of the ground state (black lines) and of the lowest triplet state (red lines) calculated as a function of the reaction field for a monomer $\mathbf{1}_{HT}$ species (left panels) and a dimer $\mathbf{[1]}_{2\ LT}$ (right panels). Top and bottom panels refer to a low polarity solvent (like CH_2Cl_2) and a strongly polar solvent (DMF), respectively. In both cases the dimer energy is lower than the monomer energy, but of course we cannot discuss the relative stability of the dimer *vs* the monomeric species because in our model we only account for the charge transfer interaction, while steric and Van der Waals interactions (among others) also affect the dimerization energy. Nevertheless, our results clearly demonstrate that in low polarity solvents both the monomer and the dimer are in a neutral state (the calculated charge on the PTM moiety is 0 in the monomer, slightly increasing to -0.34 in the dimer). Quite interestingly, for the dimer in low polarity solvents the calculated singlet-triplet gap is smaller than thermal energy, suggesting uncorrelated spins on the two PTM moieties and a sizable ESR signal in agreement with the experiments and with the dissociative character of the dimer in this media.[37] In the polar solvent (bottom panels) the monomer has a bistable behaviour, with two minima: the lowest energy minimum corresponds to a neutral state and is separated by a large energy gap from the zwitterionic state, so that only neutral monomers are observed in solution. Dimeric species instead are only stable as dimers of zwitterions, with the PTM moiety bearing a -0.9 charge. In this case the singlet triplet gap is much larger than the thermal energy, suggesting totally silent dimers in strongly polar solvents.

The model for the IET-ICT interplay proposed in Ref. 38 and extended to account for the effect of polar solvation, is fully in line with experimental observations. Indeed, in low-polarity solvents only largely neutral species are expected, either monomers in a doublet states, or dimers with basically uncorrelated spins. In either case ESR signal from unpaired electrons located on the PTM moiety is expected. On the contrary, in polar solvents at room temperature only ESR-silent dimers are expected, corresponding to dimers of zwitterions. Upon increasing the temperature, dimers are destabilized and monomers appear in solution, corresponding to neutral dyads **1**, with the unpaired spin on the PTM moiety contributing to ESR signal.

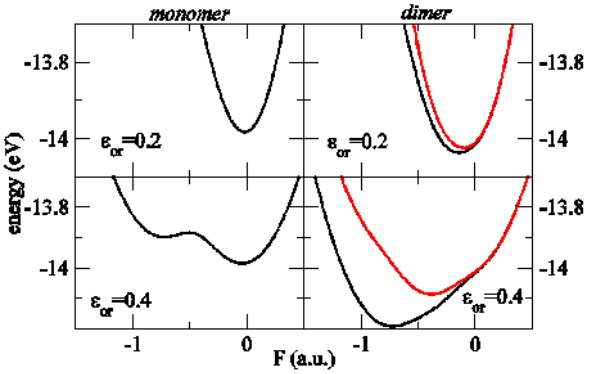

Figure 5. Evolution of the ground state energy (black lines) as a function of the solvent reaction field F, plotted for ε_{or}=0.2 and 0.4 eV (top and bottom panels, respectively) for the monomer **1** (left panels) and the dimer $\mathbf{[1]}_{2\ LT}$ (right panels). The red lines in the right panels show the energy of the lowest triplet state.

In summary, we have reported a new molecular reversible switch that exhibits changes in its optical, magnetic and supramolecular properties when using temperature as an external input. Such changes are due to the interplay of intra and intermolecular CT processes occurring between the subunits of the involved species.

ASSOCIATED CONTENT

Supporting Information. General methods for synthesis and characterization, Spectroelectrochemistry data, UV-Vis and ESR spectra and Cyclic Voltammetries of dyad **1** in DMF at 300 and 375 K, Raman and 1H-NMR spectra of **1-H** and dyad **1** at different temperatures and Reversibility studies are included. This material is available free of charge via the Internet at http://pubs.acs.org.

AUTHOR INFORMATION

Corresponding Author

* E-mail: vecianaj@icmab.es; iratera@icmab.es

Present Addresses

[⊥] Department of New Materials and Biosystems, Max Planck Institute for Intelligent Systems, Heisenberg str. 3, D-70569 Stuttgart, Germany & Department of Biophysical Chemistry, University of Heidelberg, INF 253, D-69120 Heidelberg, Germany.

Notes

The authors declare no competing financial interest.

ACKNOWLEDGMENT

This work was supported by the DGI grant (POMAs (CTQ2010-19501), the Networking Research Center on Bioengineering, Biomaterials, and Nanomedicine (CIBER-BBN), and the Generalitat de Catalunya (grant 2009SGR00516). J. G. is grateful to the Consejo Superior de Investigaciones ien tif cas (CSIC) for a JAE fellowship and M. S. to MEC for a FPU predoctoral grant.

REFERENCES

(1) Raymo, F. M. Digital Processing and Communication with Molecular Switches. *Adv. Mater.*, **2002**, *14*, 401-414.

(2) Gutlich, P.; Hauser, A.; Spiering, H. Thermal and optical switching of iron(II) complexes. *Angew. Chem. Int. Ed.***1994**, *33*, 2024-2054.

(3) Sato, O.; Tao, J.; Zhang, Y. Z. Control of Magnetic Properties through External Stimuli. *Angew. Chem. Int. Ed.,* **2007**, *46*, 2152-2187.

(4) Small, D.; Zaitsev, V.; Jung, Y. S.; Rosokha, S. V.; Head-Gordon, M.; Kochi, J. K. Intermolecular π-to-π Bonding between Stacked Aromatic Dyads. Experimental and Theoretical Binding Energies and Near-IR Optical Transitions for Phenalenyl Radical/Radical versus Radical/Cation Dimerizations. *J. Am. Chem. Soc.*, **2004**, *126*, 13850-13858.

(5) Zhong, C. J.; Kwan, W. S. V.; Miller, L. L. Self-assembly of delocalized π -stacks in solution. Assessment of structural effects. *Chem. Mater.,* **1992**, *4*, 1423-1428.

(6) Lu, J.-M.; Rosokha, S.; Kochi, J. K. Stable (long-bonded) Dimers via the Quantitative Self-association of different Cationic, Anionic, and Uncharged π-Radicals: Structures, energetic, and optical transitions. *J. Am. Chem. Soc.*, **2003**, *125*, 12161-12171.

(7) Grampp, G.; Landgraf, S.; Rasmussen, K.; Strauss. S. Dimerization of organic free radicals in solution. Temperature dependent measurements. *Spectrochimica Acta Part A,* **2002**, *58*, 1219-1226.

(8) Ratera, I.; Ruiz-Molina, D.; Vidal-Gancedo, J.; Novoa, J.J.; Wurst, K.; Letard, J.-F.; Rovira, C.; Veciana, J. Supramolecular Photomagnetic Materials: Photoinduced Dimerization of Ferrocene-Based Polychlorotriphenylmethyl Radicals. *Chem. Eur. J.* **2004**, *10*, 603-616.

(9) Ratera, I.; Ruiz-Molina, D.; Vidal-Gancedo, J.; Wurst, K.; Daro, N.; Létard, J-F.; Rovira, C.; Veciana, J. A New Photomagnetic Molecular System Based on Photoinduced Self-Assembly of Radicals. *Angew. Chem. Int. Ed.*, **2001**, *40*, 919-922.

(10) Ratera, I.; Veciana, J. Playing with organic radical as building blocks for functional molecular materials. *Chem. Soc. Rev.*, **2012**, *41*, 303-349.

(11) Venkataramani, S.; Jana, U.; Dommaschk, M.;Sönnichsen, F. D.; Tuczek, F.; Herges, R. Magnetic Bistability of Molecules in Homogeneous Solution at Room Temperature. *Science*, **2011**, *331*, 445-448.

(12) Thies, S.; Sell, H.; Schütt, C.; Bornholdt, C.; Tuczek, F.; Herges, R. Light-induced Spin by Photodissociable External Ligands: A New Principle for Magnetic Switching of Molecules. *J. Am. Chem. Soc.,* **2011**, *133*, 16243-16250.

(13) Itkis, M. E.; Chi, X.; Cordes, A. W.; Haddon, R.C. Magneto-Opto-Electronic Bistability in a Phenalenyl-Based Neutral Radica. *Science,* **2002**, *296*, 1443-1445.

(14) Morita, Y.; Suzuki, S.; Sato, K.; Takui, T. Synthetic Organic Spin Chemistry for Structurally Well-Defined Open-Shell Graphene Fragments. *Nat. Chem.* **2011**, *3*, 197-204.

(15) Hicks, R. G. A New Spin on Bistability. *Nature Chem.,* **2011**, *3*, 189-191.

(16) Pal, S. K.; Bag, P.; Sarkar, A.; Chi, X.; Itkis, M. E.; Tham, F. S.; Donnadieu, B.; Haddon, R. C. Hysteretic Spin and Charge Delocalization in a Phenalenyl-Based Molecular Conductor. *J. Am. Chem. Soc.,* **2010**, *132*, 17258-17264.

(17) Morita, Y.; *et al.* Thermochromism in an Organic Crystal Based on the Coexistance of σ- and π-dimers. *Nature Materials,* **2008**, *7*, 48-51.

(18) Rawson, J.M.; Palacio, F. Magnetic Properties of Thiazyl Radicals. *Structure and Bonding*, **2001**, *100*, 94-127.

(19) Yong, G-P.; Li, C-F.; Li, Y-Z.; Luo, S-W. New Zwitterionic Radical Salts: Dimers in Solution and Unusual Magnetic and Luminiscent Properties in the Solid State. *Chem. Commun.*, **2010**, *46*, 3194-3196.

(20) Spruell, J. M. Molecular Recognition and Switching via Radical Dimerization. *Pure Appl. Chem*., **2010**, 82, No. 12, 2281-2294.

(21) Nishinaga, T.; Komatsu, K. Persistent π radical cations: Self-association and its Steric Control in the Condensed Phase. *Org. Biomol. Chem.,* **2005**, *3*, 561-569.

(22) Hwang, I.; Ziganshina, A. Y.; Ko, Y. H.; Yun, G.; Kim, K. A new three-way supramolecular switch based on redox-controlled interconversion of hetero- and homo-guest-pair inclusion inside a host molecule. *Chem. Commun*., **2009**, *4*, 416-418.

(23) Spruell, J.M.; *et al.* Highly stable tetrathiafulvalene radical dimers in [3]catenanes. *Nature Chem*., **2010**, *2*, 870-879.

(24) Coskun, A.; *et al*. Mechanically Stabilized Tetrathiafulvalene Radical Dimers. *J. Am. Chem. Soc*., **2011**, *133*, 4538-4547.

(25) Wudl, F.; Wobschall, D.; Jufnagel, E. J. Electrical Conductivity by the bis(1,3-dithiole)-bis(1,3-dithiolium) System. *J. Am. Chem. Soc.,* **1972**, *94*, 670-672.

(26) Wudl, F.; Smith, G.M.; Hufnagel, E. J. Bis-1,3-dithiolium chloride: an usually stable organic radical cation. *J. Chem. Soc., Chem. Commun.* **1970**, 1453–1454.

(27) Khodorkovsky, V.; Shapiro, L.; Krief, P.; Shames, A.; Mabon, G.; Gorgues, A.; Giffard, M. Do π-dimers of tetrathiafulvalene cation radicals really exist at room temperature? *Chem. Commun.,* **2001**, *41*, 2736-2737.

(28) Chiang, P.-T. ; Chen, N.-C.; Lai, C.-C.; Chiu, S.-H. Direct Observation of Mixed-Valence and Radical Cation Dimer States of Tetrathiafulvalene in Solution at Room Temperature: Association and Dissociation of Molecular Clip Dimers Under Oxidative Control. *Chem. Eur. J*., **2008**, *14*, 6546-6552.

(29) Rosokha, S. V.; Kochi, J. K. Molecular and Electronic Structures of the Long-Bonded π-Dimers of Tetrathiafulvalene Cation-Radical in Intermolecular Electron Transfer and in (Solid-State) Conductivity *J. Am. Chem. Soc.,* **2007**, *129*, 828-838.

(30) Lyskawa, J. ; Sallé, M.; Balandier, J.-Y. ; Le Derf, F. ; Levillain, E.; Allain, M.; Viel, P.; Palacin, S. Monitoring the formation of TTF dimers by Na^+ complexation. *Chem. Commun.,* **2006**, *93*, 2233-2235

(31) Ziganshina, A. Y.; Ho Ko, Y.; Sung Jeon, W.; Kim, K. Stable p-dimer of a tetrathiafulvalene cation radical encapsulated in thecavity of cucurbit[8]uril. *Chem. Commun.,* **2004**, 806-807.
(32) Yoshizawa, M.; Kumazawa, K.; Fujita, M. Room-Temperature and Solution-State Observation of the Mixed-Valence Cation Radical Dimer of Tetrathiafulvalene, [$(TTF)_2$] within a Self-Assembled Cage *J. Am. Chem. Soc.,* **2005**, *127*, 13456-13457.
(33) Tanaka, K.; Kunita, T.; Ishiguro, F.; Naka, K.; Chujo, Y. Modulation of Morphology and Conductivity of Mixed-Valence Tetrathiafulvalene Nanofibers by Coexisting Organic Acid Anions. *Langmuir* **2009**, *25*, 6929–6933.
(34) Tanaka, K.; Ishiguro, F.; Kunita, T.; Chujo, Y. Transparent Conductive Films Based on Polymer Composites Containing the Mixed-Valence Tetrathiafulvalene Nanofibers. *Polym. Sci. A Polym. Chem.* **2009**, *47*, 6441–6450.
(35) Tanaka, K.; Matsumoto, T.; Ishiguro, F.; Chujo, Y. Conductivity regulation of the mixed-valence tetrathiafulvalene nanowire/poly(methyl methacrylate) composites using heterogeneous tetrathiafulvalene derivatives *J. Mater. Chem*. **2011**, *21*, 9603–9607.
(36) Hasegawa, M.; Daigoku, K.; Hashimoto, K.; Nishiwaka, H.; Iyoda, M. Face-to-Face Dimeric Tetrathiafulvalene and Their Catio Radical and Dication Species as Models for Mixed Valence and π-Dimer States. *Bull. Chem. Soc. Jpn*., **2012**, *85*, 51-60.
(37) Guasch, J.; *et al*. Induced Self-Assembly of a Tetrathiafulvalene-Based Open-Shell Dyad through Intramolecular Electron Transfer. *Angew. Chem. Int. Ed*., **2012**, *51*, 11024-11028.
(38) Guasch, J.; Grisanti, L.; Souto, M.; Lloveras, V.; Vidal-Gancedo, J.; Ratera, I.; Painelli, A.; Rovira, C.; Veciana, J. Intra- and Intermolecular Charge Transfer in Aggregates of Tetrathiafulvalene-Triphenylmethyl Radical Derivatives in Solution. *J. Am. Chem. Soc.*, **2013**, *135*, 6958-6967.
(39) Bouguessa, S.; Hervé, K.; Golhen, S.; Ouahab, L.; Fabre, J.-M. Synthesis, redox behavior and X-ray structure of bis-TTF containing a pyridine unit a potential building block in the construction of conducting magnetic materials. *New J. Chem.* **2003**, *27*, 560-564.
(40) Frei, M.; Diederich, F. Tetrathiafulvalene (TTF)-Bridged Resorcin[4]arene Cavitands: Towards New Electrochemical Molecular Switches. *Helv. Chim. Acta,* **2006**, *89*, 2040-2057.
(41) Azov, V.; Gómez, R.; Stelten, J. Synthesis of electrochemically responsive TTF-based molecular tweezers: evidence of tight intramolecular TTF pairing in solution. *Tetrahedron,* **2008**, *64*, 1909-1917.
(42) Painelli, A.; Girlando, A. Electron-molecular vibration (e-mv) coupling in charge-transfer compounds and its consequences on the optical spectra: A theoretical framework. *J. Chem Phys* **1986**, 84, 5665-5671.
(43) Casado, J.; Burrezo, P.M.; Ramírez, F.J.; López Navarrete, J. T.; Lapidus, S. H.; Stephens, P.W.; Vo, J. S. Miller, H.-L.; Mota, F.; J. J. Novoa. Evidence for Multicenter Bonding in Dianionic Tetracyanoethylene Dimers by Raman Spectroscopy. *Angew. Chem. Int. Ed*. **2013**, *52*, 6421–6425.
(44) Casado, J.; Takimiya, K.; Otsubo, T.; Ramírez, F. J.; Quirante, J. J.; Ortiz, R. P.; González, S. R.; Oliva, M. M.; Navarrete, J. T. Raman Spectroscopy Shows Interchain through Space Charge Delocalization in a Mixed Valence Oligothiophene Cation and in Its π-Dimeric Biradicaloid Dication. *J. Am. Chem. Soc.* **2008**, *130*, 14028-14029.
(45) González, M.; Segura, J. L.; Seoane, C.; Martín, N.; Garín, J.; Orduna, J.; Alcalá, R.; Villacampa, B.; Hernández, V.; López Navarrete, J. T. Tetrathiafulvalene Derivatives as NLO-phores: Synthesis, Electrochemistry, Raman Spectroscopy, Theoretical Calculations, and NLO Properties of Novel TTF-Derived Donor-π-Acceptor Dyads. *J. Org. Chem.* **2001**, *66*, 8872–8882.
(46) Bozio, R.; Girlando, A.; Pecile, C. Infrared and Raman spectra of TTF and TTF-d_4. *Chem. Phys. Lett*. **1977**, *52*, 503-508.
(47) Bozio, R.; Zanon, I.; Girlando, A.; Pecile, C. Vibrational spectroscopy of molecular constituents of onedimensional organic conductors. Tetrathiofulvalene (TTF), TTF^+, and $(TTF^+)_2$ dimer *J. Chem. Phys.* **1979**, *71*, 2282-2293.
(48) Torrance, J. B.; Scott, B. A.; Welber, B.; Kaufman, F. K.; Seiden, PP.E. Optical properties of the radical cation tetrathiafulvalenium (TTF^+) in its mixed-valence and monovalence halide salts. *Phys. Rev.,* **1979**, *19*, 730-741.
(49) D'Avino, G.; Grisanti, L.; Guasch, J.; Ratera, I.; Veciana, J.; Painelli, A. Bistability in Fc-PTM Crystals: The Role of Intermolecular Electrostatic Interactions. *J. Am. Chem. Soc.,* **2008**, *130*, 12064-12072.
(50) Grisanti, L.; D'Avino, G.; Painelli, A.; Guasch, J.; Ratera, I.; Veciana, J. Essential Models for Solvatochromism in Donor-Acceptor Molecules: The Role of the Bridge. *J. Phys. Chem.* **2009**, *113*, 4718-4725.
(51) Terenziani, F.; D'Avino, G.; Painelli, A. Multichromophores for nonlinear optics: Designing the material properties by electrostatic interactions. *Chem. Phys. Chem.*, **2007**, *8*, 2433-2444.
(52) Painelli, A. Vibronic contribution to static NLO properties: Exact results for the DA dimer. *Chem. Phys. Lett.* **1998**, *285*, 352-358.
(53) Painelli, A.; Terenziani, F. Optical spectra of push-pull chromophores in solution: A simple model *J. Phys. Chem.* **2000**, *104*, 11041–11048.
(54) Terenziani, F.; Painelli, A.; Comoretto, D. Solvation effects and inhomogeneous broadening in optical spectra of phenol blue. *J. Phys. Chem.* **2000**, *104*, 11049-11054.
(55) Boldrini, B.; Cavalli, E.; Painelli, A.; Terenziani, F. Polar dyes in solution: A joint experimental and theoretical study of absorption and emission band shapes. *J. Phys. Chem*. **2002**, *106*, 6286–6294.

Supporting Information

Thermomagnetic Molecular System Based on TTF-PTM Radical: Switching the Spin and Charge Delocalization

Manuel Souto,[†] Judith Guasch,[†,⊥] Vega Lloveras,[†] Paula Mayorga,[‡] Juan T. López Navarrete,[‡] Juan Casado,[‡] Imma Ratera,[†,*] Concepció Rovira,[†] Anna Painelli,[§] and Jaume Veciana[†,*]

[†] Institut de Ciència de Materials de Barcelona (ICMAB-CSIC)/CIBER-BBN, Campus Universitari de Bellaterra, 08193 Cerdanyola del Vallès (Barcelona), Spain
[‡] Departamento de Química Física, Universidad de Málaga, 29071-Málaga, Spain.
[§] Dipartimento Chimica, GIAF, Parma University/INSTM-UdR, I-4310 Parma, Italy

E-mails: Jaume Veciana, vecianaj@icmab.es

Contents

General methods for synthesis and characterization

UV-Vis spectra were measured using Cary 5000E Varian with temperature controller equipment. ESR spectra were performed with a Bruker ESP 300 E equipped with a rectangular cavity T102 that works with an X-band (9.5 GHz). The Raman spectra discussed in the paper are FT–Raman spectra obtained in a Bruker Equinox 55 FT–IR interferometer using a Raman accessory kit (FRA/106–S). A continuous–wave Nd–YAG laser working at 1064 nm was employed for excitation. A germanium detector operating at liquid nitrogen temperature was used. Raman scattering radiation was collected in a back–scattering configuration with a standard spectral resolution of 4 cm^{-1}. 1000-3000 scans were averaged for each spectrum. Variable temperature FT-Raman measurements were performed using a variabletemperature Linkam cell adapted to the Senterra Raman microscope from Bruker. ^{1}H-NMR spectra were recorded at 400 Hz with DMF-d_7 as solvent and Me_4Si as an internal standard using a Bruker Avance III 400 instrument. All reagents and solvents employed for the synthesis were of high purity grade and were purchased from Sigma-Aldrich Co., Merck and SDS. CH_2Cl_2 was passed through basic alumina to deactivate the acidic points of the solvent. The solvents used for optical spectroscopy and ESR measurements were of HPLC grade. The syntheses of dyad **1** and **1H** are reported elsewhere [Ref. 31].

Spectroelectrochemistry of dyad 1

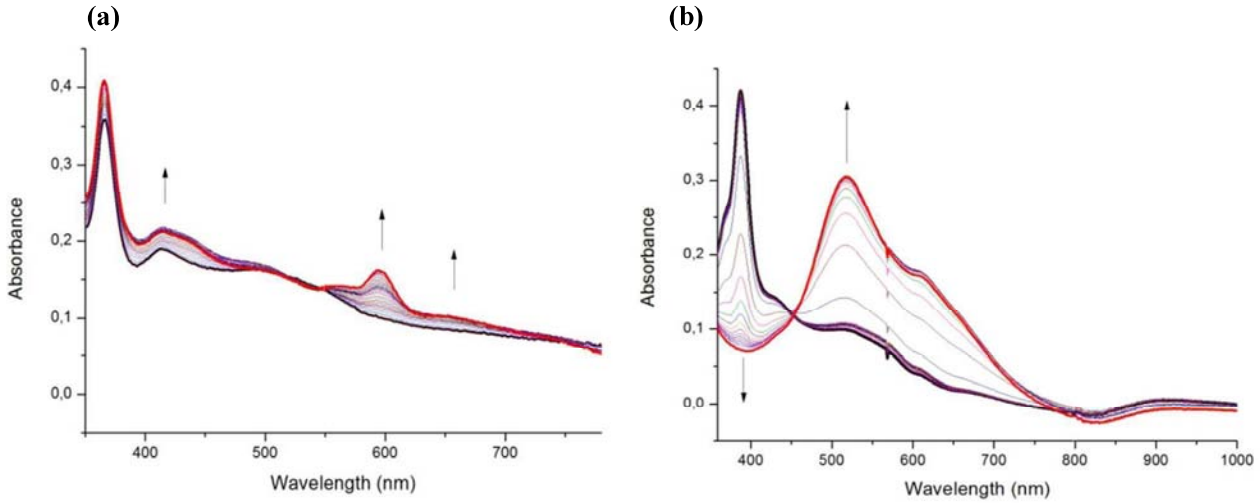

Figure S1. Absorption spectra of dyad **1** (0.05 mM) obtained in chronoamperometric experiments using fixed oxidation potentials of +1000 mV **(a)** and -1000 mV **(b),** versus Ag/AgCl, 0.1 M Bu_4NPF_6 in CH_2Cl_2 .

Absorption spectra of dyad 1 and of its oxidazed derivatives

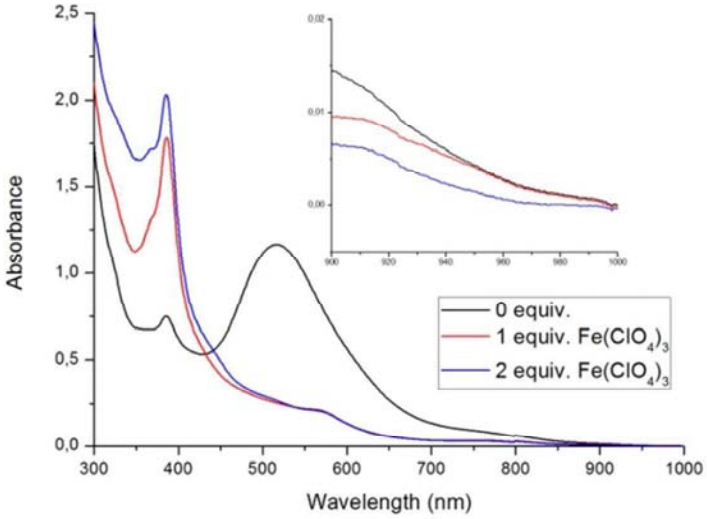

Figure S2. Absorption spectra of dyad **1** (0.2 mM) in a mixture of DMF/CH_2Cl_2 (199:1) and those of the oxidized derivatives arising from the stepwise addition of $Fe(ClO_4)_3$. Inset: Zoom of the low-energy range of the absorption spectra.

Absorption and ESR spectra of dyad 1 in DMF/CH_2Cl_2 (95:5)

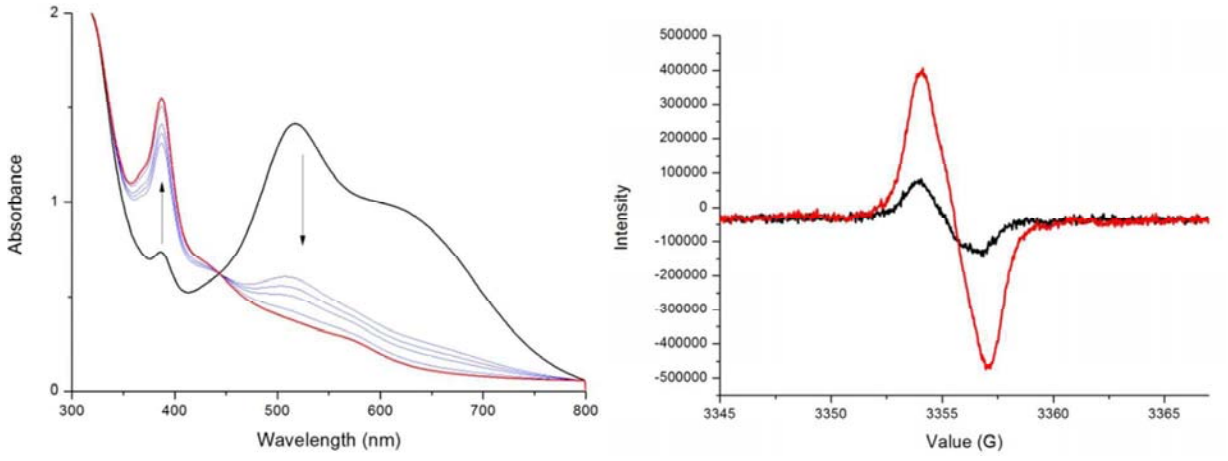

Figure S3. Absorption (left) and ESR (right) spectra of dyad **1** (0.1 mM) in DMF/CH_2Cl_2 (95:5) at 300 K (black line) and 375 K (red line).

Cyclic Voltammetries of dyad 1 in DMF

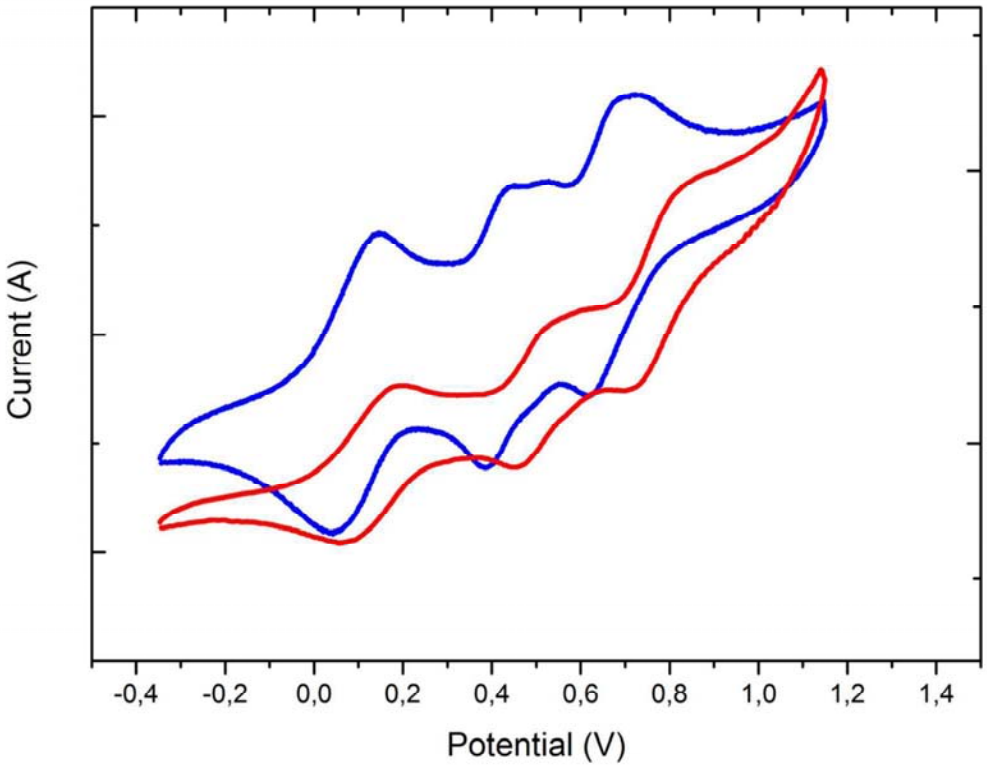

Figure S4. Cyclic voltammetry of solution of dyad **1** (0.5 mM) in DMF vs. Ag/AgCl using *n*-Bu_4PF_6 (0.1 M) as electrolyte at 300 K (blue line) and 375 K (red line) under argon at a scan rate of 0.1 V/s.

Table S1. CV data of dyad **1** (0.5 mM) in DMF solutions at 300 and 375 K vs. Ag/AgCl.

DMF	$E^{red}_{1/2}E^{red}_{1/2}$ ***(V)***	$E^{ox1}_{1/2}E^{ox1}_{1/2}$ ***(V)***	(	$E^{ox1}_{1/2}E^{ox1}_{1/2}$***' (V)***	$E^{ox2}_{1/2}E^{ox2}_{1/2}$ ***(V)***
300 K	0.09	0.42		0.51[a]	0.67
375 K[b]	0.13	0.50		-	0.78

[*a*] It has been reported that when two TTF moieties in a molecule are in sufficiently close proximity to each other, the first oxidation to the bis(radical cation) is split into two steps. In this case, the electronic stabilization of the first-formed radical cation by the π electrons of the second TTF moiety reduces the potential of the first oxidation step. If the distance between the two TTF moieties is slightly increased, the two $1e^-$ oxidation peaks merge into a single, broadened peak.
[*b*] The down shift of oxidation potentials when increasing the temperature it has been explained through an increase of the diffusion coefficient because the absolute viscosity of the solvent media decreases [Ref S1].

Raman spectra of dyad 1 and 1-H^{+} in solid state

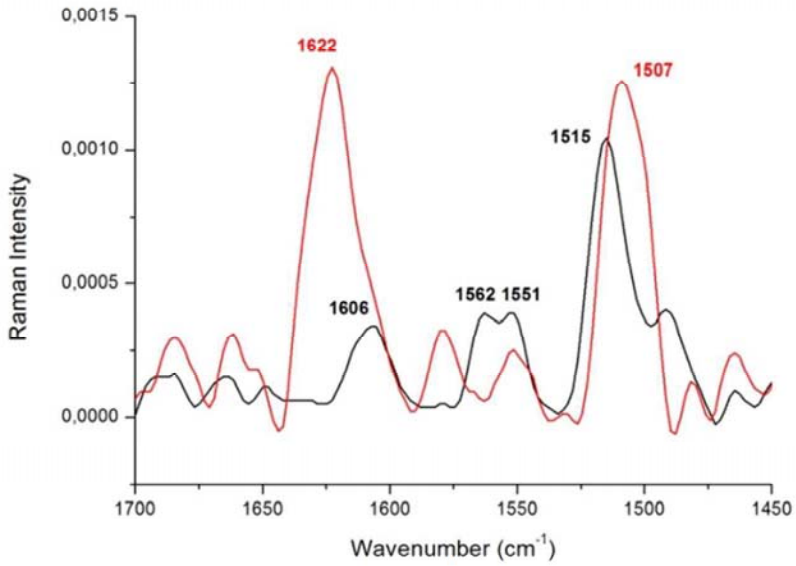

Figure S5. Raman spectra of dyad **1** (black line) and **1-H^{+}**(red line) in solid state.

^{1}H-NMR spectra of 1 and 1-H at different temperatures

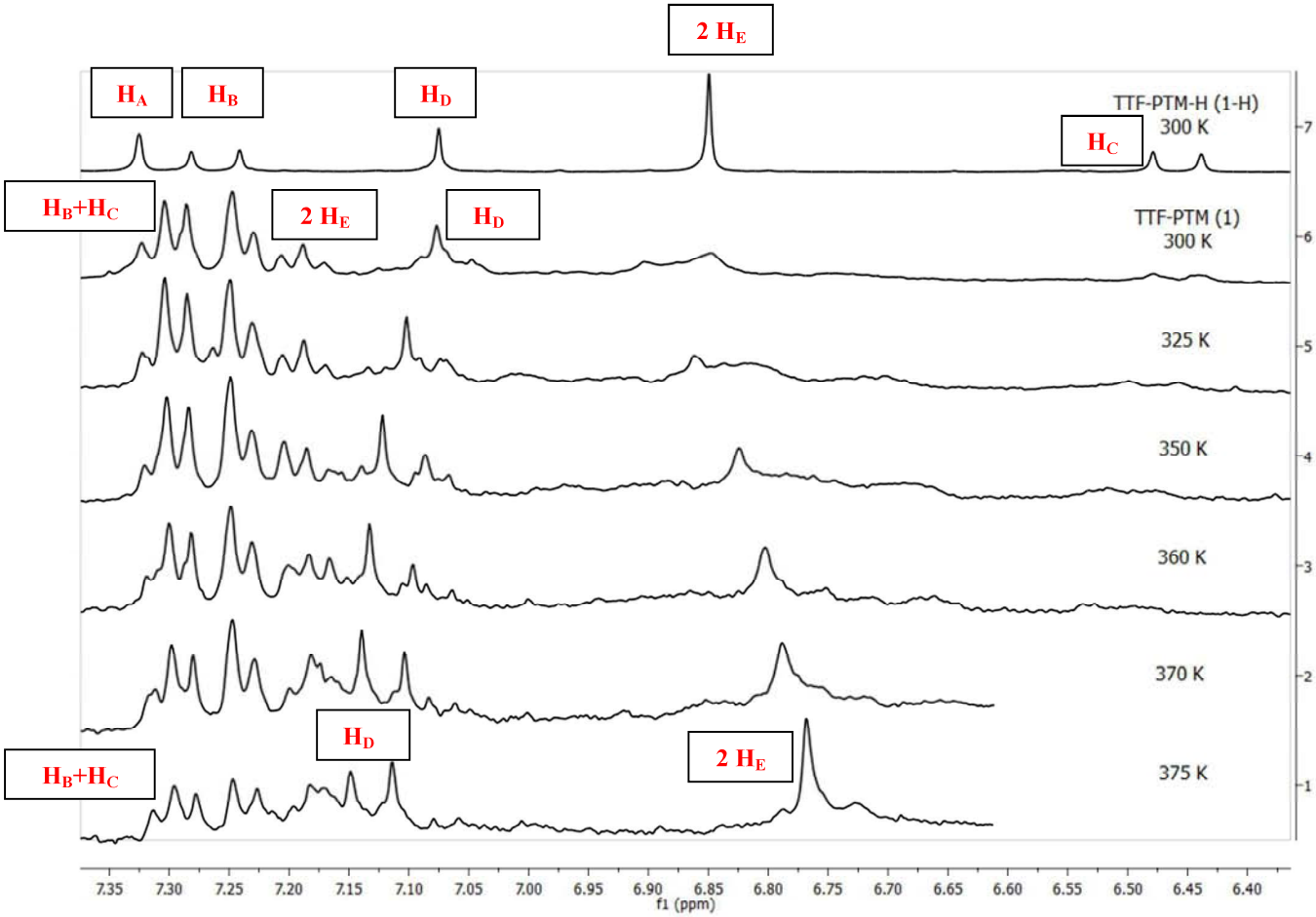

Figure S6. ^{1}H-NMR spectra of dyad **1** and **1-H** (0.01 M) at different temperatures in DMF-d_7.

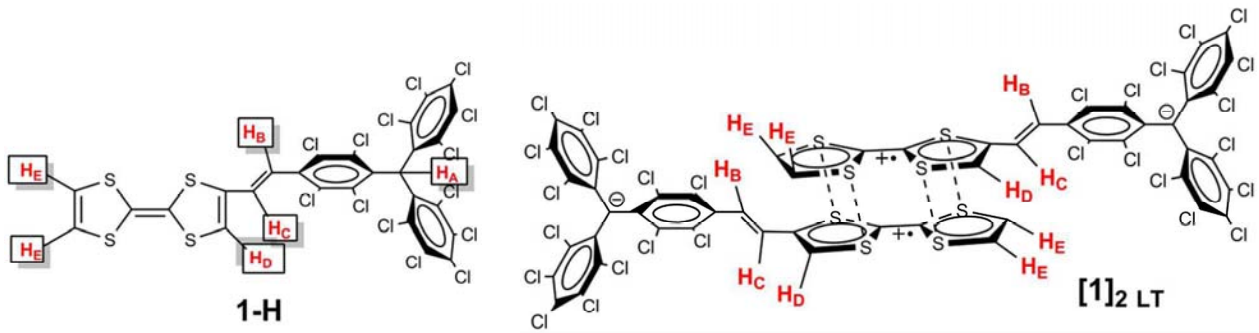

Scheme S1. Protons observed in the ^{1}H-NMR spectra.

T-dependence ESR intensities

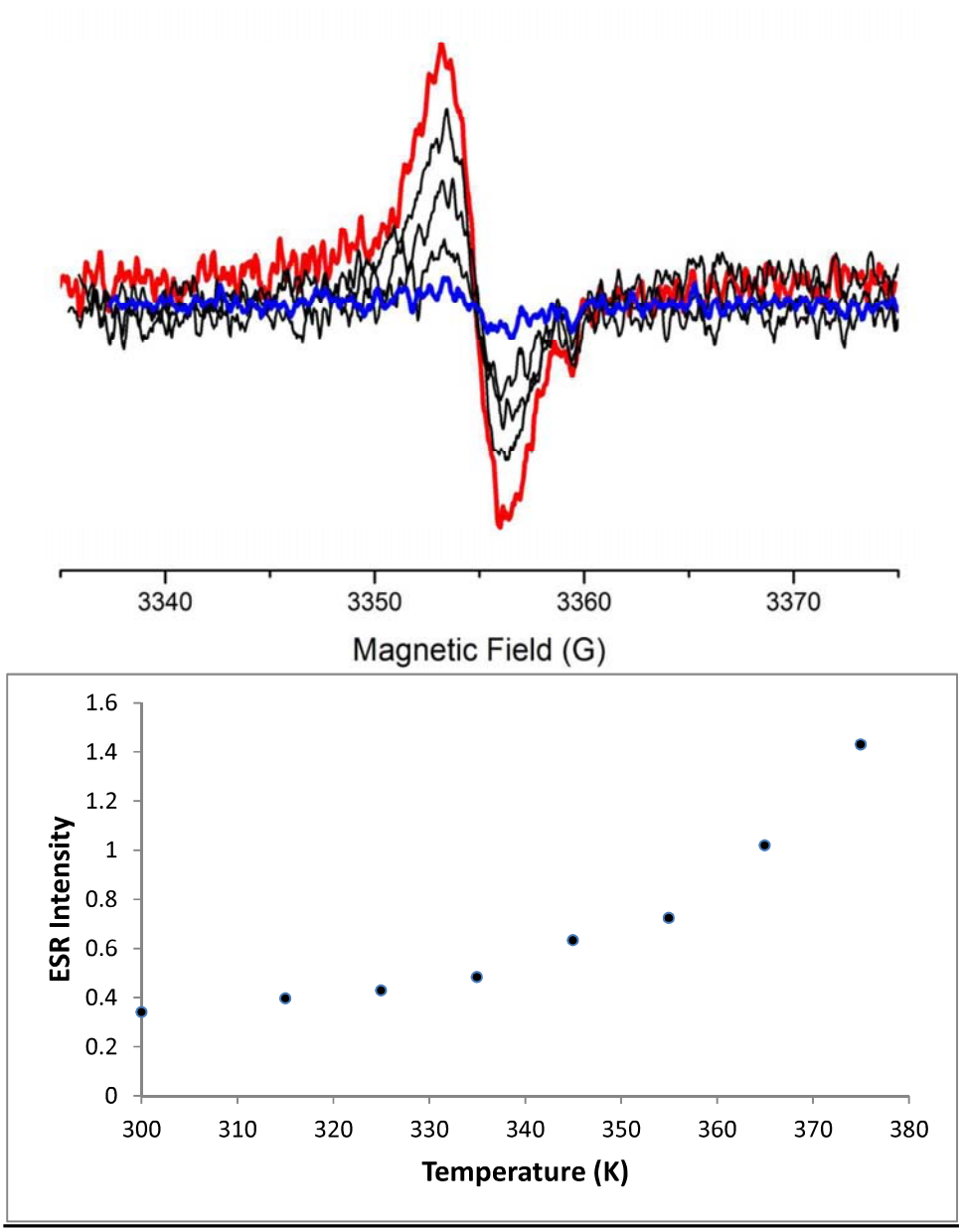

Figure S7. Top: ESR spectra of 1 in DMF (0.1 mM) at 375 (red line), 365, 355, 335 (black lines) and 300 K (blue line). Bottom: Plot of the ESR doubly-integrated signal (proportional to the monomer concentration) in the relevant region versus temperature.

Reversibility studies

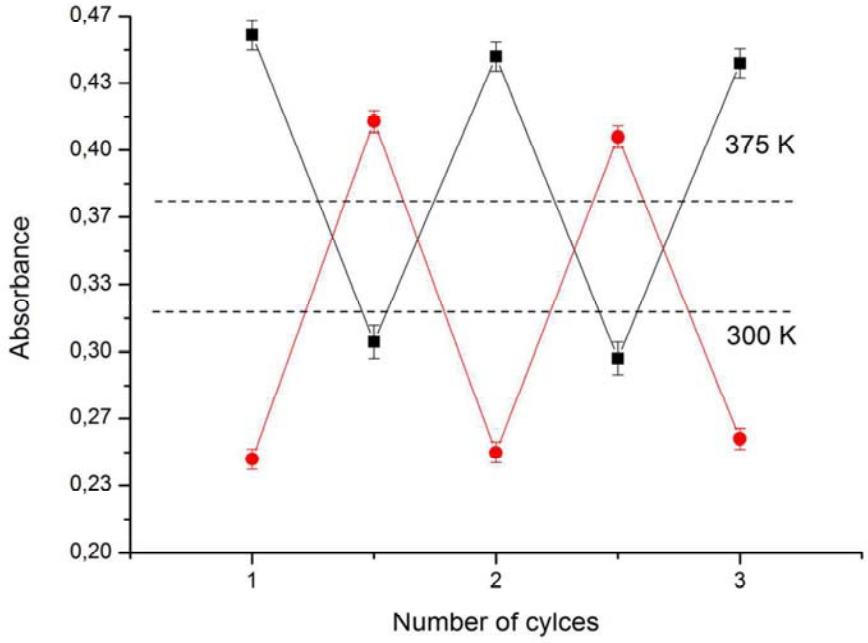

Figure S8. Absorbance changes at 387 nm (red line) and 516 nm (black line) of dyad **1** (0.1 mM) in DMF during switching cycles at 300 and 375 K.

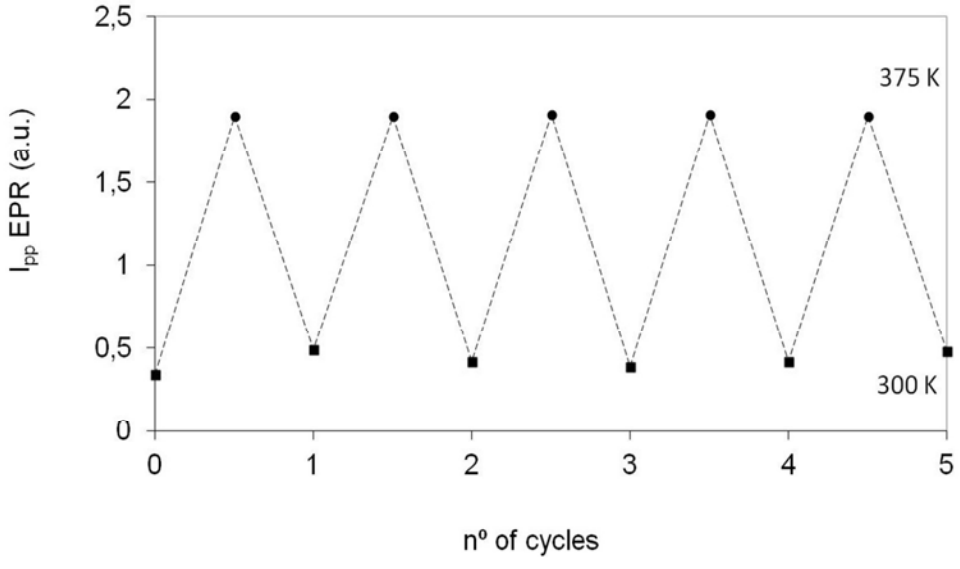

Figure S9. Plot of ESR intensities at 300 K (squares) and 375 K (circles) *vs.* number of cycles.

The model

Details of numerical calculations:

For the sake of clarity we write here explicitly the four-site Hamiltonian relevant to 2.2, 1.2 and 1.1 dimers. Sites 1 and 4 refer to PTM units, sites 2 and 3 to TTF units:

$$H = -\tau \sum_{\sigma=\alpha,\beta} \left(a_{1\sigma}^{\dagger} a_{2\sigma} + a_{2\sigma}^{\dagger} a_{1\sigma}\right) - \tau \sum_{\sigma=\alpha,\beta} \left(a_{3\sigma}^{\dagger} a_{4\sigma} + a_{4\sigma}^{\dagger} a_{3\sigma}\right) - t \sum_{\sigma=\alpha,\beta} \left(a_{2\sigma}^{\dagger} a_{3\sigma} + a_{3\sigma}^{\dagger} a_{2\sigma}\right) + U\left(n_{2\alpha} n_{2\beta} + n_{3\alpha} n_{3\beta}\right)$$
$$+ U_P\left(n_{1\alpha} n_{1\beta} + n_{4\alpha} n_{4\beta}\right) + \Delta\left(n_{1\alpha} + n_{1\beta} + n_{4\alpha} + n_{4\beta}\right) - F_1\mu_1 - F_1\mu_1 + \frac{F_1^2}{4\varepsilon_{or}} + \frac{F_2^2}{4\varepsilon_{or}}$$

Where $a_{i\sigma}^{+}a_{i\sigma}^{+}$, $a_{i\sigma}$ $a_{i\sigma}$ are the creation and destruction operators, respectively, for an electron with spin σ on site *i*, and $n_{i\sigma} = a_{i\sigma}^{+}a_{i\sigma}n_{i\sigma} = a_{i\sigma}^{+}a_{i\sigma}$ counts electrons with spin σ on site *i*. As explained in ref. 6b, U_P and Δ are set to large values as to make their specific values irrelevant, while maintaining finite the energy gap between the neutral and zwitterionic forms of each dyad, $2z=U_P-\Delta-U$. Specifically, calculations were run setting $U_P=10$ eV, and adjusting Δ to obtain the required 2z. F_1 and F_2 are the two reaction fields generated in polar solvents at the location of dyad 1 and dyad 2, respectively. Each field is coupled with the dipole moment operator relevant to each dyad: $\mu_1=(n_2-n_1-1)/2$, $\mu_2=(n_3-n_4-1)/2$, where $n_i = n_{i\alpha}+n_{i\beta}n_i = n_{i\alpha}+n_{i\beta}$ counts the total number of electrons on site *i*. Molecular parameters are taken from ref. 6b: 2z=0.45 eV, τ=0.1 eV, t=0.34 eV, U=1.29 eV. Solvent relaxation energies ε_{or} are set to 0.2 eV to mimic a mildly polar solvent like CH_2Cl_2 and to 0.4 eV to mimic a strongly polar solvent like DMF. Results for monomers are simply obtained setting the intermolecular hopping integral to zero, t=0.

Figure S10 shows the variation of the ground state energy as a function of the solvation fields. In all cases the absolute minima are found along the main diagonal ($F_1=F_2$). For this reason in the main text we only discuss the behavior of the system with $F_1=F_2$

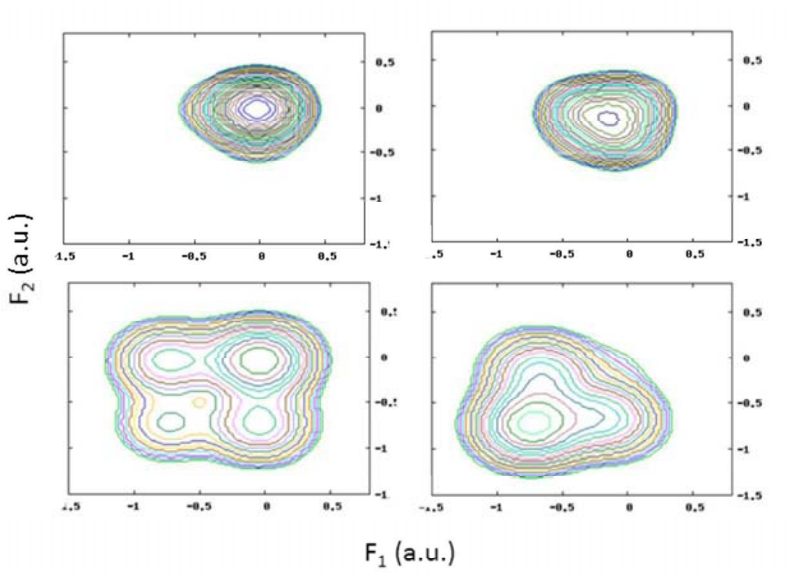

Figure S10. Potential energy surfaces (PES) shown in terms of equipotential profiles calculated for a couple of non-interacting (t=0) dyads (left panels) and a dimer (t=0.34 eV, right panel). Results refer to a weakly polar solvent (ε_{or}=0.2 eV, top panels) and a strongly polar solvent (ε_{or}=0.4 eV, bottom panels). In the low-polarity solvent the PES of either the monomer or the dimer show a minimum at $F_1 = F_2 \sim 0$, corresponding to a largely neutral state. In the high polarity solvent the monomer (bottom left panel) shows four minima: the minimum at $F_1 = F_2 \sim 0$, corresponding to the neutral dyad, has by far the lowest energy, representing the only populated state. Metastable states are recognized at $F_1 = F_2 \sim$-0.7 corresponding to a state where both molecules are zwitterionic and at $F_1 \sim$-0.0 and $F_2 \sim$-0.7 (or viceversa) where one of the molecule is in a zwitterionic state and the other is in a neutral state. Finally, for the dimer (t=0.34 eV) in a strongly polar solvent the (bottom right panel) the only stable state describes a dimer where both molecules are in a zwitterionic state.

References:

1 Tsierkos, N. K. Cyclic Voltammetric Studies of Ferrocene in Nonaqueous Solvents in The Temperature Range from 284.15 to 298.15 K. *J. Solution Chem.*, **2007**, *36*, 289-302.

Publication #2

Title: Three Redox States of a Diradical Acceptor-Donor-Acceptor Triad: Gating the Magnetic Coupling and the Electron Delocalization

Authors: Manuel Souto, Vega Lloveras, Sergi Vela, Maria Fumanal, Imma Ratera, and Jaume Veciana

Publication: *J. Phys. Chem. Lett.* 2016, 7, 2234−2239

Three Redox States of a Diradical Acceptor-Donor-Acceptor Triad: Gating the Magnetic Coupling and the Electron Delocalization

Manuel Souto, [†] *Vega Lloveras,* [†] *Sergi Vela,* [‡] *Maria Fumanal,* [‡] *Imma Ratera,* [†,*] *and Jaume Veciana*[†,*]

[†] Institut de Ciència de Materials de Barcelona (ICMAB-CSIC)/CIBER-BBN, Campus Universitari de la UAB, 08193 Cerdanyola del Vallès (Barcelona), Spain

[‡] Laboratoire de Chimie Quantique, Université de Strasbourg, 4 rue Blaise Pascal, F-67000 Strasbourg, France

AUTHOR INFORMATION

Corresponding Author

*E-mail: vecianaj@icmab.es, iratera@icmab.es

ABSTRACT: The diradical acceptor-donor-acceptor triad **1**$^{\cdot\cdot}$, based on two polychlorotriphenylmethyl (PTM) radicals connected through a tetrathiafulvalene(TTF)-vinylene bridge, has been synthesized. The generation of the mixed-valence radical anion, **1**$^{\cdot-}$, and triradical cation species, $1^{\cdot\cdot\cdot+}$, obtained upon electrochemical reduction and oxidation, respectively, was monitored by optical and ESR spectroscopy. Interestingly, the modification of

electron delocalization and magnetic coupling was observed when the charged species were generated and the changes have been rationalized by theoretical calculations.

TOC GRAPHICS

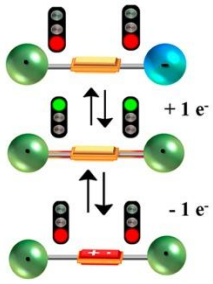

In the last few years, there is an increasing interest in the design and synthesis of novel organic materials exhibiting intramolecular electron transfer (IET) phenomena. Challenging are dyadic systems formed by donor (D) and acceptor (A) units connected by conjugated bridges due to their potential applications as molecular wires or switches.[1-8] Organic mixed-valence (MV) compounds containing at least two redox sites with two different oxidation states connected through a conjugated bridge are good examples for this kind of compounds.[9-14] On the other hand, research on organic molecules containing several stable radical centres linked through ferromagnetic coupling bridges have also received much attention during the past decades.[15-22] In fact, there are recent examples of diradical compounds that can switch the magnetic interaction between the radical centres by changing the chemical nature of the bridge.[19,20] Thus, switching the magnetic response of organic molecular materials through the application of an external stimulus is an interesting phenomenon since they mimic elemental electronic operations.

In our group, we have recently reported an organic radical D-A dyad, based on the electron π-donor tetrathiafulvalene (TTF) connected to the electron acceptor

polychlorotriphenylmethyl (PTM) radical, that exhibits bistability in solution through the application of external stimuli such as the polarity of the solvent or temperature.[23-28] In order to study the effect of having two acceptor PTM units linked to the same TTF moiety, we have synthesized and characterized the quadrupolar species based on a diradical acceptor-donor-acceptor (A-D-A) triad **1**$^{\cdot\cdot}$ consisting on two PTM radical units connected by a bis-vinylene-TTF bridge. Moreover, we have studied the reversible formation of the mixed-valence **1**$^{\cdot-}$ and triradical cation **1**$^{\cdot\cdot\cdot+}$ species by one-electron reduction and oxidation respectively (Scheme 1). Both species exhibit different optical and magnetic properties as the electron delocalization was suppressed for the generated charged species. This molecular tristable redox system can gate their physical properties upon the application of an electrical input in a reversible way under ambient conditions.

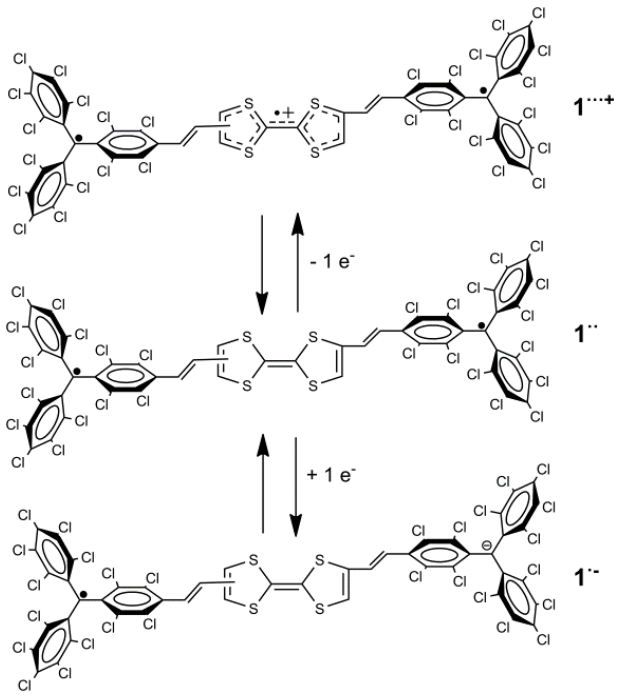

Scheme 1. Molecular structures of diradical **1**$^{\cdot\cdot}$, mixed-valence **1**$^{\cdot-}$ and triradical cation **1**$^{\cdot\cdot\cdot+}$.

Diradical triad **1**¨ was synthesized in three steps as shown in Scheme 2. First, the precursor diformyl TTF **2** was obtained as a mixture of (*E*) and (*Z*) isomers, as previously reported.[29] It is important to note that all the reported compounds derived from **2** were obtained as a mixture of isomers,[30-34] which are difficult to isolate due to the easiness of a *E*-*Z* isomerisation during the chromatographic separation.[35] Crystallization also resulted fruitless for their purification. Compound **4** was obtained through a Horner-Wadsworth-Emmons reaction of diformyl TTF **2** and two equivalents of phosphonated PTM derivative **3.**[9] The two vinylene units were obtained in *trans*-configuration according to the coupling constants in the ^{1}H-NMR spectra and to the nature of the base (*tert*-butoxide) that always favours the formation of *trans*-olefins[36] (see Figure S1). DFT calculations show that *E* and *Z* isomers of **4** lie extremely close in energy (*ca.* 0.1 kcal/mol). In addition the computational analysis suggests that the *cis* configuration of the vinylene units is *ca.* 2 kcal/mol disfavoured with respect to the *trans* one (see Table S4). Finally, subsequent deprotonation of **4** with two equivalents of TBAOH and oxidation of corresponding dicarbanions using silver nitrate yield diradical **1**¨ (*E* + *Z*) in 71%, as a brownish powder.

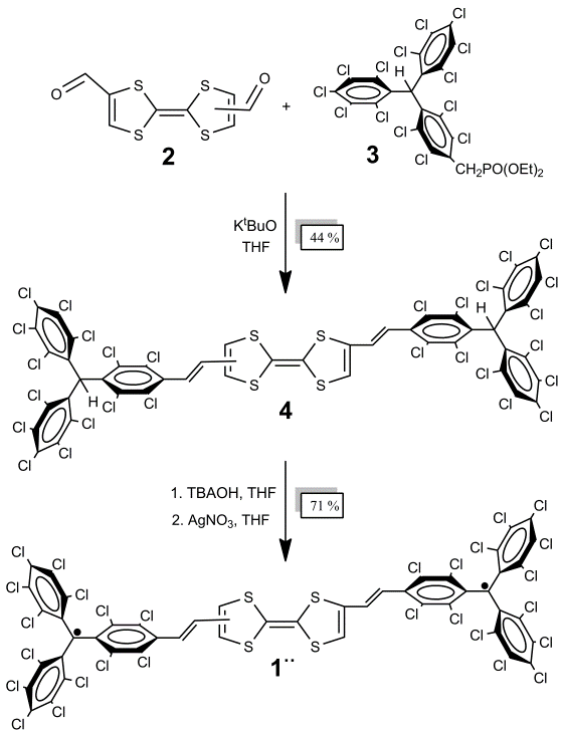

Scheme 1. Three-step synthesis of **1**$^{\cdot\cdot}$. TBAOH = tetrabutylammonium hydroxide.

Cyclic voltammetry (CV) of diradical **1**$^{\cdot\cdot}$ was recorded in CH_2Cl_2 at room temperature, with [(*n*-Bu)$_4$N] PF_6 (0.1 M) as supporting electrolyte, a Pt wire as a working electrode, and Ag/Ag^+ as the reference electrode (Figure 1). The spectrum of **1**$^{\cdot\cdot}$ shows two reversible oxidation processes (0.59 and 1.06 V vs Ag^+/Ag) assigned to the oxidation of the TTF bridge to $TTF^{+\cdot}$ and TTF^{2+} respectively, and one reversible reduction process (-0.21 V) that involves the simultaneous transfer of two electrons due to the reduction of the two PTM radical subunits. The CV suggests a negligible or very weak interaction between the two PTM radical subunits since we would expect to observe two electrochemical reduction waves in the case of a strong interaction between the two subunits.

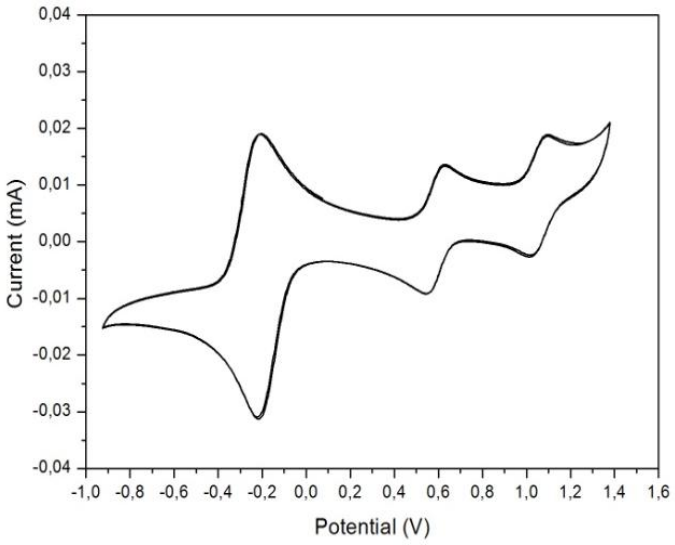

Figure 1. Cyclic voltammetry of solution of diradical **1**·· in CH_2Cl_2 vs. Ag/AgCl using *n*-Bu_4PF_6 (0.1 M) as electrolyte at 300 K under argon at a scan rate of 0.1 V/s.

UV-Vis-NIR spectrum of diradical **1**·· was obtained in CH_2Cl_2 at 300 K (Figure 2) showing an intense band at 385 nm, characteristic of PTM radical chromophores. The shoulders around 420 and 540 nm are attributed to the electronic conjugation of the unpaired electron into the π-framework. Regarding the low-energy region, the weak broad band that appears around 900 nm is assigned to the intramolecular charge transfer process from the electron-donor TTF bridge to the two electron-acceptor PTM radical subunits. TDDFT calculations confirmed such assignments enabling to ascribe each band to certain MO transitions (see Table S3).

Formation of radical anion mixed-valence species **1**·- was carried out either by electrochemical or by chemical reduction using metallic Cu with $[(Ph)_4P]Br$ (0.1 M) as supporting electrolyte in CH_2Cl_2 (see Figures 2 and S8). The reduction process was followed by UV-Vis-NIR spectroscopy until the mixed-valence species was completely generated. It was

observed two isosbestic points at 480 and 730 nm during the course of the reduction indicating that there are no byproducts due to decompositions or further reactions. During the reduction, the initial band at 385 nm, characteristic of PTM radical chromophore, gradually decreases and two new intense bands at 520 and 604 nm appear which are attributed to the PTM anion chromophore. Moreover, the lowest-energy band at 900 nm gradually decreases indicating the suppression of charge transfer from the TTF bridge to one of the PTM radical subunit as the later group is not electron-acceptor anymore. It is important to note that it was not observed any band in the NIR region that could be assigned to the intervalence transition (IVT) as observed for other mixed-valence compounds indicating a weak coupling of the two terminal PTM subunits.[13] Finally, triradical cation $\mathbf{1}^{\cdot\cdot\cdot+}$ was generated either by electrochemical or by chemical oxidation of $\mathbf{1}^{\cdot\cdot}$ using $FeCl_3$ (see Figures 2 and S9)**.** Absorption spectrum of the oxidized species shows a decreasing in intensity of the shoulders at 420 and 540 nm and the appearance of two new bands at 550 and 690 nm associated with the formation of $TTF^{\cdot+}$ species.[37-39] Moreover, the band at 900 nm attributed to the IET gradually decreases in agreement with the lack of intramolecular charge transfer when the TTF bridge loses its electron-donor character.

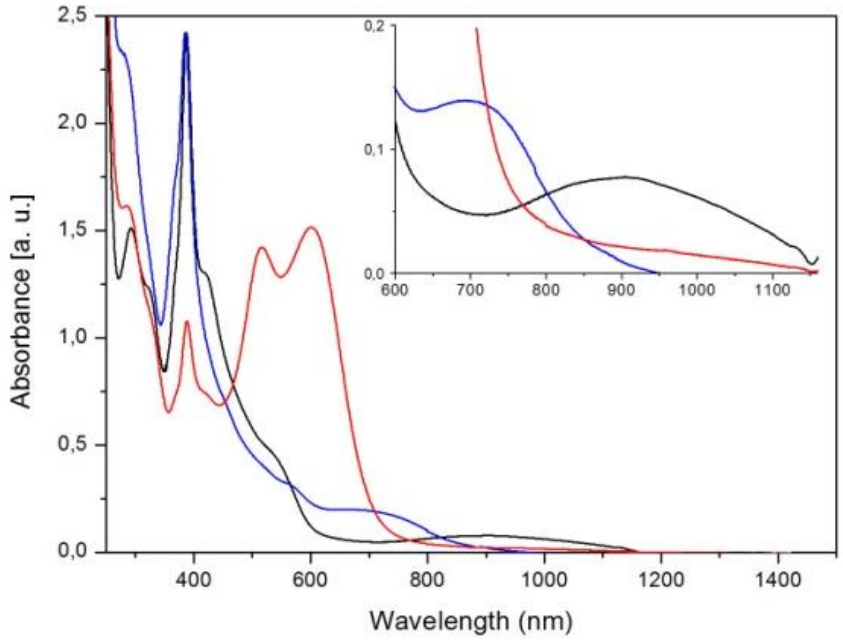

Figure 2. UV-Vis-NIR spectra of a solution 0.05 mM of diradical **1**$^{\bullet\bullet}$ (black line), mixed-valence species **1**$^{\bullet-}$ (red line) and triradical cation **1**$^{\bullet\bullet+}$ (blue line) in CH_2Cl_2. Inset shows the low-energy range of the absorption spectra.

CW X-band ESR spectra of **1**$^{\bullet\bullet}$ were recorded in CH_2Cl_2 in the temperature range of 300-200 K (Figure S10). The spectrum of **1**$^{\bullet\bullet}$ at 240 K (Figure 3) shows at g_{iso} of 2.0027 three overlapped lines that are attributed to the coupling of the unpaired electron with two equivalent protons with a coupling constant a_H = 0.9 G (ΔH_{pp} = 0.9 G) which is half of the value showed by a PTM monoradical with one vinylene bridge (a_H = 2 G). The appearance of three symmetrical lines indicate that the magnetic interaction of the two electrons of the PTM radicals have a magnetic exchange coupling constant, *J,* that fulfils the condition $|J| >> |a_i|$, as it has been already observed for other PTM diradicals.[9-13] The weak observed satellite lines are attributed to the hyperfine couplings with the naturally abundant ^{13}C nuclei of the PTM subunits with coupling constants of $a_{C,\alpha}$ = 14.9 G and $a_{C,arom}$ = 6.9 and 4.8 G that are also half the values for

typical PTM monoradicals. The spectrum of diradical **1**¨ was also recorded in frozen CH_2Cl_2 at 140 K and it was possible to observe the forbidden $\Delta m_s = 2$ transitions at half field in the ESR spectra suggesting the presence of the thermally-populated triplet state in the molecule (Figure S11). DFT calculations confirmed that the two unpaired electrons of **1**¨ are localized in each PTM unit (see Table S1 and Figure S15 in SI), and are coupled by an almost-negligible magnetic interaction (J_1, see Table S2 and Figure S16 in SI). This is in agreement with the CV measurements discussed above. Even if the computed ground state is an open-shell singlet, the strength of the coupling suggests that the system effectively behaves as a paramagnet, with *ca.* 75% population of triplet states.

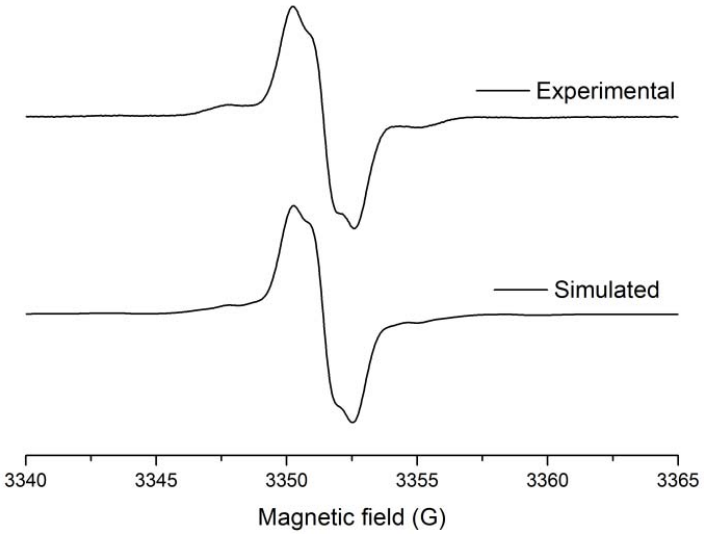

Figure 3. Experimental and simulated ESR spectra of 0.05 mM solution of diradical **1**¨ in CH_2Cl_2 at 240 K.

On the other hand, ESR spectra of the mixed-valence **1**·⁻ in CH_2Cl_2 species were recorded in the temperature range of 220-300 K (Figure S12). All the recorded spectra at different temperatures show two symmetrical lines at a *g* value of 2.0026 which indicates the coupling of the unpaired electron with only one hydrogen atom of the ethylene moiety directly linked to the

PTM radical with the isotropic hyperfine coupling constants typical for a PTM monoradical with a vinylene bridge (a_H = 1.7 G; ΔH_{pp} = 1.4 G) (Figure 4).[11] This result, together with the lack of an intervalence (IVT) band transition in the absorption spectra, suggests that at these temperatures the unpaired electron of the radical anion $\mathbf{1}^{\bullet-}$ is always localized on only one half of the molecule, like in a monoradical (i.e. the intramolecular electron transfer rate is below the EPR time scale) showing that this MV compound belongs to Class I.

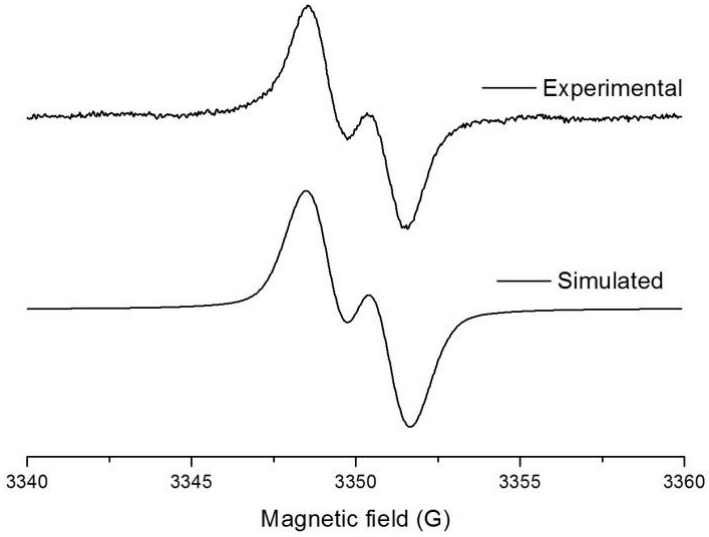

Figure 4. Experimental and simulated ESR spectra of 0.05 mM solution of mixed-valence $\mathbf{1}^{\bullet-}$ in CH_2Cl_2 at 240 K.

This localization effect observed for the radical anion $\mathbf{1}^{\bullet-}$ is in contrast to other fused A-D-A triads using a TTF as a bridge where the MV compounds have delocalized the unpaired electron at high temperatures.[40-45] However, in all these examples the molecules are almost planar and in our case the molecule has several degrees of conformational freedom. Also it is important to mention the influence of the different topologies of the possible isomers on the ease of the electron transfer as it has been previously studied.[9]

Finally, ESR spectra of the oxidized $\mathbf{1}^{\bullet\bullet\bullet+}$ triradical cation species were recorded in CH_2Cl_2 in the temperature range of 240-300 K (Figure S13). The ESR spectrum of $\mathbf{1}^{\bullet\bullet\bullet+}$ consists of two

separated groups of lines centered at *g*-values of 2.0085 and 2.0034 that are attributed to the open-shell $TTF^{\cdot+}$ and $PTM^{\cdot}$ radical subunits, respectively, that appear uncoupled (Figure 5). The ESR lines associated to the TTF bridge show a symmetric 5-lines signal indicating the coupling of the unpaired electron of the $TTF^{\cdot+}$ with two protons from the TTF subunit and two from the vinylene units ($a_{H,TTF}$ = 1.3 and $a_{H,vin}$ = 0.8 G)**.** On the other hand, the group of lines corresponding to the PTM radical subunits shows only two overlapped symmetrical lines due to the coupling of the unpaired electron of the PTM subunits with only one proton of the bridge ($a_{H,vin}$ = 1.5 G). The fact that the two group of lines related to the $TTF^{\cdot+}$ and $PTM^{\cdot}$ radicals appear uncoupled and separated suggests that the electrons at the two terminal PTM radical subunits remain localized at the ESR time scale. A worth noticing point is the moderately-strong antiferromagnetic (AFM) interactions calculated for $\mathbf{1}^{\cdots+}$ between the oxidized TTF and each of the PTM moieties ($J_2 \approx J_3 \approx -60$ cm^{-1}) (Table S2). Therefore, the resulting ground state is a doublet, with three unpaired electrons localized in the TTF and PTM (x2) units (see Figure S17). The quadruplet state lies higher in energy and, as a result, is poorly populated, which explains why the forbidden transition at half field in the ESR is not observed anymore. On the other hand, when temperature is lowered, the lines associated to the $TTF^{\cdot+}$ bridge do not disappear indicating the absence of dimerization process in contrast to the reported monoradical TTF-PTM dyad.[27] This is probably due to the steric hindrance of the two bulky PTM units that avoid the close interaction between the $TTF^{\cdot+}$ units.

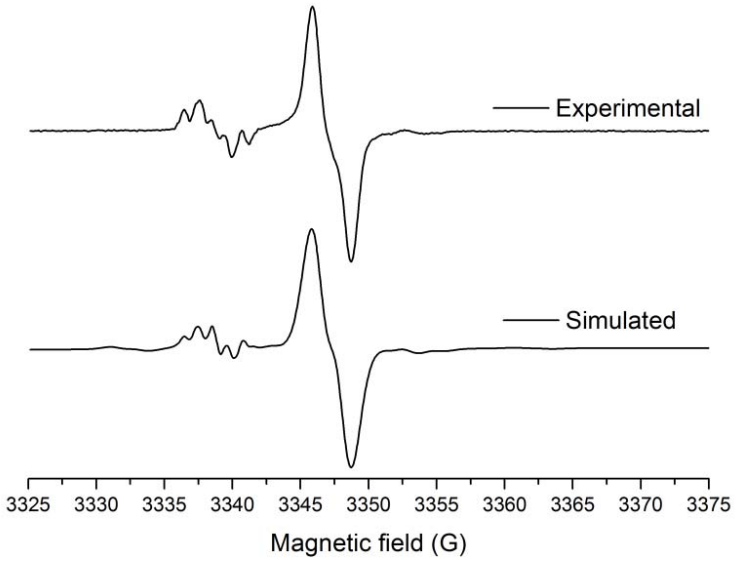

Figure 5. Experimental and simulated ESR spectra of 0.05 mM solution of radical cation $\mathbf{1}^{\bullet\bullet+}$ in CH_2Cl_2 at 240 K.

In order to demonstrate the reversibility of the system, we have carried out electrochemical redox reactions starting from $\mathbf{1}^{\bullet\bullet}$ that is oxidized to $\mathbf{1}^{\bullet\bullet+}$, then reduced to $\mathbf{1}^{\bullet-}$ and oxidized back to the diradical species using CH_2Cl_2 with $[(n\text{-}Bu)_4N]\ PF_6$ (0.1 M) as supporting electrolyte, Pt wire as a working electrode, and Ag/Ag+ as the reference electrode (Figure 6). We performed several cycles and the electrochemical oxidation and reduction processes were monitored by UV-Vis spectroscopy at the wavelength of 650 nm showing that the absorbance intensity is completely recovered after each step demonstrating the high reversibility and stability of the resulted species.

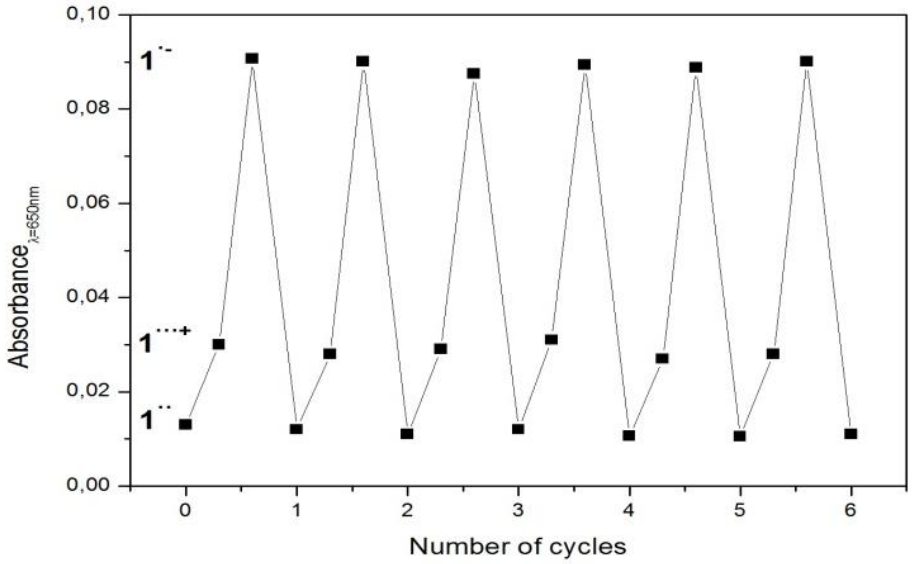

Figure 6. Evolution of the UV-Vis intensity at 650 nm recorded during the stepwise oxidation and reduction cycles of **1**••.

In conclusion, we have reported a diradical A-D-A triad composed by two PTM radical subunits connected through a TTF-vinylene bridge that can reversible modulate the optical, electronic and magnetic properties by one-electron reduction and oxidation in a reversible way. Interestingly, the suppression of the electron delocalization was observed when passing from the diradical to the anion radical mixed-valence species indicating the preferable localization of the unpaired electron on only one of the two PTM radical moieties. On the other hand, the switching from an almost negligible ferromagnetic (FM) magnetic interaction to a moderate-strong antiferromagnetic (AFM) interaction between TTF and PTM moieties was observed when the TTF bridge was oxidized. Finally, the system was found to be highly reversible and can be viewed as a promising building block for the development of molecular switches.

ASSOCIATED CONTENT

Supporting Information. General methods, synthesis and characterization, chemical reduction and oxidation of $\mathbf{1}^{\cdot\cdot}$, ESR spectra of $\mathbf{1}^{\cdot\cdot}$, $\mathbf{1}^{\cdot-}$ and $\mathbf{1}^{\cdot\cdot\cdot+}$ at different temperatures, and computational analysis are included.

AUTHOR INFORMATION

Notes

The authors declare no competing financial interests.

ACKNOWLEDGMENT

This work was supported by the DGI grant (CTQ2013- 40480-R), the Networking Research Center on Bioengineering, Biomaterials, and Nanomedicine (CIBER-BBN), and the Generalitat de Catalunya (grant 2014-SGR-17). M. S. is enrolled in the Material Science Ph.D. program of UAB and is grateful to MEC for a FPU predoctoral grant. S.V. and M.F. are thankful to the LabEx-Chemistry of Complex Systems for post-doctoral grants (ANR-10-LABX-0026CSC) and to the regional High-Performance Computing (HPC) center in Strasbourg for computational resources. We thank Amable Bernabé for the MALDI spectroscopy.

REFERENCES

(1) Nishida, S.; Morita, Y.; Fukui, K.; Sato, K.; Shiomi, D.; Takui, T.; Nakasuji, L. Spin Transfer and Solvato-/Thermochromism Induced by Intramolecular Electron Transfer in a Purely Organic Open-Shell System. *Angew. Chem. Int. Ed.* **2005**, *44*, 7277-7280.

(2) Yamamoto, Y.; et al. Photoconductive Coaxial Nanotubes of Molecularly Connected Electron Donor and Acceptor Layers. *Science* **2006**, *314*, 1761-1764.

(3) Scott, A.; Ricks, A. B.; Colvin, M. T.; Wasielewski, M. R. Comparing spin-selective charge transport through donor-bridge-acceptor molecules with different oligomeric aromatic bridges. *Angew. Chem. Int. Ed.* **2010**, *49*, 2904-2908.

(4) Kirk, M. L.; Shultz, D. A.; Stasiw, D. E.; Habel-Rodriguez, D.; Stein, B.; Boyle, P. D. Electronic and exchange coupling in a cross-conjugated D-B-A biradical: Mechanistic implications for quantum interference effects. *J. Am. Chem. Soc.* **2013**, *135*, 14713-14725.

(5) Sukegawa, J.; Schubert, C.; Zhu, X.; Tsuji, H.; Guldi, D. M.; Nakamura, E. Electron transfer through rigid organic molecular wires enhanced by electronic and electron-vibration coupling. *Nat. Chem.* **2014**, *6*, 899-905.

(6) Gilbert, M.; Albinssion, B. Photoinduced charge and energy transfer in molecular wires. *Chem. Soc. Rev.* **2015**, *44*, 845-862.

(7) Bergkamp, J. J.; Decurtins, S.; Liu, S. Current advances in fused tetrathiafulvalene donor-acceptor systems. *Chem. Soc. Rev.* **2015**, *44*, 863-874.

(8) Venneri, S.; Wilson, J.; Rawson, J. M.; Pilkington, M. Structural, Magnetic and DFT studies on a Charge Transfer Salt of a TTF-pyridyl-(1,5-diisopropyl)verdazyl Diradical Cation. *ChemPlusChem*, **2015**, *80*, 1624-1633.

(9) Rovira, C.; Ruiz-Molina, D.; Elsner, A.; Vidal-Gancedo, J.; Bonvoisin, J.; Launay, J.-P. Veciana, J. Influence of topology on the long-range electron-transfer phenomenon. *Chem. Eur. J.* **2001**, *7*, 240-250.

(10) Dumur, F.; *et al.* Novel Fused D-A Dyad and A-D-A Triad Incorporating Tetrathiafulvalene and p-Benzoquinone. *J. Org. Chem.*, **2004**, *69*, 2164-2177.

(11) Lloveras, V.; Vidal-Gancedo, J.; Ruiz-Molina, D.; Figueira-Duarte, T. M. Nierengarten, J. F.; Veciana, J.; Rovira, C. Influence of bridge topology and torsion on the intramolecular electron transfer. *Faraday Discuss.* 2006, **131**, 291-305.

(12) Hankache, J.; Wenger, O. S. Organic mixed valence. *Chem. Rev*. **2011**, *111*, 5138-5178.

(13) Lloveras, V.; Vidal-Gancedo, J.; Figuerira-Duarte, T. M.; Nierengarten, J.-F.; Novoa, J. J.; Mota, F.; Ventosa, N.; Rovira, C.; Veciana, J. Tunneling versus hopping in mixed-valence oligo- p -phenylenevinylene polychlorinated bis(triphenylmethyl) radical anions. *J. Am. Chem. Soc*. **2011**, *133*, 5818-583.

(14) Heckmann, A.; Lambert, C. Organic mixed-valence compounds: A playground for electrons and holes. *Angew. Chem. Int. Ed.* **2012**, *51*, 326-392.

(15) Elsner, O.; Ruiz-Molina, D.; Vidal-Gancedo, J.; Rovira, C.; Veciana, J. Ferromagnetic interactions between triphenylmethyl radicals through an organometallic coupler. *Chem. Commun.* **1999**, 579-580.

(16) Elsner, O.; Ruiz-Molina, D.; Ratera, I.; Vidal-Gancedo, J.; Rovira, C.; Veciana, J. Ferrocene as a ferromagnetic coupler. Synthesis and characterization of a ferrocene bridged polychlorotriphenylmethyl diradical. *J. Organomet. Chem.* **2001**, *637-639*, 251-257.

(17) Ito, A.; Nakano, Y.; Urabe, M.; Kato, T.; Tanaka, K. Triradical cation of p-phenylenediamine having two nitroxide radical groups: spin alignment mediated by delocalized spin. *J. Am. Chem. Soc*. **2006**, *128*, 1948-2953.

(18) Rajca, A.; Shiraishi, K.; Rajca, S. Stable diarylnitroxide diradical with triplet ground state. *Chem. Commun.* **2009**, 4372-4374.

(19) Suzuki, S.; et al. Trinitroxide-Trioxytriphenylamine: Spin-State Conversion from Triradical Doublet to Diradical Cation Triplet by Oxidative Modulation of a p-Conjugated System. *Angew. Chem. Int. Ed.* **2012**, *51*, 3193-3197.

(20) Shil, S.; Herrmann, C. Increasing Magnetic Coupling through Oxidation of a Ferrocene Bridge. *Inorg. Chem.* **2015**, *54*, 11733−11740.

(21) Bhattacharya, D.; Shil, S.; Misra, A.; Bytautas, L.; Klein, D. J. Borazine: Spin blocker or not? *Phys. Chem. Chem. Phys.* **2015**, *17*, 14223-14237.

(22) Ratera, I.; Veciana, J. Playing with organic radicals as building blocks for functional molecular materials. *Chem. Soc. Rev.* **2012**, *41*, 303–349.

(23) Grisanti, L.; D'Avino, G.; Painelli, A.; Guasch, J.; Ratera, I.; Veciana, J. Essential state models for solvatochromism in donor-acceptor molecules: The role of the Bridge. *J. Phys. Chem. B* **2009**, *113 (14),* 4718–4725.

(24) D'Avino, G.; Grisanti, L.; Guasch, J.; Ratera, I.; Veciana, J.; Painelli, A. Bistability in Fc-PTM crystals: The role of intermolecular electrostatic interactions. *J. Am. Chem. Soc.* **2008**, *130 (36),* 12064–12072.

(25) Ratera, I.; Ruiz-Molina, D.; Vidal-Gancedo, J.; Novoa, J. J.; Wurst, K.; Letard, J.-F.; Rovira, C.; Veciana, J. Supramolecular photomagnetic materials: photoinduced dimerization of ferrocene-based polychlorotriphenylmethyl radicals. *Chem. Eur. J.* 2004, **10**, 603-616.

(26) Guasch, J.; *et al.* Induced self-assembly of a tetrathiafulvalene-based open-shell dyad through intramolecular electron transfer. *Angew. Chem. Int. Ed*. **2012**, *51*, 11024-11028.

(27) Guasch, J.; *et al.* Intra- and intermolecular charge transfer in aggregates of tetrathiafulvalene-triphenylmethyl radical derivatives in solution. *J. Am. Chem. Soc*. **2013**, *135*, 6958-6967.

(28) Souto, M.; *et al.* Thermomagnetic molecular system based on TTF-PTM radical: Switching the spin and charge delocalization. *J. Phys. Chem. Lett*. **2013**, *4*, 2721-2726.

(29) Andreu, R.; Garín, J.; Orduna, J.; Savíron, M.; Cousseau, J.; Gorgues, A.; Morisson, V.; Nozdryn, T.; Becher, J.; Clausen, R. P.; Bryce, M. R.; Skabara, P. J.; Dehaen, W. The first allylic alcohol derivatives of tetrathiafulvalene. A route to new covalently linked donors. *Tetrahedron Lett.* **1994**, *35*, 9243-9246.

(30) Andreu, R.; Garín, J.; Orduna, J.; Savirón, M.; Uriel, S.; Cousseau, J.; Morrison, V.; Gorgues, A. *Synth. Met.* **1995**, *70*, 1111-1112.

(31) Terkia-Derdra, N.; *et al.* π Conjugation Across the Tetrathiafulvalene Core: Synthesis of Extended Tetrathiafulvalene Derivatives and Theoretical Analysis of their Unusual Electrochemical Properties. *Chem. Eur. J.*, 2000, **6**, 1199-1213.

(32) Saha, E.; Johansson, A.; Flood, H.; Tseng, H.; Zink, J. I.; Stoddart, J. F. A photoactive molecular triad as a nanoscale power supply for a supramolecular machine. *Chem. Eur. J.*, **2005**, *11*, 6846-6858.

(33) Hoi, S. H.; Frisbie, C. D. Transition from Tunneling to Hopping Transport in Long, Conjugated Oligo-imine Wires Connected to Metals. *J. Am. Chem. Soc*., **2010**, *132*, 16191-16201.

(34) Luo, L.; Balhorn, L.; Vlaisavljevich, B.; Ma, D.; Gagliardi, L.; Frisbie, C. D. Hopping Transport and Rectifying Behavior in Long Donor–Acceptor Molecular Wires. *J. Phys. Chem. C* **2014**, *118*, 26485-26497.

(35) Souizi, A.; Robert, A.; Batail, P.; Lahcene, L. Acid-mediated trans-cis isomerization of substituted tetrathiafulvalenes. Selective precipitation of the trans isomer. *J. Org. Chem.* **1987**, *52*, 1611-1613.

(36) Müllen, K.; Wegner, G. Electronic Materials: the Oligomer Approach, Wiley-VCH: Weinheim, Germany; 1998.

(37) Chiang, P.-T.; Chen, N.-C.; Lai, C.-C.; Chiu, S.-H. Direct observation of mixed-valence and radical cation dimer states of tetrathiafulvalene in solution at room temperature: association and dissociation of molecular clip dimers under oxidative control. *Chem. Eur. J.* **2008**, *14*, 6546 – 6552.

(38) Hasegawa, M.; Doigoku, K.; Hashimoto, K.; Nishikawa, H.; Iyoda, M. Face-to-Face Dimeric Tetrathiafulvalenes and Their Cation Radical and Dication Species as Models of Mixed Valence and Dimer States. *Bull. Chem. Soc. Jpn.* **2012**, *85*, 51-60.

(39) Tian, J.; Ding, Y.-D.; Zhou, T.-Y.; Zhang, K.-D.; Zhang, X.; Zhao, Z.; Wang, H.; Zhang, D.-W.; Liu, Y.; Li, Z.-T. Self-assembly of three-dimensional supramolecular polymers through cooperative tetrathiafulvalene radical cation dimerization. *Chem. Eur. J.* **2014**, *20*, 575-584.

(40) Gautier, N.; Dumur, D.; Lloveras, V.; Vidal-Gancedo, J.; Veciana, J.; Hudhomme, P. Intramolecular Electron Transfer Mediated by a Tetrathiafulvalene Bridge in a Purely Organic Mixed-Valence System. *Angew. Chem.* **2003**, *115*, 2871-2874.

(41) Dumur, F.; *et al.* Novel Fused D-A Dyad and A-D-A Triad Incorporating Tetrathiafulvalene and p-Benzoquinone. *J. Org. Chem.* **2004**, *69*, 2164-2177.

(42) Jia, C.; *et al.* An Experimental and Computational Study on Intramolecular Charge Transfer: A Tetrathiafulvalene-Fused Dipyridophenazine Molecule. *Chem. Eur. J.* **2007**, *13*, 3804-3812.

(43) Otón, F.; Lloveras, V.; Mas-Torrent, M.; Vidal-Gancedo, J.; Veciana, J.; Rovira, C. Coupling tetracyanoquinodimethane to tetrathiafulvalene: A fused TCNQ-TTF-TCNQ triad. *Angew. Chem.* **2011**, *123*, 11094-11098.

(44) Calbo, J.; Argó, J.; Otón, F.; Lloveras, V.; Mas-Torrent, M.; Vidal-Gancedo, J.; Veciana, J.; Rovira, C.; Ortí, E. Tetrathiafulvalene-based mixed-valence acceptor-donor-acceptor triads: A joint theoretical and experimental approach. *Chem. Eur. J.* **2013**, *19*, 16656-16664.

(45) Calbo, J.; Aragó, J.; Ortí, E. Theoretical study of the benzoquinone–tetrathiafulvalene–benzoquinone triad in neutral and oxidized/reduced states. *Theor. Chem. Acc.* **2013**, *132*, 13.

Electronic Supporting Information (16 pages)

Three Redox States of a Diradical Acceptor-Donor-Acceptor Triad: Gating the Magnetic Coupling and the Electron Delocalization

Manuel Souto, [†] *Vega Lloveras,* [†] *Sergi Vela,* [‡] *Maria Fumanal,* [‡] *Imma Ratera,* [†,*] *and Jaume Veciana*[†,*]

[†] Institut de Ciència de Materials de Barcelona (ICMAB-CSIC)/CIBER-BBN, Campus Universitari de la UAB, 08193 Cerdanyola del Vallès (Barcelona), Spain

[‡] Laboratoire de Chimie Quantique, Université de Strasbourg, 4 rue Blaise Pascal, F-67000 Strasbourg, France

*E-mail: vecianaj@icmab.es, iratera@icmab.es

Table of Content

General methods for synthesis and characterization

All reagents and solvents employed for the syntheses were of high purity grade and were purchased from Sigma-Aldrich Co., Merck, and SDS. ^{1}H NMR spectra were recorded using a Bruker Avance 250, 400, 500 instruments and Me_4Si as an internal standard. Infrared spectra were recorded with Spectrum One FT-IR Spectroscopy instrument and UV/Vis/NIR spectra were measured using Cary 5000E Varian. ESR spectra were performed with a Bruker ESP 300 E equipped with a rectangular cavity T102 that works with an X-band (9.5 GHz). The solutions were degassed by argon bubbling before the measurements. LDI/TOF MS were recorded in a Bruker Ultraflex LDI-TOF spectrometer. Cyclic voltammetry measurements were obtained with a potentiostat 263a from EG&G Princeton Applied Research in a standard 3 electrodes cell. Dry solvents were used in the chemical reactions and in the cyclic voltammetries. The solvents used for optical spectroscopy and ESR measurements were of HPLC grade (ROMIL-SpS). In addition, for cyclic voltammetry experiments, CH_2Cl_2 was filtered over basic alumina to eliminate the acidic residues.

Synthesis of 2:

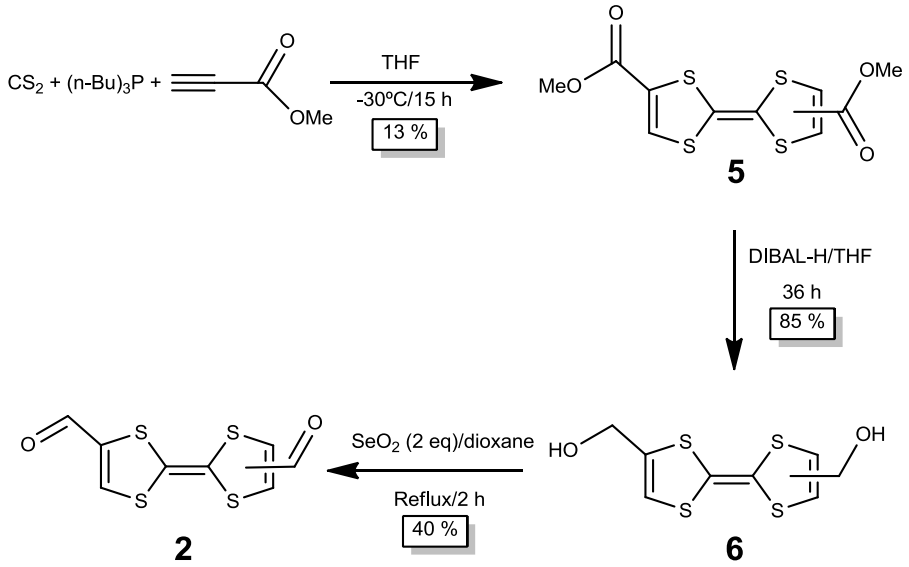

Scheme S1. Synthesis of the diformyl-TTF derivative **2**.

Compound 5: Tributylphosphine (20.3 g, 0.1 mol) was added dropwise to a solution of 10 ml of carbon disulfide in 50 ml of tetrahydrofuran at -10ºC under inert conditions and the deep maroon solution was stirred at room temperature for 1 hour. Next the mixture was cooled to -40ºC and a solution of methyl propiolate (8.4 g, 0.1 mol) in 20 ml of tetrahydrofuran was added dropwise. The temperature was maintained between -30ºC and -50ºC during the addition. The solution was warmed to room temperature and stirred overnight. Finally solvents were evaporated under reduced pressure, the residue was stirred with ether to crash out the product that and was filtered and washed with Et_2O. Then the product was purified by column chromatography using CH_2Cl_2 as eluent to give 4.2 g (13 %) of the red microcrystalline powder **5**. Characterization: ^{1}H-NMR (250 MHz, $CDCl_3$, δ(ppm): 7.35 (d, 2H, CH, J = 7.34 Hz); 3.82 (s, 6H, CH_3). FT-IR (ν cm^{-1}): 2956 (w); 2922 (w); 2852 (w); 1712 (s, C=O); 1548 (s); 1434 (m); 1244 (s); 1199 (m); 1045 (m); 940 (m); 829 (m); 820 (m); 763 (m); 725 (m). LDI-TOF (positive mode): *m/z* (amu/e$^-$): 320.377 ($M^{+\cdot}$).

Compound 6: 30 ml of DIBAL-H (1 M in THF) was added dropwise to a solution of **5** (1 g, 3.12 mmol) in 60 ml of tetrahydrofuran cooled at -70ºC under strict inert conditions. The color of the solution changes from red to yellow during the first hour of reaction. Then the solution was allowed to warm to room temperature and stirred overnight. The absence of TTF diester was confirmed by TLC and the reaction was hydrolyzed by the carefully addition of 10 ml of MeOH/HCl 12 M (3:1) mixture to the solution previously cooled with an ice bath. Then ether was

added to the mixture and the organic phase was washed with three portions of water (100 ml), dried with anhydrous $MgSO_4$ and solvents were evaporated under reduced pressure. Finally the product was purified by column chromatography of silica gel using a mixture of ether and hexane to obtain 738 mg (85 %) of TTF diol **6** as a light brown solid. Characterization: ^{1}H-NMR (250 MHz, DMSO-D_6, δ(ppm): 6.52 (s, 2H); 5.48 (t, 2H, *J* = 5.9 Hz); 4.20 (d, 4H, *J* = 5.84 Hz, CH_2OH). FT-IR (ν cm^{-1}): 3338 (s, OH); 3256 (s, OH); 2947 (m); 2918 (m); 2858 (m); 1587 (w); 1459 (m); 1443 (m); 1430 (m); 1369 (m); 1228 (m); 1092 (s); 1012 (s); 969 (m); 839 (w); 773 (w); 741 (w) 709 (w). LDI-TOF (positive mode): *m/z* (amu/e$^-$): 263.926 ($M^{+\cdot}$).

Compound 2: A solution of **6** (750 mg, 2.84 mmol) and 2 equivalents of selenium dioxide (630 mg)was heated under reflux for 2 h in dry dioxane (70 mL); the solution turned from yellow to dark red. Cooling of the solution resulted in the formation of a black precipitate of elemental selenium, which was filtered and washed thoroughly with dichloromethane. The solvent mixture was then evaporated under reduced pressure to produce a dark red oil, which was purified by SiO_2 column chromatography (eluent: hexane: Et_2O) to obtain **2** (295 mg, 40%) as a brownish powder. Characterization: ^{1}H-NMR (250 MHz, DMSO-D_6, δ(ppm): 9.54 (s, 2H, CHO); 8.27 and 8.28 (s, 2H). LDI-TOF (positive mode): *m/z* (amu/e$^-$): 259.729($M^{+\cdot}$).

Synthesis of diradical 1$^{\cdot\cdot}$:

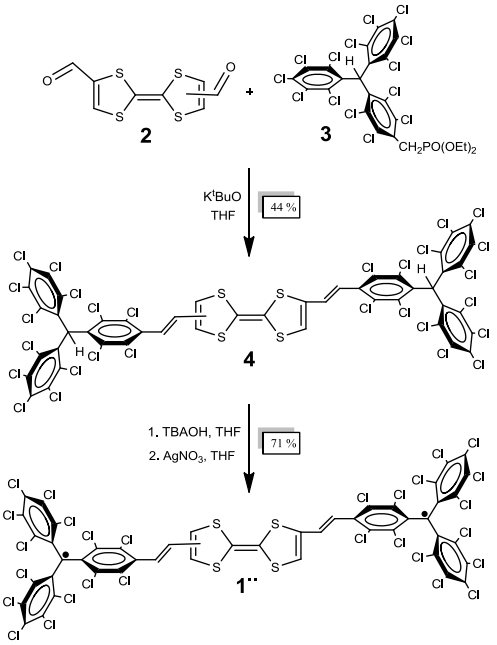

Scheme S2. Final synthetic steps of diradical **1**$^{\cdot\cdot}$. TBAOH = Tetrabutylammonium hydroxide.

Compound 4: 585 mg (0.67 mmol) of the phosphonated PTM derivative **3** were dissolved in 60 ml of anhydrous THF under strict inert conditions. The solution was cooled down to -78 ºC. Next, 150 mg (1.33 mmol) of potassium *tert*-butoxide were added and stirred for 20 minutes to form the yellow-orange ylide. Then 101 mg (0.39 mmol) of **2** were added and the reaction was warmed up to room temperature and stirred for 3 days. Then the mixture was washed with water, dried with anhydrous $MgSO_4$ and solvents were evaporated under reduced pressure. Finally the product was purified by column chromatography of silica gel using a mixture of ether and hexane to obtain to obtain 250 mg (44 %) of **4** (*E*+*Z*) as a red powder. Characterization: ^{1}H-NMR (250 MHz, C_6D_6, δ(ppm): 7.22 (s, 1H, αH); 7.21 (s, 1H, αH); 6,32 (dd, *J* = 16.0, 2.5 Hz, 2H, CH=CH); 6.18 (dd, *J* = 16.1, 6.2 Hz, 2H CH=CH); 5.53 (s, 2H, TTF). FT-IR (ν cm^{-1}): 2956 (w); 2922 (w); 2855 (w); 1614 (m, CH=CH); 1528 (m); 1455 (m); 1369 (m); 1336 (s); 1296 (s); 1276 (w); 1238 (w); 1206 (w); 1137 (m); 944 (m); 863 (w); 826 (w); 808 (s); 778 (m) 751 (m); 719 (w); 693 (m). LDI-TOF (positive mode): *m/z* (amu/e$^-$): 1704.559 ($M^{+\cdot}$); (negative mode): 1704.147 ($M^{-\cdot}$). Cyclic voltammetry (Bu_4NPF_6 0.15 M in CH_2Cl_2 as electrolyte): $E_{½}{}^1$=0.621 V; $E_{½}{}^2$=1.103 V.

Diradical 1¨: 70 mg (0.04 mmol) of **4** were dissolved in 20 ml of distilled THF and 100 μl (0.10 mmol) of TBAOH 1.0 M in MeOH were added and stirred for 3 h under Ar atmosphere. Then 20 mg (0.12 mmol) of $AgNO_3$ were added and immediately stirred for 10 minutes. The solution was concentrated and the product was purified by flash column chromatography of silica gel using hexane as eluent to produce 50 mg (71 %) of a brownish powder. Characterization: FT-IR (ν cm^{-1}): 2952 (w); 2922 (w); 2855 (w); 1603 (m, CH=CH); 1504 (m); 1460 (m); 1376 (w); 1355 (2); 1335 (s); 1320 (s); 1278 (m); 1259 (s); 1162 (m); 1138 (w); 1118 (w); 935 (s); 866 (w); 817 (m); 777 (m) 752 (m); 735 (m); 711 (m). UV-VIS-NIR (CH_2Cl_2, λ_{max} in nm, ε in $M^{-1}\cdot cm^{-1}$): 299 (30752); 325 (27461); 387 (26506); 426 (16192); 522 (6303); 938 (1087). LDI-TOF (positive mode): *m/z* (amu/e^-): 1700.947 $[M]^{+\cdot}$; 1630.060 $[M\text{-}70]^+$; (negative mode): 1704.913 $[M]^{-\cdot}$; 1632.412 $[M\text{-}70]^+$. Cyclic voltammetry (Bu_4NPF_6 0.15 M in CH_2Cl_2 as electrolyte): $E_{½}^1$= -0.213 V; $E_{½}^2$= 0.591 V; $E_{½}^3$ =1.064 V. ESR (Toluene:CH_2Cl_2): g = 2.0027; a_1(H)=0.8 G (Half field at 1675 G).

^{1}H-NMR of 4

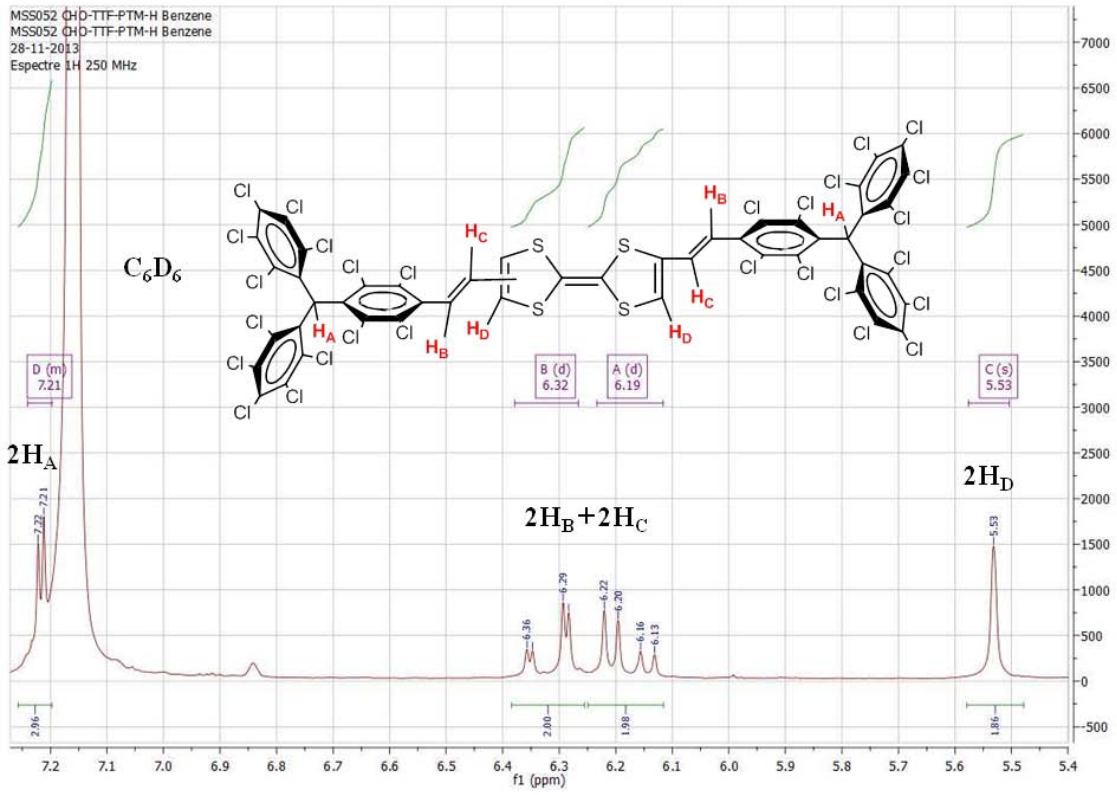

Figure S1. ^{1}H-NMR spectrum of compound **4** in C_6D_6 and protons observed in the ^{1}H-NMR spectrum.

Cyclic Voltammetry of 4

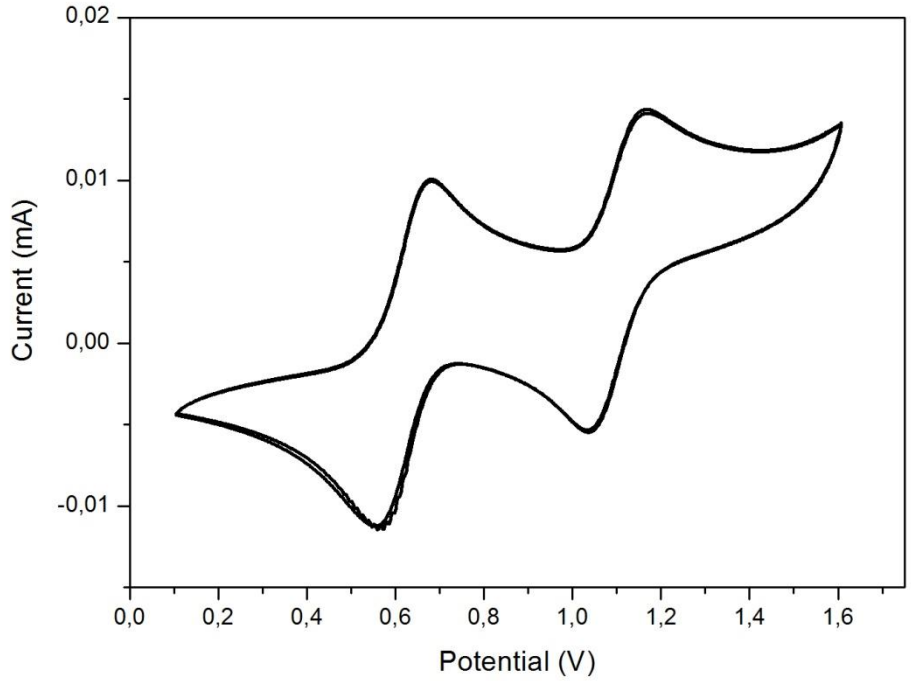

Figure S2. Cyclic voltammetry of solution of compound **4** in CH_2Cl_2 vs. Ag/AgCl using *n*-Bu_4PF_6 (0.1 M) as electrolyte at 300 K under argon at a scan rate of 0.1 V/s.

UV-vis spectrum of 4

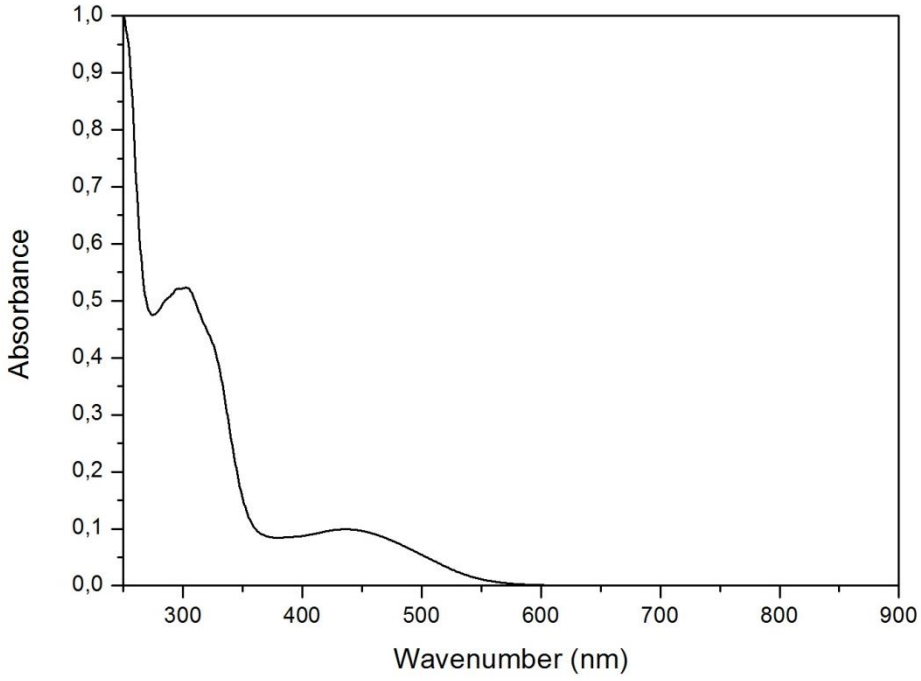

Figure S3. UV-Vis spectrum of a solution 0.05 mM of compound **4** in CH_2Cl_2 (black line).

IR spectra of 4 and 1¨

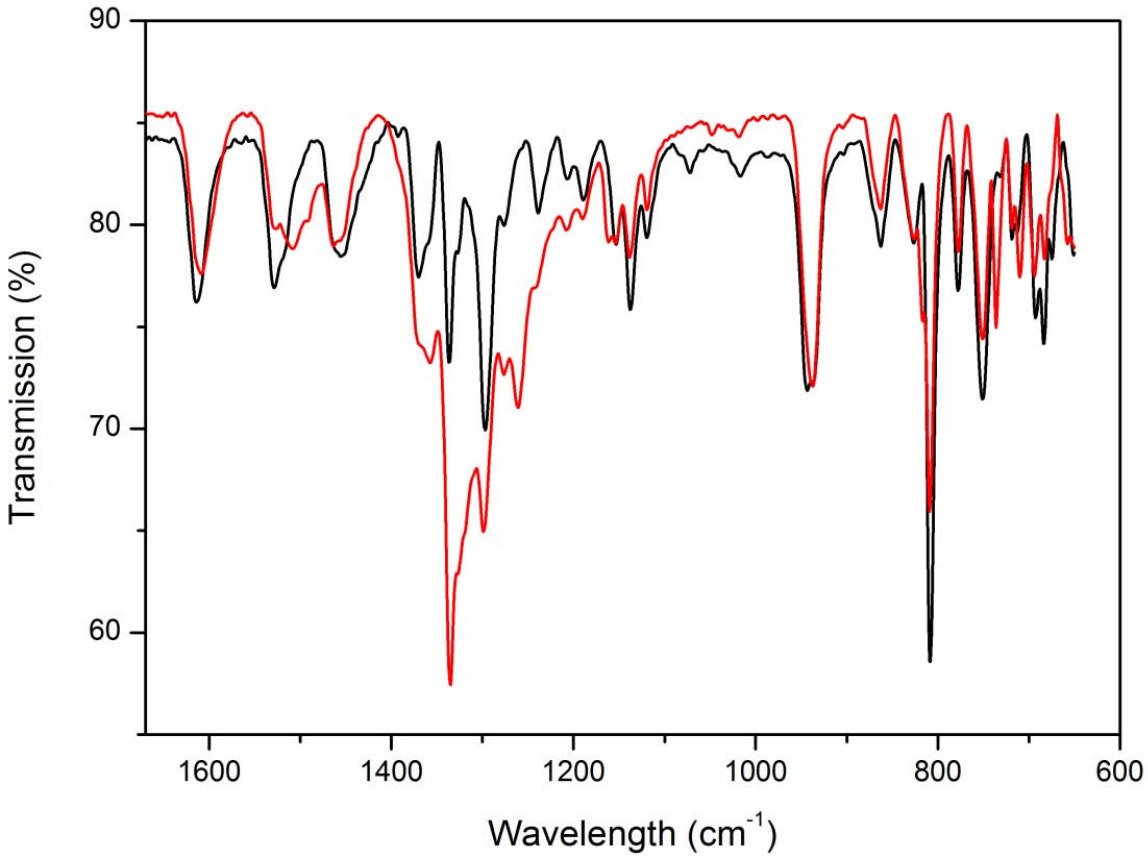

Figure S4. FT-IR spectra of compounds **4** (black line) and diradical **1¨** (red line).

MALDI-TOF spectrum of 1··

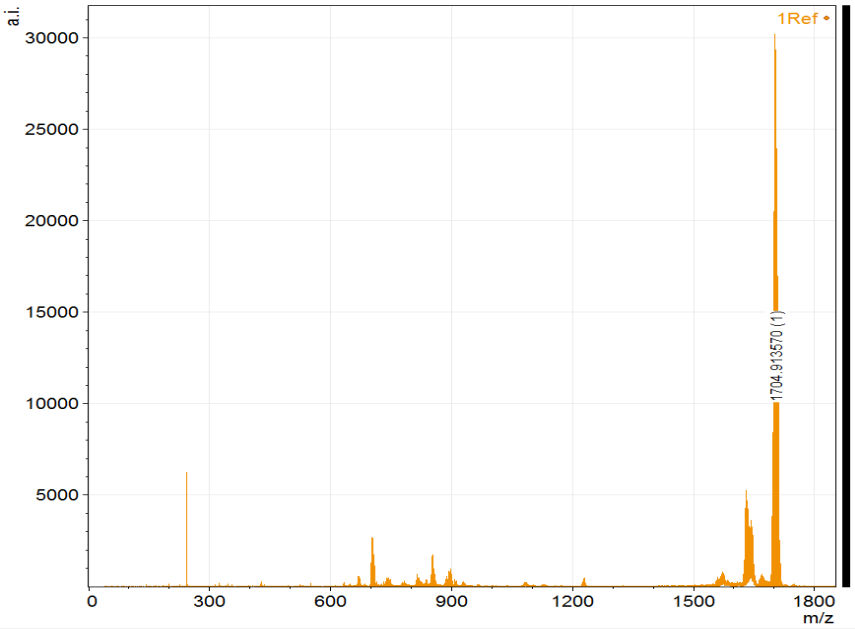

Figure S5. MALDI-TOF spectrum of diradical **1¨** (negative mode) indicating the molecular mass of the compound.

Electrospray ionization for mass spectrometry (ESI-MS)

Instrument: LC/MSD-TOF (2006) (Agilent Technologies)
Intrumental conditions:

Capillary: 3.5 KV (negative)
Fragmentor: 225 V
Gas temperature: 325ºC
Nebulizing Gas: N_2 Pressure = 15 psi
Drying Gas: N_2 Glow = 7.0 l /min

Sample introduction. Samples (microliters) are introduced into the source with an HPLC system (Agilent 1100), using a mixtue of H_2O:CH_3CN 1:1 as eluent (100 ml/min),

ESI-MS spectrum of compound 4

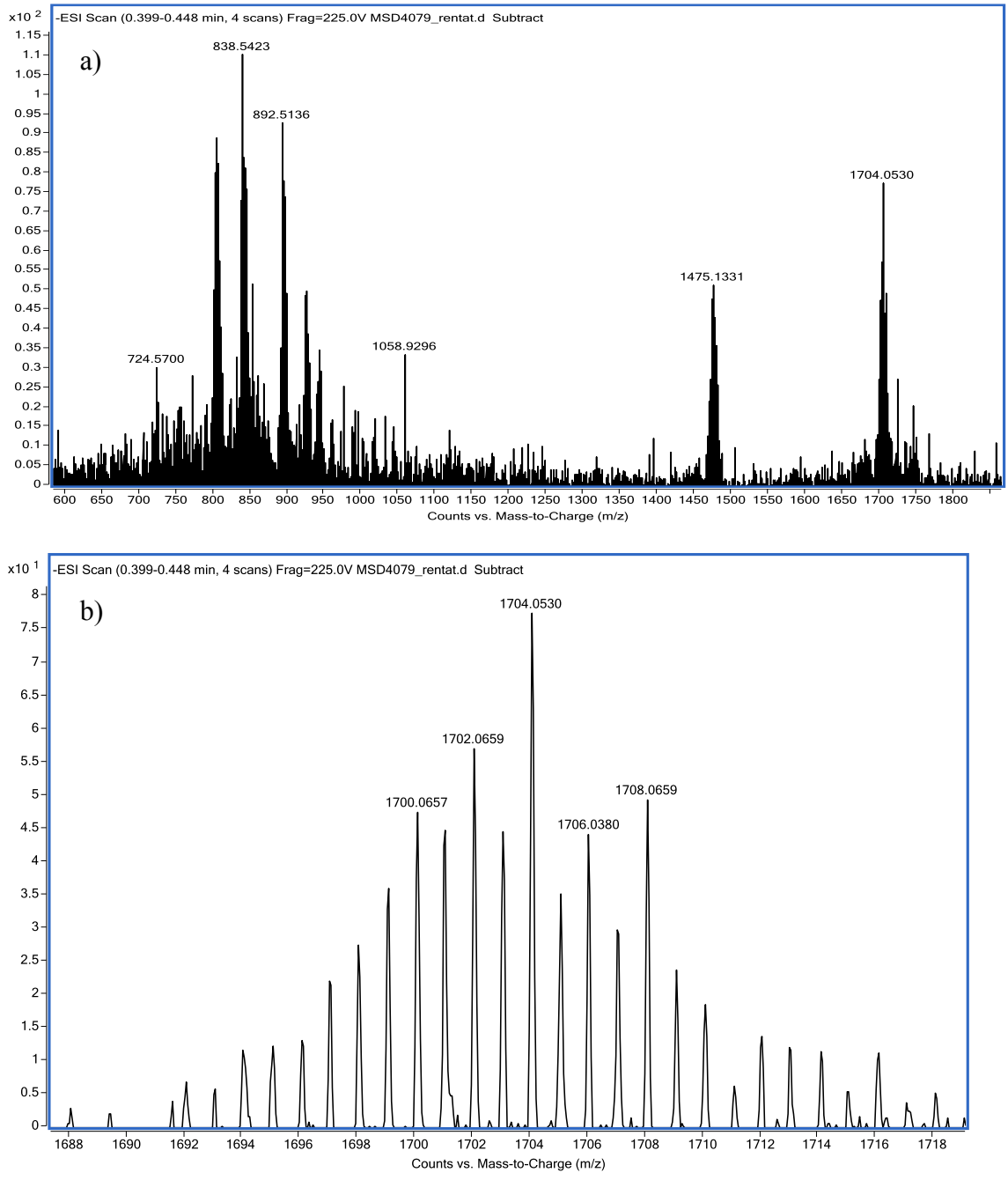

Figure S6. a) ESI-MS spectrum of compound **4** (mz/1705.06) and b) mass isotopic distribution of **4** (negative mode).

ESI-MS spectrum of compound 1··

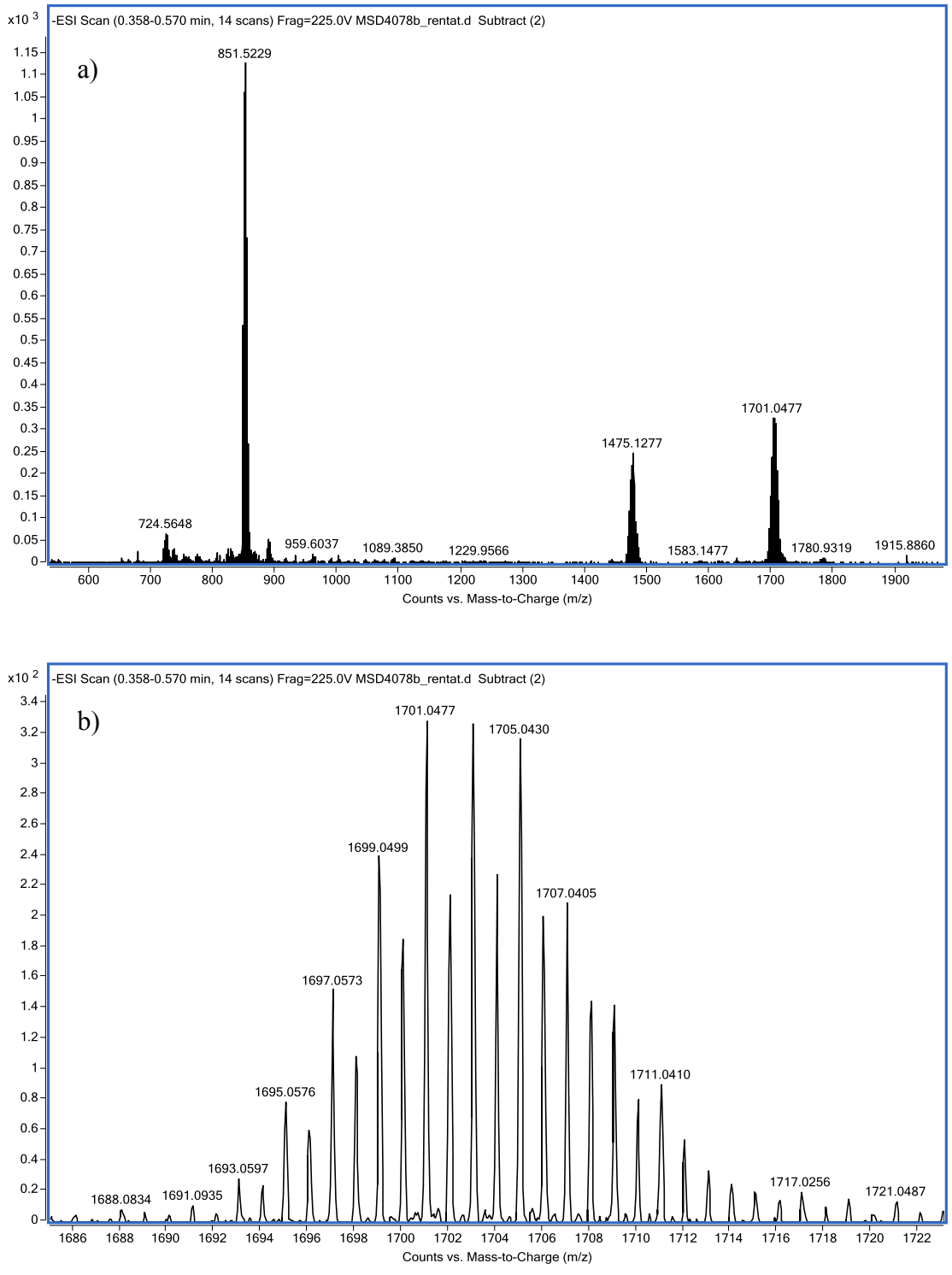

Figure S7. a) ESI-MS spectrum of compound **1··** (mz/1703.04) and b) mass isotopic distribution of **1··** (negative mode).

Chemical reduction of $1^{\cdot\cdot}$

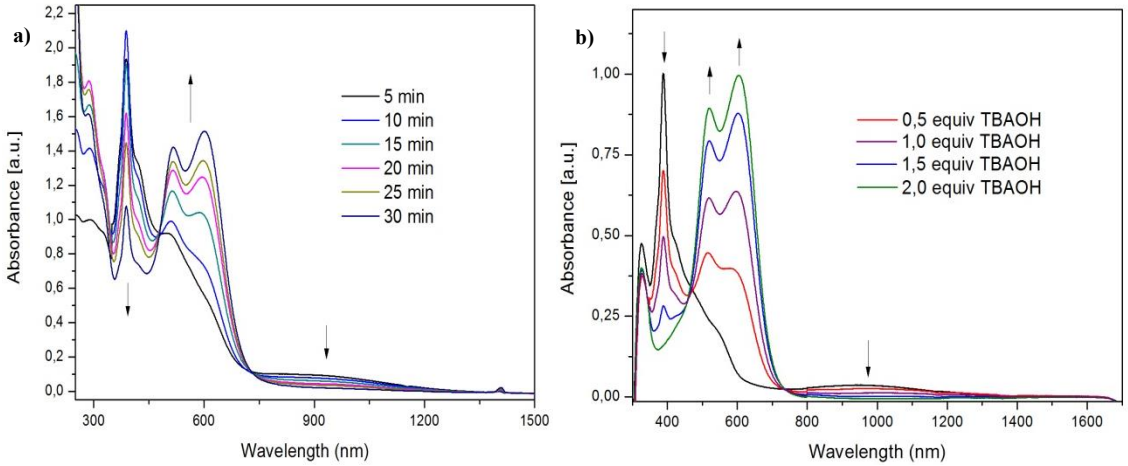

Figure S8. (*a*) Evolution of the UV-vis-NIR during the course of the formation of radical anion mixed-valence $\mathbf{1}^{\cdot-}$ in CH_2Cl_2 with metallic Cu. **(b)** Evolution of the UV-vis-NIR spectra during the course of the reduction of diradical $\mathbf{1}^{\cdot\cdot}$ to the formation of the radical anion $\mathbf{1}^{\cdot-}$ (1 equiv.) followed by the dianaion $\mathbf{1}^{2-}$ (2 equiv.) in THF arising from the subsequent addition of equivalent amounts of tetrabutylammonium hydroxide (TBAOH) until the formation of dianion.

Chemical oxidation of $1^{\cdot\cdot}$

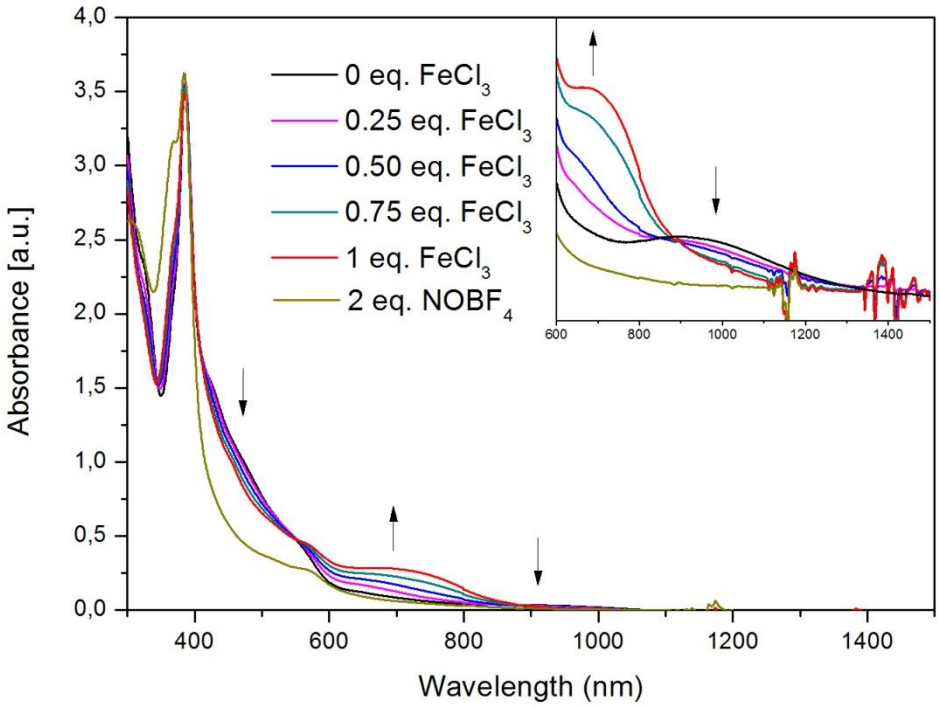

Figure S9. Evolution of the UV-vis-NIR spectra during the course of the oxidation of diradical $\mathbf{1}^{\cdot\cdot}$ in CH_2Cl_2 arising from the subsequent addition of equivalent amounts of $FeCl_3$ until the formation of $\mathbf{1}^{\cdot\cdot+}$ (red line) and further oxidation using nitrosium tetrafluoroborate to form $\mathbf{1}^{++}$ (brown line).

ESR of 1$^{\cdot\cdot}$

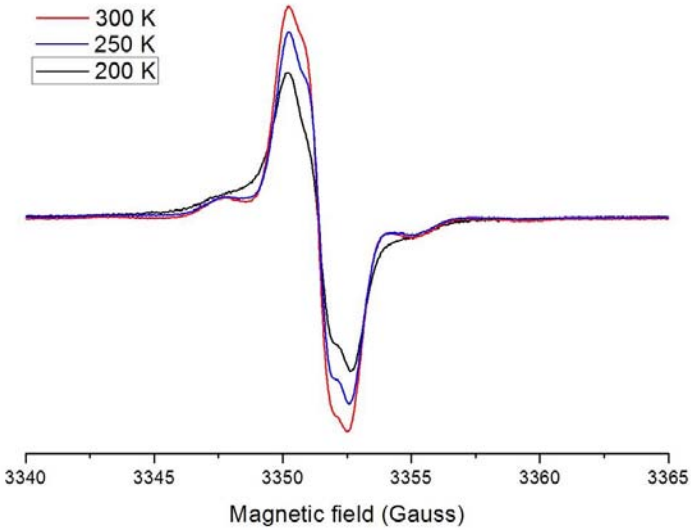

Figure S10. ESR spectra of 0.05 mM solution of diradical **1**$^{\cdot\cdot}$ in CH_2Cl_2 at 300 (red line), 250 (blue line) and 200 K (black line).

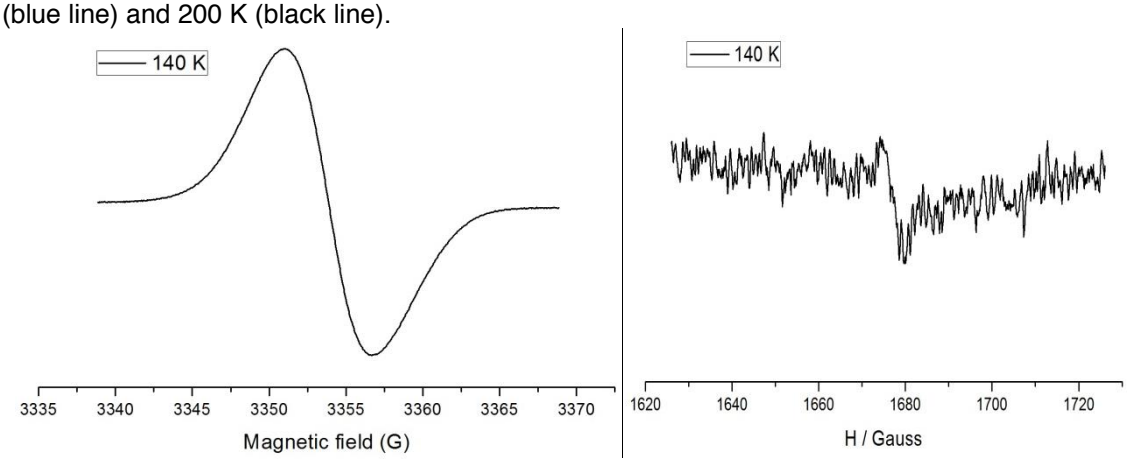

Figure S11. a) ESR spectra of 1 mM solution of diradical **1**$^{\cdot\cdot}$ in CH_2Cl_2 at 140 K. b) ESR spectra of 1 mM solution of diradical **1** in CH_2Cl_2 at 140 K at the half-field region.

ESR of radical-anion 1$^{\cdot-}$

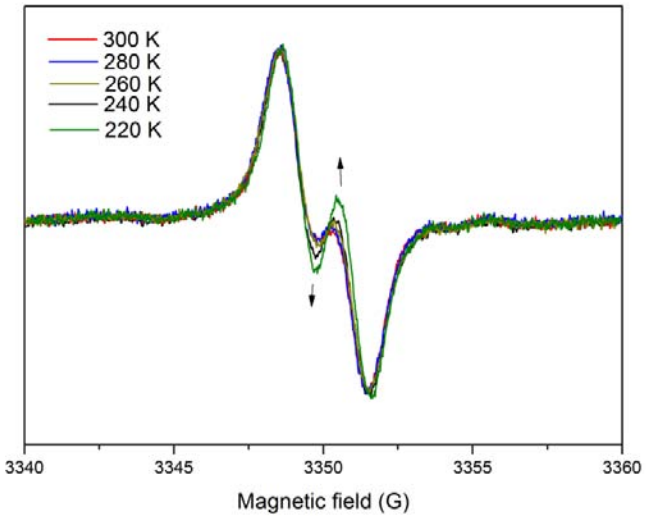

Figure S12. ESR spectra of 0.05 mM solution of mixed-valence **1**$^{\cdot-}$ in toluene/CH_2Cl_2 at 300 (red line), 280 (blue line), 260 (brown line), 240 (black line) and 220 K (green line).

ESR of triradical cation $1^{\bullet\bullet\bullet+}$

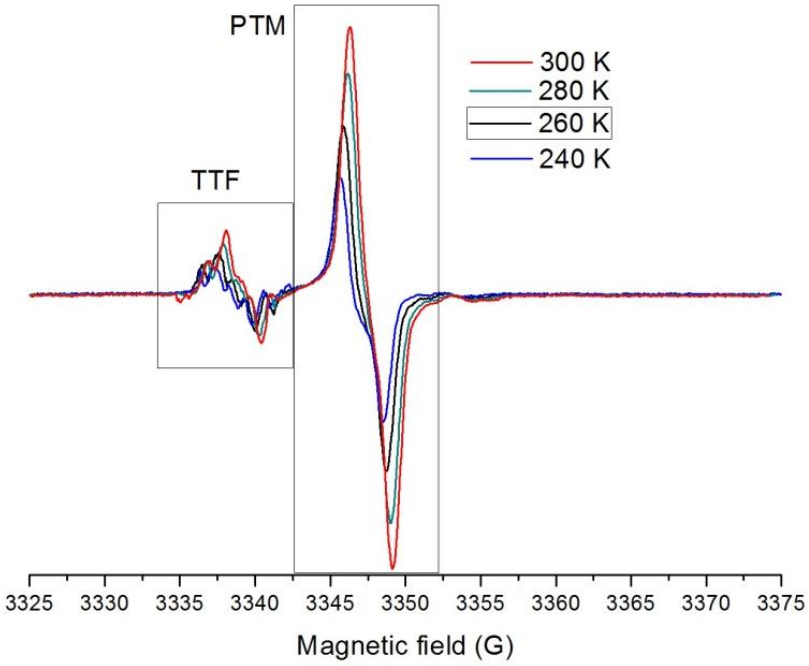

Figure S13. ESR spectra of 0.05 mM solution of triradical cation $\mathbf{1}^{\bullet\bullet\bullet+}$ in CH_2Cl_2 at 300 (red line), 280 (green line), 260 (black line) and 240 (blue line).

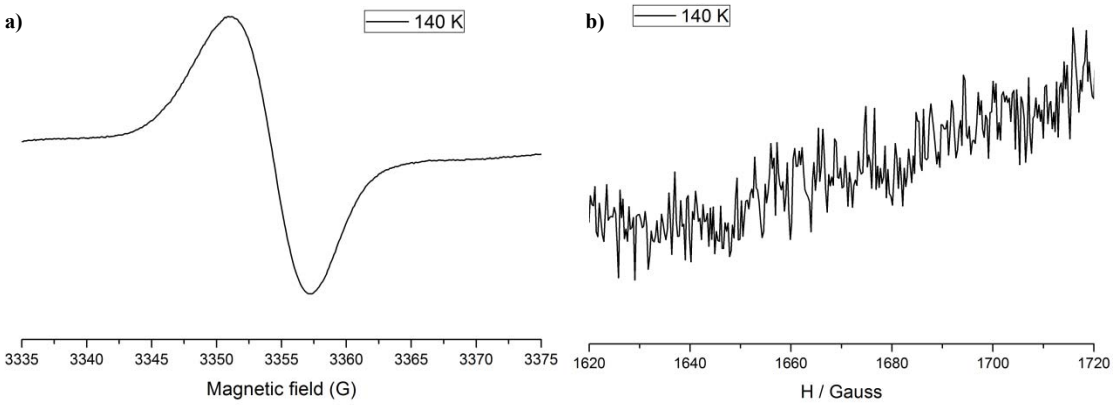

Figure S14. a) ESR spectra of 1 mM solution of triradical cation $\mathbf{1}^{\bullet\bullet\bullet+}$ CH_2Cl_2 at 140 K. b) ESR spectra of 1 mM solution of triradical cation $\mathbf{1}^{\bullet\bullet\bullet+}$ in CH_2Cl_2 at 140 K at the half-field region.

Computational Details

Structures. The molecular geometries of the diradical (**1**¨) and triradical cation (**1**¨˙⁺) species have been optimized in their low-spin (LS, Singlet for **1**¨, Doublet for **1**¨˙⁺) and high-spin states (HS, Triplet for **1**¨, Quadruplet for **1**¨˙⁺), both for the *Z* and *E* isomers. All calculations have been performed at the UB3LYP/TZVP level using the D2 dispersion correction of Grimme[S1] as implemented in Gaussian 09.[S2] Dichloromethane solvent has been modelled using the PCM method.

Magnetic Properties. The magnetic exchange couplings (J_{AB}) have been evaluated on those structures at the same level of calculation. For **1**¨, we have calculated the energy of the triplet and Broken-Symmetry singlet and their energy difference has been directly used to compute J_1 using the isotropic Heisenberg Hamiltonian $\hat{H} = -2\sum_{A,B}^{N} J_{AB}\hat{S}_A\hat{S}_B$. In turn, for the triradical cation **1**¨˙⁺, we have calculated the energy of one quadruplet and three doublet states (one for each possible combination of two unpaired alpha and one beta electrons on the three magnetic units) and the resulting energy differences have been used to extract J_{1-3}.

Optical Properties. The absorption spectra have been calculated on the optimized geometries of the *Z* isomer of the neutral diradical and cationic-triradical species in their HS state. We have used the UB3LYP/TZP scheme as implemented in ADF 2013.[S3] Dichloromethane has been modelled using the PCM method.

Computational analysis of 1¨ and 1¨˙⁺:

Magnetic Properties. The ground state of **1**¨ is an open-shell singlet, with the two unpaired electrons localized in the PTM units (see Figure S15 and Table S1). They are coupled by an almost-negligible magnetic interaction (J_1, see Figure S16 and Table S2 and), whose strength indicates that no magnetic ordering would be observed even at low temperatures and that the system would effectively behave as paramagnet, with *ca.* 75% population of triplet states. This is consistent with the CV measurements and with the observation of the Δm_s = 2 transitions in the ESR spectrum.

In turn, the ground state of **1**¨˙⁺ is a doublet with three unpaired electrons localized in the TTF and PTM (x2) units (see Figure S17). The calculations indicate that the weak coupling between PTM units observed for **1**¨ is maintained, whereas moderately-strong antiferromagnetic (AFM) interactions appear between the oxidized TTF and each of the PTM moieties ($J_2 \approx J_3 \approx$ –60 cm^{-1}).

Finally, it is worth mentioning that the anionic monoradical compound **1**¨⁻ has not been analyzed due to the well-known difficulty of describing mixed-valence states with DFT.[S4-S6]

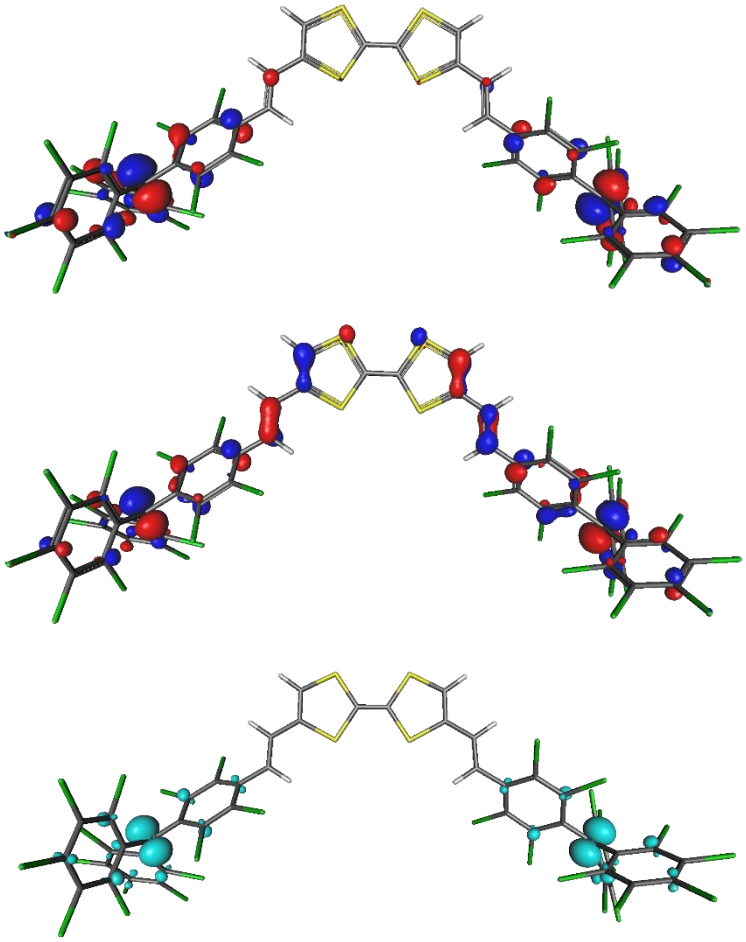

Figure S15. Singly-Occupied Molecular Orbital (SOMO) and spin density distribution obtained for the HS states of $\mathbf{1}^{\cdot\cdot}$ (Isomer Z). SOMO isovalue = 0.04, Spin Density isovalue = 0.01.

Table S1. Spin density contained in the different constituents of $\mathbf{1}^{\cdot\cdot}$ and $\mathbf{1}^{\cdot\cdot\cdot+}$.

	$\mathbf{1}^{\cdot\cdot}$		$\mathbf{1}^{\cdot\cdot\cdot+}$	
Fragment	***Z***	***E***	***Z***	***E***
TTF	0.040	0.072	0.974	0.975
Vinylene Bridge	0.014	0.064	0.050	0.119
PTM #1	0.972	0.889	0.988	0.918
PTM #2	0.974	0.974	0.988	0.989
Total	2.000	2.000	3.000	3.000

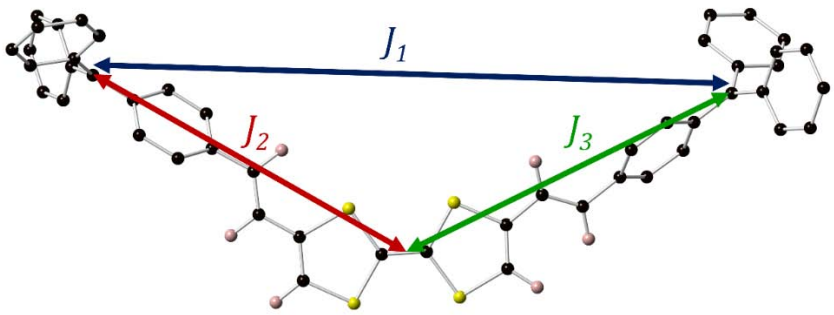

Figure S16. Representation of the magnetic interactions between the potential spin-carrying units of **1**. For clarity, the Cl atoms of the PTM moieties are not shown.

Table S2. Magnetic exchange couplings (J_{AB}, value in cm^{-1}) between unpaired electrons of the *Z* and *E* Isomers of **1**$^{\cdot}$ and **1**$^{\cdot\cdot+}$, labelled according to Figure S15.

1$^{\cdot}$		J_1	
Isomer-*Z*		<|0.05|	
Isomer-*E*		–0.6	
1$^{\cdot\cdot+}$	J_1	J_2	J_3
Isomer-*Z*	–0.7	–66.2	–62.9
Isomer-*E*	–0.5	–62.5	–59.3

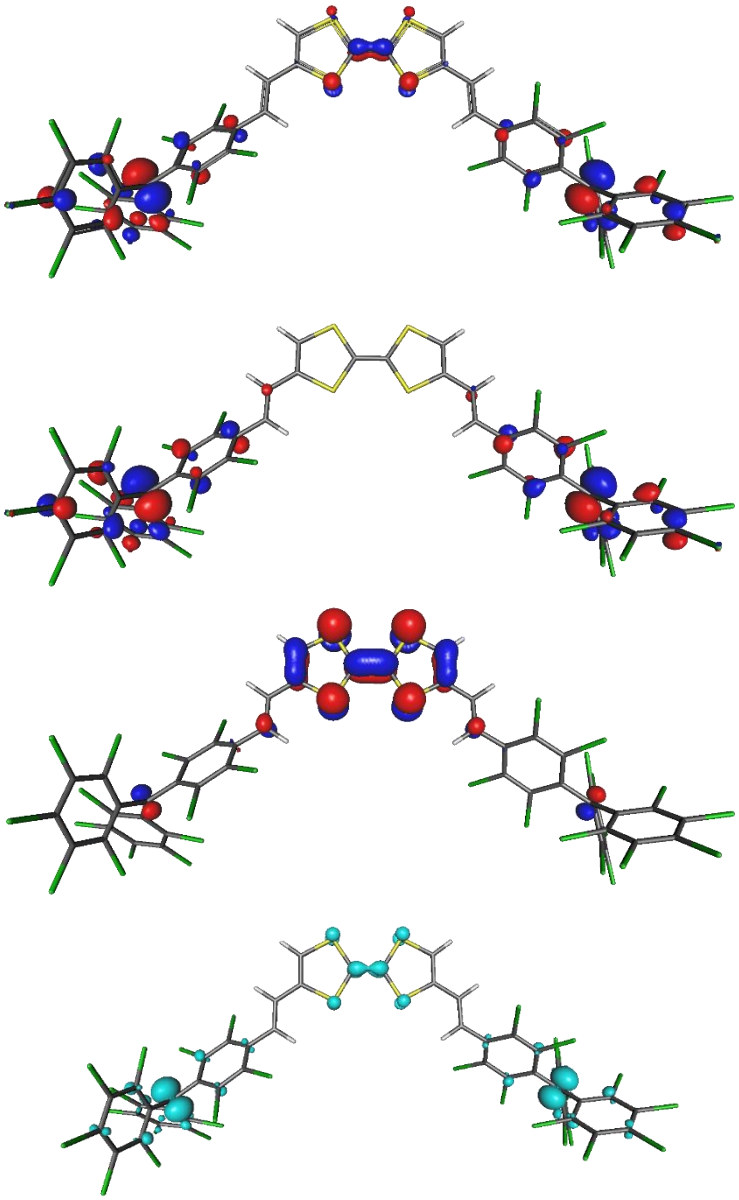

Figure S17. Singly-Occupied Molecular Orbital (SOMO) and spin density distribution obtained for the HS states of **1**$^{\cdot\cdot+}$ (Isomer Z). SOMO isovalue = 0.04, Spin Density isovalue = 0.01.

Optical Properties. TDDFT calculations shed some light on the optical properties of the studied compounds. Even if the position of the calculated bands displays a shift toward larger energies - smaller wavelengths -, such analisys is useful to complement the rationalization of the spectra obtained experimentally. For compound **1**$^{\bullet\bullet}$, the calculations predict three main bands (Table S3). One in the near-IR (1401nm, oscillator stregth *fosc* = 0.1), corresponding to the charge transfer from the TTF HOMO to the PTM SUMO orbitals (see Figure S15). Since the two PTM units are not strictly equivalent, this transition apears as a double band (also 1338 nm, *fosc* = 0.03). This computed band corresponds to the experimental band observed at 900 nm, and the red-shift is associated to (*i*) the accuracy of the calculation, which implies larger shifts in the low-energy region, and (*ii*) to the simplicity of our inspection, which does not account for the effects derived from the fast *E-Z* isomerization. Two higher energy bands are also observed at 590 nm (*fosc* = 0.25) and 520 nm (*fosc* = 0.44). The first one corresponds to the transition from the TTF HOMO-1 to the PTM SUMO and the second one to the TTF HOMO to an unoccupied orbital delocalized over the Vinylene-PTM system.

Table S3. Main bands of the absorption spectra computed for (a) **1**$^{\bullet\bullet}$ and (b) **1**$^{\bullet\bullet\bullet+}$ in dichloromethane

1$^{\bullet\bullet}$	
Band	Type
520 nm, *fosc* = 0.44	TTF [HOMO] - Vinylene-PTM
590 nm, *fosc* = 0.25	TTF [HOMO-1] - PTM [SUMO]
1401 nm, *fosc* = 0.1	TTF [HOMO] - PTM [SUMO]
1$^{\bullet\bullet\bullet+}$	
Band	Type
510 nm, *fosc* = 0.65	TTF [SOMO] - Vinylene-PTM
687 nm, *fosc* = 0.45	TTF [HOMO] - PTM [SUMO]

Regarding **1**$^{\bullet\bullet\bullet+}$, our calculations yield two bright bands at 687 nm (*fosc* = 0.45) and 510 nm (fosc = 0.65) (see Table S3). The first one corresponds mainly (95%) to a transition from the TTF^+ HOMO (HOMO-1 of the neutral TTF) to the PTM SUMO (see Figure S15). It is, thus, equivalent to the transition observed at 590 nm for the neutral compound. In turn, the second one is a mixture of several transitions, being dominant the one from the TTF^+ SOMO (HOMO of the neutral TTF) to the Vinylene-PTM system, as observed for the neutral compound (band at 520 nm). As expected, the low-energy band observed for the neutral specie disappears upon TTF oxidation.

Structure. The molecular geometries of the diradical (**1**$^{\bullet\bullet}$) and triradical cation (**1**$^{\bullet\bullet\bullet+}$) species have been optimized in their low-spin (LS, Singlet for **1**$^{\bullet\bullet}$, Doublet for **1**$^{\bullet\bullet\bullet+}$) and high-spin states (HS, Triplet for **1**$^{\bullet\bullet}$, Quadruplet for **1**$^{\bullet\bullet\bullet+}$), both for the *Z* and *E* isomers and several conformations of the two vinylene bridges. Some of the values reported in Tables S4 and S5 have been used to extract the magnetic exchange couplings reported in Table S2.

Table S4. Computed energy differences (in kcal/mol) of the Z- and E- isomers of **1**$^{\bullet\bullet}$ in several conformations of the two vinylene bridges. The values are given with respect to the most stable one. The energy of the high-spin and low-spin states have been evaluated at each optimized structure.

Isomer	**Bridge 1**	**Bridge 2**	**Geometry**	**Spin State**	
				T	**S**
Z	cis	trans	S	2.90	2.90
Z	cis	trans	T	2.90	2.90
Z	trans	trans	S	0.02	0.02
Z	trans	trans	T	0.02	0.02
E	cis	trans	S	2.88	2.87
E	cis	trans	T	2.88	2.87
E	trans	trans	S	0.00	0.00
E	trans	trans	T	0.00	0.00

Table S5. Computed energy differences (in kcal/mol) of the Z- and E- isomers of $\mathbf{1}^{\cdot\cdot+}$ in several conformations of the two vinylene bridges. The values are given with respect to the most stable one. The energy of the high-spin and low-spin states have been evaluated at each optimized structure. For simplicity, we only include one possible doublet state, in which two alpha electrons are in the PTM units and one beta electron in the TTF.

Isomer	Bridge 1	Bridge 2	Geometry	Spin State	
				Q	D
Z	cis	trans	D	1.96	1.67
Z	cis	trans	Q	1.93	1.67
Z	trans	trans	D	0.37	0.00
Z	trans	trans	Q	0.33	0.01
E	cis	trans	D	2.00	1.74
E	cis	trans	Q	1.96	1.73
E	trans	trans	D	0.43	0.08
E	trans	trans	Q	0.39	0.09

References:

[S1] S. Grimme, *J. Comput. Chem.* **2006**, *27*, 1787-1799.

[S2] M. J. Frisch, G. W. Trucks, H. B. Schlegel, G. E. Scuseria, M. A. Robb, J. R. Cheeseman, G. Scalmani, V. Barone, B. Mennucci, G. A. Petersson, H. Nakatsuji, M. Caricato, X. Li, H. P. Hratchian, A. F. Izmaylov, J. Bloino, G. Zheng, J. L. Sonnenberg, M. Hada, M. Ehara, K. Toyota, R. Fukuda, J. Hasegawa, M. Ishida, T. Nakajima, Y. Honda, O. Kitao, H. Nakai, T. Vreven, J. A. Montgomery Jr., J. E. Peralta, F. Ogliaro, M. Bearpark, J. J. Heyd, E. Brothers, K. N. Kudin, V. N. Staroverov, R. Kobayashi, J. Normand, K. Raghavachari, A. Rendell, J. C. Burant, S. S. Iyengar, J. Tomasi, M. Cossi, N. Rega, J. M. Millam, M. Klene, J. E. Knox, J. B. Cross, V. Bakken, C. Adamo, J. Jaramillo, R. Gomperts, R. E. Stratmann, O. Yazyev, A. J. Austin, R. Cammi, C. Pomelli, J. W. Ochterski, R. L. Martin, K. Morokuma, V. G. Zakrzewski, G. A. Voth, P. Salvador, J. J. Dannenberg, S. Dapprich, A. D. Daniels, Ö. Farkas, J. B. Foresman, J. V. Ortiz, J. Cioslowski and D. J. Fox, 2009.

[S3] ADF2013, SCM, Theoretical Chemistry, Vrije Universiteit, Amsterdam, The Netherlands.

[S4] M. Kaupp, M. Renz, M. Parthey, M. Stolte, F. Wurthner and C. Lambert, *Phys. Chem. Chem. Phys.* **2011**, *13*, 16973-16986.

[S5] V. Lloveras, J. Vidal-Gancedo, T. M. Figueira-Duarte, J.-F. Nierengarten, J. J. Novoa, F. Mota, N. Ventosa, C. Rovira and J. Veciana, *J. Am. Chem. Soc.* **2011**, *133*, 5818-5833.

[S6] M. Fumanal, F. Mota, J. J. Novoa and J. Ribas-Arino, *J. Am. Chem. Soc.* **2015**, *137*, 12843-12855.